

# **DEVELOPMENT OF ORGANIC SOLAR CELLS AND THEIR PERFORMANCE CHARACTERIZATION**

*By*

**ABHAY GUSAIN**

(ENGG01201104015)

**Bhabha Atomic Research Centre**

*A thesis submitted to the*

*Board of Studies in Engineering Sciences Strategic Studies*

*In partial fulfillment of requirements*

*for the Degree of*

**DOCTOR OF PHILOSOPHY**

*Of*

**HOMI BHABHA NATIONAL INSTITUTE**

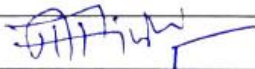
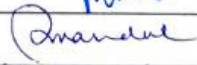
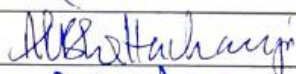
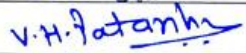
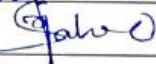
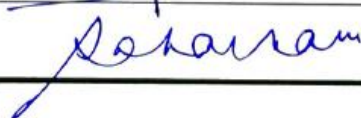


**Oct. 2016**

# Homi Bhabha National Institute

## Recommendations of the Viva Voce Committee

As members of the Viva Voce Committee, we certify that we have read the dissertation prepared by **Abhay Gusain** entitled "**Development of Organic Solar Cells and Their Performance Characterization**" and recommend that it may be accepted as fulfilling the thesis requirement for the award of Degree of Doctor of Philosophy.

Chairman - Prof. A. P. Tiwari		27/10/16
Guide / Convener - Prof. D. K. Aswal		27/10/16
Co-guide Prof. P. V. Varde		27/10/16
Examiner - Prof. P. K. Mondal		27.10.16
Member 1- Prof. A. K. Bhattacharjee		27/10/2016
Member 2- Prof. V. H. Patankar		27.10.2016
Member 3- Prof. D. C. Kar		27/11/2016
Member 4- Prof. N. K. Sahoo		27-X-2016
Member 5- Prof. S. Basu		27/10/16

Final approval and acceptance of this thesis is contingent upon the candidate's submission of the final copies of the thesis to HBNI.

I/We hereby certify that I/we have read this thesis prepared under my/our direction and recommend that it may be accepted as fulfilling the thesis requirement.

Date: 27.10.16

Place: Mumbai

<Signature>

Co-guide (if applicable)

  
27/10/16

<Signature>

Guide

## **STATEMENT BY AUTHOR**

This dissertation has been submitted in partial fulfillment of requirements for an advanced degree at Homi Bhabha National Institute (HBNI) and is deposited in the Library to be made available to borrowers under rules of the HBNI.

Brief quotations from this dissertation are allowable without special permission, provided that accurate acknowledgement of source is made. Requests for permission for extended quotation from or reproduction of this manuscript in whole or in part may be granted by the Competent Authority of HBNI when in his or her judgment the proposed use of the material is in the interests of scholarship. In all other instances, however, permission must be obtained from the author.

Abhay Gusain  
DGFS-Ph.D

## **DECLARATION**

I, hereby declare that the investigation presented in the thesis has been carried out by me. The work is original and has not been submitted earlier as a whole or in part for a degree / diploma at this or any other Institution / University.

Abhay Gusain  
DGFS-Ph.D

## **CERTIFICATE**

I hereby certify that I have read this dissertation prepared under my supervision and recommend that it may accepted for fulfilling the dissertation requirement.

D. K. Aswal

## **ACKNOWLEDGEMENTS**

Firstly, I take an honored privilege to express my heartiest gratitude to my research guide Prof. D. K. Aswal, for his continuous guidance during the thesis work. It is my pleasure to express my grateful thanks to Prof. P. V. Varde for his encouragement and support. I express my deep gratitude to Prof. S.K. Gupta and Prof. S. C. Gadkari, Head, Technical Physics Division, for their supports and guidance during the course of thesis work.

I sincerely thank Dr. K. P. Muthe, Dr. Niranjana Ramgir and Dr. Nirav Joshi for their constant motivation and support during this thesis work and their untiring efforts towards bringing the thesis into the present form.

<b>S.No.</b>	<b>CONTENTS</b>	<b>PAGE</b>
<b>Chapter 1.</b>		
<b><i>Introduction</i></b>		
	1.1 Solar Cells	1
	1.2 Solar Energy Spectrum	2
	1.3 Basic semiconductor physics of solar cells	3
	1.3.1 Fundamentals of parameters of solar cells	4
	1.3.1.1 Open circuit voltage ( $V_{OC}$ )	5
	1.3.1.2 Short circuit current density ( $J_{SC}$ )	5
	1.3.1.3 Fill Factor (FF)	5
	1.3.1.4 Efficiency ( $\eta$ )	5
	1.4 Generations of the solar cells	9
	1.4.1 First generation monocrystalline and amorphous Si (Silicon) based solar cells:	11
	1.4.2 Second generation monocrystalline and amorphous Si (Silicon) based solar cells	11
	1.4.3 Third generation thin film organic solar cells	13
	1.4.3.1 Polymer solar cells	13
	1.5 Literature survey	23
	1.6 Objectives of the present thesis	31
<b>Chapter 2.</b>		
<b><i>Experimental Techniques</i></b>		
	2.1 Materials used	39
	2.1.1 Materials used for the device fabrication	39
	2.1.1.1 ITO base substrates	39
	2.1.1.2 PEDOT:PSS	40
	2.1.1.3 Donor polymers	40
	2.1.1.4 Acceptor Fullerene	41

	2.1.1.5 Aluminum	41
	2.1.2 Kelvin clips	41
	2.1.3 Solvent materials	41
	2.1.4 Materials used for device encapsulation	42
	2.2 Fabrication of BHJ solar cells	42
	2.2.1 MBraun glove box	42
	2.2.2 Fabrication steps	43
	2.2.2.1 Patterning	43
	2.2.2.2 Cleaning steps	43
	2.2.2.3 Deposition of the PEDOT:PSS	44
	2.2.2.4 Deposition of PCDTBT:PCBM	44
	2.2.2.5 Deposition of Aluminum electrode	46
	2.2.2.6 Encapsulation of the solar cells device	47
	2.3 Characterization techniques	47
	2.3.1 UV-Visible spectroscopy	47
	2.3.2 Fourier Transform Infrared Spectroscopy	48
	2.3.3 Atomic force microscopy	50
	2.3.4 Kelvin probe microscopy	51
	2.3.5 Raman spectroscopy	52
	2.3.6 X-ray reflectometry	52
	2.3.7 X-ray photoelectron spectroscopy	53
	2.3.8 Photovoltaic characterization	53
	2.3.8.1 Current-voltage characterization	53
	2.3.8.2 Incident photon to current conversion efficiency (IPCE)	54
	2.3.8.3 Electrochemical impedance spectroscopy	54

<b>Chapter 3.</b>	<b><i>S-kinks in BHJs and Efficiency Enhancement by Solvent Annealing</i></b>	
	3.1 Introduction	56
	3.2. XRR experiments	62
	3.3 Results and discussion	63
	3.4. Efficiency enhancement by solvent annealing	73
	3.4.1 Adoption of a new approach for fabrication of the PCDTBT:PCBM solar cells with higher thickness	74
	3.4.2 Advantages offered by layer by layer deposition	76
	3.4.3 Fabrication of the PCDTBT:PCBM solar cells	77
	3.4.2 JV Results	78
	3.4.4 Encapsulation and stability studies on PCDTBT:PCBM solar cells	80
	3.4.5 Effects of interface on the photovoltaic performance	81
	3.4.6 Thermal and solvent annealing of the different layer PCDTBT:PCBM devices	83
	3.4.7 Intensity variation of the input light on the different layer devices	84
	3.4.8 Approach for efficiency enhancement in multilayer devices using solvent annealing	86
	3.4.9 Experimental	88
	3.4.10 Results and discussion	91
	3.5 Conclusions	99

<b>Chapter 4.</b>	<b><i>Efficiency Enhancement in BHJ Solar Cells using Graphene Nanosheets</i></b>	
	4.1 Introduction	103
	4.1.1 Preparation of graphene for graphene-PCBM composite as acceptor type material	104
	4.1.2 Fabrication of the P3HT:PCBM solar cells	105
	4.1.3 Characterization of the P3HT:PCBM solar cells and graphene composites	106
	4.1.3.1 Cyclic Voltammetry	106
	4.1.3.2 Morphological characterization	109
	4.1.3.3 Raman characterization	110
	4.1.3.4 JV characterization	111
	4.1.4 Efficiency enhancement in PCDTBT:PCBM using graphene nanosheets	113
	4.1.4.1 Experimental details	114
	4.1.4.2 Results and discussion	115
	4. 2 Conclusions	117
<b>Chapter 5.</b>	<b><i>Summary and Conclusions</i></b>	
		118

## Publications

### Journals

1. Electron density profile at the interfaces of bulk heterojunction solar cells and its implication on the S-kink, Abhay Gusain, S. Singh, A.K. Chauhan, V. Saxena, P. Jha, P. Veerender, A. Singh, P. V. Varde, Saibal Basu, D.K. Aswal and S.K. Gupta, *Chem. Phys. Lett.* 646, 6–11 (2016). **(Thesis work)**
2. Flexible NO gas sensor based on conducting polymer poly[*N*-9'-heptadecanyl-2,7-carbazole-alt-5,5-(4',7'-di-2-thienyl-2',1',3'-benzothiadiazole)] (PCDTBT), Abhay Gusain, Nirav Joshi, P. V. Varde, D.K. Aswal, *Sens. Actuators B Chem.* , 239, 734–745, (2017). **(Thesis work)**
3. Different physical mechanisms underlying the performance of the polymer solar cells, Abhay Gusain, Niranjan Ramgir, K. P. Muthe, S. C. Gadkari, under preparation. **(Thesis work)**
4. Graphene composite for improvement in the conversion efficiency of flexible poly 3-hexyl-thiophene:[6,6]-phenyl C<sub>71</sub> butyric acid methyl ester polymer solar cells, A. K. Chauhan, Abhay Gusain, P. Jha, S. P. Koiry, V. Saxena, P. Veerender, D. K. Aswal, and S. K. Gupta, *Appl. Phys. Lett.* 104, 133901 (2014). **(Thesis work)**
5. Interfacial charge trapping in PCDTBT:PCBM solar cells and its elimination by solvent annealing, A.K. Chauhan, Abhay Gusain, P. Jha, P. Veerender, D.K. Aswal, and S.K. Gupta, D. Taguchi, T. Manaka, M. Iwamoto, *AIP Advances*, 6, 095012 (2016). **(Thesis work)**

6. XPS, UV-Vis, FTIR and EXAFS Studies to Investigate the Binding Mechanism of N719 Dye Onto Oxalic Acid Treated TiO<sub>2</sub> and Its Implication on Photovoltaic Properties, J. Singh, Abhay Gusain, V.Saxena, A. K. Chauhan, P.Veerender, S. P.Koiry, P.Jha, A. Jain, D. K.Aswal, S. K. Gupta, *J. Phys. Chem. C.* 117 (41), 21096-21104 (2013).
7. Air-stability and bending properties of flexible organic field-effect transistors based on poly [N-9'-heptadecanyl-2, 7-carbazole-alt-5, 5-(4', 7'-di-2-thienyl-2', 1', 3'-benzothiadiazole)], P.Jha, S.P.Koiry, V.Saxena, P.Veerender, Abhay Gusain, A.K. Chauhan, A.K. Debnath, D.K. Aswal, S.K .Gupta, *Org. Electron.*14 (10), 2635-2644 (2013).
8. Incorporation of non-conjugated polymer chain in conjugated polymer matrix: A new single step strategy for free standing non-volatile polymer memory, P. Jha, S. P. Koiry, V. Saxena, P. Veerender, Abhay Gusain, A. K. Chauhan, D. K. Aswal, S. K. Gupta, *Org. Electron.*14 (11), 2896-2901 (2013).
9. Free-standing polypyrrole films as substrate-free and Pt-free counter electrodes for quasi-solid dye-sensitized solar cells, P. Veerender, V.Saxena, P. Jha, S.P. Koiry, Abhay Gusain, S. Samanta, A.K. Chauhan, D.K. Aswal, S.K. Gupta, *Org. Electron.* 13(12), 3032-3039 (2012).
10. Co-sensitization of N719 and RhCL dyes on carboxylic acid treated TiO<sub>2</sub>for enhancement of light harvesting and reduced recombination, V.Saxena, P Veerender, AbhayGusain, P.Jha, J. Singh, S.P.Koiry, P.V.Varde, A.K. Chauhan, D.K.Aswal, S.K. Gupta, *Org. Electron.*14 (11), 3098-3108 (2013).

11. Probing the annealing induced molecular ordering in bulk heterojunction polymer solar cells using in-situ Raman spectroscopy, P Veerender, V.Saxena, A.K. Chauhan, S.P.Koiry, P.Jha, Abhay Gusain, S. Choudhury, D.K.Aswal, S.K. Gupta, *Sol. Energ. Mat. Sol. Cells*,120, 526-535 (2013).

## Conferences

1. Investigation on the effects of thermal annealing on PCDTBT: PCBM bulk-heterojunction polymer solar cells, Abhay Gusain, V.Saxena, P.Veerender, P.Jha, S.P.Koiry, A.K. Chauhan, D.K.Aswal, S.K. Gupta, *AIP Conf. Proc.* 776, 1512 (2013).
2. Efficiency Enhancement in PCDTBT:PCBM polymer solar cells using grapheme nansheets, Abhay Gusain, V.Saxena, P.Veerender, P.Jha, S.P.Koiry, A.K. Chauhan, P.V. Varde, D.K.Aswal, S.K. Gupta, *AIP Conf. Proc.* 1665, 050122 (2015).
3. Effect Of Interfaces On Charge Transfer In PCDTBT:PCBM Solar Cells,Abhay Gusain, P. V. Varde, D. K. Aswal, S. K. Gupta,*AIP Conf. Proc.*(2016) in press.
4. Active layer Thickness dependence of open circuit voltage in PCDTBT:PCBM polymer solar cells and their stability studies, Abhay Gusain, A. K. Chauhan, P. Veerender, V.Saxena, S. P. Koiry, P. Jha, P.V. Varde, D. K. Aswal, S. K. Gupta, *EUPVSEC*,Amsterdam, (2014).
5. Encapsulation and stability studies on PCDTBT:PCBM polymer solar cells, Abhay Gusain, A. K. Chauhan, P. Veerender, V.Saxena, S. P. Koiry, P. Jha, D. K. Aswal, S. K. Gupta, *DAE-BRNS Conference on Organic Devices: The Future Ahead, (ODEFA)*, (2014).
6. Active layer Thickness dependence of open circuit voltage in PCDTBT:PCBM polymer solar cells, Abhay Gusain, A. K. Chauhan, P. Veerender, V.Saxena, S. P. Koiry, P. Jha,

- D. K. Aswal, S. K. Gupta, *DAE-BRNS Conference on Organic Devices: The Future Ahead, (ODEFA)*, (2014).
7. Effect of Graphene Incorporation in the Hole Transport Layer of P3HT:PCBM Polymer Solar Cells, A. K. Chauhan, V.Saxena, S. P. Koiry, P. Jha, P. Veerender, Abhay Gusain, D. K. Aswal, S. K. Gupta, *DAE SSPS Conference, (2014)*.
  8. Power conversion efficiency enhancement of P3HT:PCBM polymer solar cells using graphene in active layer, A. K. Chauhan, Abhay Gusain, P. Jha, S. P. Koiry, V.Saxena, P. Veerender, D. K. Aswal, S. K. Gupta, *DAE-BRNS Conference on Organic Devices: The Future Ahead, (ODEFA)*, (2014).
  9. Novel free standing polypyrrole films as counter electrodes for dye sensitized solar cells, P. Veerender, V.Saxena, P. Jha, S. P. Koiry, Abhay Gusain, A. K. Chauhan, D. K. Aswal, S. K. Gupta, *DAE-BRNS Conference on Organic Devices: The Future Ahead, (ODEFA)*, (2014).
  10. Ferroelectric like characteristics in redox active polymers, S. P. Koiry, V.Saxena, P. Jha, P. Veerender, Abhay Gusain, A. K. Chauhan, D. K. Aswal, S. K. Gupta, *DAE-BRNS Conference on Organic Devices: The Future Ahead, (ODEFA)*, (2014).
  11. Conducting polymers based counter electrodes for dye-sensitized solar cells, P. Veerender, V.Saxena, Abhay Gusain, P. Jha, S.P. Koiry, A.K. Chauhan, D.K. Aswal, S.K. Gupta, *DAE SSPS Conference, (2014)*.
  12. Poly (2, 7-carbazole) derivative based air stable and flexible organic field effect transistor, P.Jha, P Veerender, SP Koiry, V.Saxena, A Gusain, A. K. Chauhan, D. K.Aswal, S. K. Gupta, *AIP Conf. Proc. 772, 1512 (2013)*.

13. Effect of Co-sensitization and acid treatment on TiO<sub>2</sub> photoanodes in dye-sensitized solar cells, P Veerender, V.Saxena, Abhay Gusain, P Jha, S.P.Koiry, A. K. Chauhan, D. K. Aswal, S. K. Gupta, *AIP Conf. Proc.* 778, 1512 (2013).
14. Improved efficiency of organic dye sensitized solar cells through acid treatment, P Veerender, V. Saxena, Abhay Gusain, P Jha, S.P. Koiry, A. K. Chauhan, D. K. Aswal, S. K. Gupta, *AIP Conf. Proc.* 774, 1512 (2013).
15. Dye Sensitized Solar Cells Based On Metal-Free Organic Dyes and Aqueous Electrolytes, P Veerender, V. Saxena, Abhay Gusain, D. K. Aswal, S. K. Gupta, *Fuelling the Future: Advances in Science and Technologies for Energy Generation, Transmission and Storage*, (2012).

## **Awards**

1. ***Innovative Research Award*** at *DAE-BRNS Conference on Organic Devices: The Future Ahead*, 2014.



# ODeFA-2014



## Innovative Research Award

is conferred to Dr./Mr./Mrs./Ms **Abhay Gusain** of Technical Physics Division, Bhabha Atomic Research Centre, Mumbai - 85 for his/her work on "Power Conversion Efficiency Enhancement of P3HT: PCBM Polymer Solar Cells using Graphene in Active Layer" presented in the DAE-BRNS Conference on "Organic Devices: The Future Ahead" (ODeFA-2014) held at Bhabha Atomic Research Centre, Mumbai – 400 085, India on March 3-6, 2014.

**Dr. D.K. Aswal**  
**Convener**

## List of Figures

- Fig. 1.1 Solar spectrum and spectral photon flux density as a function of the wavelength  $\lambda$  of incident photon (Data from ASTM) ASTM Reference Spectra. <http://rredc.nrel.gov/solar/spectra/am1.5/ASTMG173/ASTMG173.html>).
- Fig. 1.2 Charge generation in solar cell after the absorption of the light photons.
- Fig. 1.3 Photovoltaic parameters of the solar cells.
- Fig. 1.4 Equivalent circuit model of a solar cell.
- Fig. 1.5 Different generations of solar cells with reported efficiencies.
- Fig. 1.6 Schematic of the first generation single crystal Si solar cell.
- Fig. 1.7 Schematic of the second generation thin film CdTe, CiGS and a-Si solar cells.
- Fig. 1.8 Structure of polymer solar cell.
- Fig. 1.9 Schematic representation underlying the working principle of polymer solar cell.
- Fig. 1.10 Charge carrier generation in polymer solar cell.
- Fig. 1.11 Charge carrier diffusion and recombination in polymer solar cell.
- Fig. 1.12 Architecture of polymer solar cell.
- Fig. 1.13 Variation in the efficiency with bandgap of polymer solar cell.
- Fig. 2.1 Cleaning procedure of the ITO substrates.
- Fig. 2.2 Deposition of the PCDTBT:PCBM active layer and thermal evaporation of the aluminum electrodes.
- Fig. 2.3 Encapsulated polymer solar cell.
- Fig. 2.4 Encapsulated PCDTBT:PCBM solar cells.
- Fig. 2.5 FTIR spectrophotometer.

- Fig. 2.6 Atomic Force Microscopy.
- Fig. 3.1 Chemical structures of (a) PCDTBT and (b) P3HT.
- Fig. 3.2 (a) JV characteristics, (b) UV-Vis and (c) Raman spectrum of PCDTBT:PCBM solar cells before and after thermal annealing.
- Fig. 3.3 Typical experimental J–V curves recorded for devices under 1 sun (AM 1.5 G), 100 mW/cm<sup>2</sup> illumination for (a) devices without S-kink, (b) devices with S-kink and (c) appearance of S-kink after annealing (100°C for 4 h) the devices representing (a). The inset shows the energy levels of the materials employed in device fabrication, and represents the injection barrier for holes.
- Fig. 3.4 Work function mapping of (a) filtered and (b) unfiltered PEDOT:PSS layers recorded using Kelvin Probe exhibiting average work function value of 5.1 and 5.3 eV, respectively.
- Fig. 3.5 (a) Structure of PEDOT:PSS and (b) S2p and O1s XPS spectra of the PEDOT:PSS samples (b) and (d), and (c) and (e) corresponding to average work function value of (a) 5.1 and (b) 5.3 eV for the samples, respectively.
- Fig. 3.6 (a) Fitting of GXRR data for a typical ITO/PEDOT:PSS/PCDTBT:PCBM/Al bulk heterojunction solar cell using the different electron density profiles shown in the inset. It is seen that the best fitting is observed only when an additional interface between PCDTBT:PCBM and PEDOT:PSS is taken into account.(b) Fitting of GXRR data for devices with and without S-kink in their J-V characteristics and (c) the resultant electron density profile.
- Fig. 3.7 The electron density profile of the device with diode-like J-V characteristics annealed at 100°C for different period of time. Annealing leads to increase in the

electron density at the PCDTBT:PCBM/ PEDOT:PSS as well as increase in the roughness of all the interfaces.

- Fig. 3.8 Conventional approach of deposition of the single thick active layer on substrate through spin coating.
- Fig. 3.9 New layer by layer deposition approach of deposition of the thick active layer on substrate through spin coating.
- Fig. 3.10 Two substrates of each layer with nine devices were fabricated and characterized.
- Fig. 3.11 JV characteristics of single-layer and five-layer cells under varying input intensity.
- Fig. 3.12 Variation of open circuit voltage and short circuit current density with time for (a) unsealed and (b) encapsulated devices.
- Fig. 3.13 Charge accumulation across the interfaces in the various layers of the device.
- Fig. 3.14 (a) Chemical structure of PCDTBT and PCBM (b) Typical device structure (c) Bottom Gate Top Contact FET configuration of mobility measurements (d) solvent annealing setup.
- Fig. 3.15 Optical absorption spectra of single and multilayer films.
- Fig. 3.16 J-V characteristics of (a) different layers devices under 1 sun (b) for single layer device before and after solvent annealing (c) for multilayer device before and after solvent annealing (red plots for solvent annealed films).
- Fig. 3.17 Impedance spectra of BHJ solar cells for 1- 5 layer devices, equivalent circuit models used for fitting the impedance spectra for(a) thin and(b)thick active layer, respectively. Impedance spectra of devices having (c)active layer of different

thickness and (d) thick active layer after solvent annealing, under illumination of 1 sun intensity.

- Fig. 3.18 FET transfer characteristics of single layer and 5-layer PCDTBT:PCBM films.
- Fig. 3.19. AFM images of the PCDTBT films before solvent annealing (a) single layer and (b) thick active layer and after solvent annealing (c) single layer and (d) thick active layer.
- Fig. 4.1 Cyclic voltammograms recorded for the solution of (a) P3HT and P3HT + graphene-sheets and (b) PCBM and PCBM + graphene-sheets.  $(\alpha h\nu)^2$  vs  $(h\nu)$  plots obtained for (c) P3HT and (d) PCBM films.
- Fig. 4.2 Energy level diagrams for the solar cell structures:ITO/PEDOT/P3HT:PCBM/Al and ITO/PEDOT/P3HT:PCBM-graphenesheets/Al.
- Fig. 4.3 AFM images of active layer blend films of (a) P3HT:PCBM and (b) P3HT:PCBM-graphene-sheets. The shown line profile is scaled in nm. (c) Raman spectra recorded for the films of pure graphene-sheets, P3HT:PCBM and P3HT:PCBM-graphene composite.
- Fig. 4.4 JV characteristics for the bulk heterojunction solar cells fabricated using different active layers: (a) P3HT:PCBM, (b) P3HT:PCBM-graphene-sheets, and (c) P3HT:PCBM-graphene-flakes.
- Fig. 4.5 JV characteristics with different set of devices under  $30 \text{ mW/cm}^2$ .

## List of Tables

- Table 1.1 Summary of efficiencies of different polymer BHJ solar cells.
- Table 3.1 Summary of photovoltaic parameters of different BHJ solar cells and estimated parameters of the (PCDTBT:PCBM)/(PEDOT:PSS) interface using GXRR measurements.
- Table 3.2 Variation of Photovoltaic Parameters under AM1.5G with thickness.
- Table 3.3 Short circuit current density values under the different input light intensities.
- Table 3.4 Thickness of different layers estimated using optical absorption and profilometry.
- Table 3.5 Summary of photovoltaic parameters of BHJ solar cells with different layers under input intensity of  $100 \text{ mW/cm}^2$ .
- Table 3.6 Device parameters for different layer devices at input intensity of  $100 \text{ mW/cm}^2$  (after solvent annealing).
- Table 3.7 Impedance Spectroscopy of different layered devices.
- Table 3.8 Hole mobilities in single and five layer device.
- Table 4.1 Summary of various photovoltaic parameters obtained for flexible bulk-heterojunction solar cells using different active layer.
- Table 4.2 Photovoltaic parameters with different set of devices under  $30 \text{ mW/cm}^2$ .
- Table 5.1 Major achievements and evolution of the polymer solar cells

## Abbreviations

<b>ITO</b>	Indium doped Tin Oxide
<b>PEDOT</b>	poly (3,4-ethylene dioxythiophene)
<b>PSS</b>	poly (styrenesulfonate)
<b>P3HT</b>	poly (3-hexylthiophene-2,5-diyl)
<b>PCBM</b>	phenyl-C <sub>71</sub> butyric acid methyl ester
<b>PTPTB</b>	poly N-dodecyl-2,5-bis(2'thienyl)pyrrol(2,1,3-benzothiadiazole)
<b>PEOPT</b>	poly(3-(4-(1'',4'',7''-trioxaoctyl)phenyl)thiophene)
<b>PFDTBT</b>	poly(2,7-(9-(2'-ethylhexyl)-9-hexyl-fluorene)-alt-5,5-(4',7'-di-2-thienyl-2',1',3'-benzothiadiazole))
<b>MDMO-PPV</b>	9-(diethylamino)-5H-benzo[a]phenoxazin-5-one (nilered), poly(2-methoxyl-5-(3,7-dimethyloctyloxy)para-phenylene-vinylene)
<b>ICBA</b>	indene-C <sub>60</sub> bisadduct
<b>PDTP-DFBT</b>	poly[2,7-(5,5-bis-(3,7-dimethyloctyl)-5H-dithieno[3,2-b:2',3'-d]pyran)-alt-4,7-(5,6-difluoro-2,1,3-benzothiadiazole)]
<b>PTB7</b>	polythieno[3,4-b]-thiophene/benzodithiophene
<b>PDVT-10</b>	poly[2,5-bis(alkyl)pyrrolo[3,4-c]pyrrole-1,4(2H,5H)-dione-alt-5,5'-di(thiophene-2-yl)-2,2'-(E)-2-(2-(thiophen-2-yl)vinyl)thiophene]
<b>PBDTTT-EFT</b>	poly[4,8-bis(5-(2-ethylhexyl)thiophen-2-yl)-benzo[1,2-b;4,5-b']dithiophene-2,6-diyl-alt-(4-(2-ethylhexyl)-3-fluorothieno[3,4-b]thiophene-)-2-carboxylate-2,6-diyl]

<b>PBDTP-DTBT</b>	poly(4,8-bis(4-(2-ethylhexyl)-phenyl)-benzo[1,2-b:4,5-b']dithiophene-alt-[4,7-di(4-(2-ethylhexyl)-2-thienyl)-2,1,3-benzothiadiazole)-5, 5'-diyl])
<b>PCPDTBT</b>	poly(4,4-dialkyl-4H-cyclopenta[2,1-b:3,4-b']dithiophene-2,6-diyl-alt-2,1,3-benzothiadiazole-4,7-diyl)
<b>PBDTTT-EFT</b>	poly[4,8-bis(5-(2-ethylhexyl)thiophen-2-yl)-benzo[1,2-b:4,5-b <sub>0</sub> ]dithiophene-2,6-diyl-alt-(4-(2-ethylhexyl)-3-fluorothiopheno[3,4-b]thiophene-)-2-carboxylate-2-6-diyl]
<b>BHJ</b>	bulk heterojunction
<b>PCDTBT</b>	poly[N-9'-heptadecanyl-2,7-carbazole-alt-5,5-(4',7'-di-2-thienyl-2',1',3'-benzothiadiazole)]
<b>GIXRR</b>	Grazing Incident X-ray Reflectometry
<b>PEN</b>	polyethylene naphthalate
<b>DCB</b>	1,2-dichlorobenzene
<b>Al</b>	Aluminum

## SYNOPSIS

With the demand of the global energy increased upto 15,500 TWh and a significant reduction of conventional energy sources (e.g. coal and petroleum) has led to increased research and development to tap renewable energy sources, including solar, wind and geothermal etc. Renewable energy sources have additional advantages in terms of protecting the global environment. Solar energy has gained attention as it can be implemented economically. As India receives continuous supply of the incident sun radiation, the solar energy sector provides huge opportunity for harnessing solar energy for various applications. Various types of solar cells have been developed till date which can be categorized as: First generation i.e. Si (Silicon) based monocrystalline and amorphous solar cells; Second generation i.e. multi-junction CdTe, CdSe and GaAs; Third generation i.e. thin film solar cells, including organic solar cells and Fourth generation i.e. organic/inorganic hybrid solar cells. Among these, the research on organic (polymer) solar cells is of current international focus as they offer several advantages such as low processing cost, ease of processing, faster processing and flexibility.

A typical BHJ polymer solar cell consists of an active layer (i.e. blend of a donor conducting polymer and an acceptor fullerene-derivative) sandwiched between hole and electron transporting layers/electrodes. Upon light exposure, the electrons in the donor are excited from HOMO (Highest Occupied Molecular Orbital) to LUMO (Lowest Unoccupied Molecular Orbital) of the polymer and form excitons (i.e. electron-hole pairs). The excitons are dissociated at the donor/acceptor interface, wherein the electrons are transferred from the LUMO of donor to LUMO of the acceptor, which are finally collected at the anode. Similarly, the holes jump from HOMO of the donor to the HOMO of the HTL, which are collected at the cathode. The most commonly used conducting polymers for the BHJs are P3HT and PCDTBT. On the other hand,

the acceptor has been limited to PCBM. In literature, though the highest reported efficiencies for the BHJ solar cells have been upto 12%, however their reproducibility from lab-to-lab has been poor as most of the time the obtained efficiencies are much lower i.e. <5%. In addition, the environmental stability of the BHJ solar cells has been poor, owing to the factors like unfavourable band gap, unintended energy level misalignments and material properties susceptible to the degradation by atmospheric oxygen and moisture. One of the direct outcome of these factors is the appearance of a S-shaped like current-voltage characteristics (known as S-kink), which drastically reduces all the photovoltaic parameters viz. open circuit voltage, short circuit current density and fill factor, and consequently the overall efficiency of the solar cells. The appearance of S-kink essentially is related to the poor quality interfaces, and therefore, the ineffective charge transfer across the interfaces and reduced surface recombination. The quality of interface is governed by several factors including oxygen doping, presence of organic impurities, vertical phase segregation, formation of charge dipole etc. Thus it is important to understand the underlying mechanism for the appearance of the S-kinks in the BHJ solar cells. In order to understand this mechanism, the S-kinks in the current-voltage characteristics in PCDTBT:PCBM based BHJ solar cells were studied using non-destructive X-ray reflectivity, which is a powerful technique to estimate the electron density profile across the BHJ solar cells. A direct correlation is observed between the enhanced electron density at PEDOT:PSS/PCDTBT:PCBM interface and appearance of S-kink in J-V characteristics, which is also supported by X-ray photoelectron spectroscopy and Kelvin probe measurements. It has been found that at the interfaces of the devices with S-kinks, the charge transfer is not effective as compared to the devices without S-kinks. Thus for the improvement of the efficiency of the BHJ solar cells with S-kinks, the charge transfer across the interfaces must be improved. In order

to address the issue of the S-kinks in the J-V characteristics of the devices an approach of the solvent annealing of the active layer of PCDTBT:PCBM has been adopted.

Additionally, for efficiency improvement in the BHJ polymer solar cells based on PCDTBT:PCBM, an approach of enhancing the active layer thickness was adopted. The efficiency of PCDTBT:PCBM based BHJ solar cell is limited by the thickness of the active layer. In order to improve the efficiency of the BHJ solar cell by a mixed approach of use of thicker active layer as well as solvent annealing was adopted. It is observed that 290 nm thick PCDTBT:PCBM active layer via multilayer deposition aids in more light absorption as compared with thin (75 nm) active layer. The BHJ solar cells fabricated using thick active layer show enhanced open circuit voltage, and reduced short circuit current density and fill factor as compared with devices fabricated using thin active layer. The solvent annealing of the thick active layer by tetrahydrofuran vapors results in all photovoltaic parameters and therefore, results in overall efficiency improvement of 3.9% as compared to 3.55% for device using thin layer. The efficiency improvement has been attributed to the suppression of the resistive losses occurring at various interfaces of the active layer as supported by impedance spectroscopy measurements.

One of the most important factors determining the performance of the polymer solar cells is their stability in performance over longer period of times. The thesis also addresses the issues related to the stable operation of the solar cell. As the active layer materials used in the fabrication of the solar cells are prone to degradation in the ambient atmosphere due to oxygen and moisture, these devices must be encapsulated in order to prevent their exposure to the atmosphere. Thus the encapsulation of the devices of the different layers and the comparison in the stability in the performance of the encapsulated and unencapsulated devices with time was done. Prior and after the encapsulation procedure, the devices are characterized inside the Glove

Box to ensure that encapsulation procedure does not cause any degradation of the photovoltaic performance of the solar cells. It has been confirmed that the devices do not undergo any degradation after encapsulation confirming that encapsulation has no effect on the performance of the devices.

In addition to the effective charge transfer across the interfaces of the BHJ device, the efficiency of the BHJ device also depends upon the effective charge transfer across the bulk of the active layer. This effective charge transfer across the bulk has been achieved by the addition of graphene in the BHJ device. The experiments were carried out on BHJ solar cells based on P3HT:PCBM using the composites of the graphene mixed in PCBM in the active layer of the BHJ solar cell. The solution of thin graphene-sheets obtained from a simple ultrasonic exfoliation process was found to chemically interact with PCBM molecules. The thinner graphene-sheets have significantly altered the positions of highest occupied molecular orbital and lowest unoccupied molecular orbital of PCBM, which is beneficial for the enhancement of the open circuit voltage of the solar cells. Flexible BHJ solar cells fabricated P3HT:PCBM-graphene exhibited a power conversion efficiency of 2.51%, which is a 2-fold increase as compared to those fabricated using P3HT:PCBM. Inclusion of graphene-sheets not only improved the open-circuit voltage but also enhanced the short-circuit current density owing to an improved electron transport.

*Thus, in order to improve the efficiency of BHJ solar cells it is imperative to understand in detail the origin of the S-kinks as well as improve the charge transport in the active layer, and therefore, this thesis is aimed at these two targets. Both of these targets have been addressed by using novel approaches of application of solvent annealing (to improve charge transfer across the interfaces) and use of graphene in the active layer (to improve the*

*charge transfer across the bulk of the device). Using both of these approaches, the efficiencies of the solar cells have been improved significantly.*



## **1.1.Solar Cells**

With the demand of the global energy increased upto 15,500 TWh [1] and the significant reduction of the conventional sources like coal and petroleum used for the production of the energy for world consumption has led to switching over the renewable sources of energy. This switching is also significantly led in addition due to the global environmental problems created by the conventional sources of the energy. The most promising of such renewable sector of the energy is the solar energy which has been a continuous subject of attention as well as its practically economic implementation for harnessing the solar energy. This is achieved by the solar cell devices which convert the light photons of the solar spectrum incident on the surface of the earth into electric current. As a result major efforts have been put forward for the basic understanding of the functioning and development of the solar cells as well as technology development for commercialization of the solar cells on global scale. The significant progress made in the silicon industry also provided the necessary infrastructure for the large scale development of the solar cell devices. As the progress in the silicon industry scaled up, the efficiencies of the solar cells based on silicon also went up. The work in the silicon based solar cells began in 1959 in Bell Labs [2]. With initial efficiencies as low as 1%, with the development of the different generation of the solar cells, the efficiencies also enhanced upto 25.6% in few decades [3]. This was achievable with different structural changes in the architecture of the silicon solar cells that was achieved within this duration of the development of these solar cells. As India receives continuous supply of the incident sun radiation, the solar energy sector provides huge opportunity for harnessing solar energy for various applications.

## 1.2. Solar Energy Spectrum

The earth's surface receiving the spectrum of the sunlight is distributed into a range of the wavelengths, most of which falls under the electromagnetic spectrum. The solar spectral irradiance or spectral flux density is defined as energy per unit area per unit time transmitted by the sun and received at certain distance above the earth's surface. The solar spectrum is thus the plot between the solar spectral irradiance and the energy of the sunlight quantized for each photon ( $h\omega$ ) for different wavelength (defined as the product of Planck's constant,  $h$  and the frequency of the light,  $\omega$ ). This plot is shown in the Fig. 1.1. It can be seen from the solar spectrum plot that the most of the solar energy is concentrated at infrared range at 1.4 eV (340 THz, 880 nm).

The solar spectrum, however, varies in its values at the same wavelength for different distance above the earth surface as the solar energy received at these distances undergo significant changes due to the absorption by the various atmospheric compositional gases like nitrogen, oxygen, CO<sub>2</sub> and dust particles and other materials across the various layers of the atmosphere. These different energy distribution or solar spectrum at various distances above the earth's surface is thus dependent upon the mass of the air in the earth's atmosphere and thus defined accordingly. The air mass (AM) is defined as  $1/\cos(\alpha)$  with the angle of incidence  $\alpha$  measured to the vertical to the earth's surface and is actually the ratio of the actual path travelled by the sun light beam to the vertical distance between the top of the earth's atmosphere and earth's surface. The solar spectrum, AM 0 (Air Mass 0) is defined at the distance above the earth's atmosphere and is quantitatively given with an integral radiant flux of 1353 W/m<sup>2</sup>. Similarly the solar spectrum of AM 1 is defined at the earth's surface after the sun light beam has crossed vertically the earth's atmosphere. However, for using a global standardization, AM 1.5G

is defined as solar spectrum when the incident sun rays at an incidence angle of  $48^\circ$ . The integral radiant flux for AM 1.5G thus reduces down to  $1000 \text{ W/m}^2$ . This is the value that is taken into account for the standard characterization of the solar cells globally.

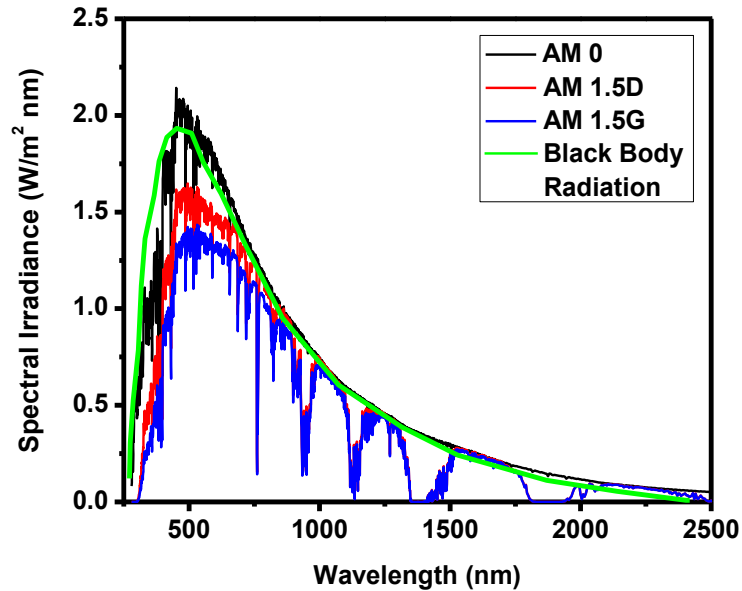


**Fig. 1.1.** Solar spectrum and spectral photon flux density as a function of the wavelength  $\lambda$  of incident photon (Data from ASTM) ASTM Reference Spectra.

<http://rredc.nrel.gov/solar/spectra/am1.5/ASTMG173/ASTMG173.html>).

### 1.3. Basic semiconductor physics of solar cells

The solar cell is a transducer which actually converts the incident sunlight energy into electric current. In all the different types of the solar cells, two types of materials – a donor and acceptor are sandwiched between the electrodes. The difference between the energy levels of these materials is defined as energy bandgap. In case of the silicon solar cells, the bandgap is defined as the difference between the valence band and the conduction band of the n-type and p-type semiconductor material while in the case of polymer solar cells the band gap is defined by the difference between the HOMO of the donor polymer and the LUMO of the acceptor fullerene

derivative. In any case, the photon is absorbed by the donor material and the energy of the photon ( $h\nu$ ) is used to excite the electron from HOMO/valence band to the LUMO/conduction band. This electron-hole pair is then dissociated across the donor/acceptor interface and through the electrodes is transferred to the external load circuitry.

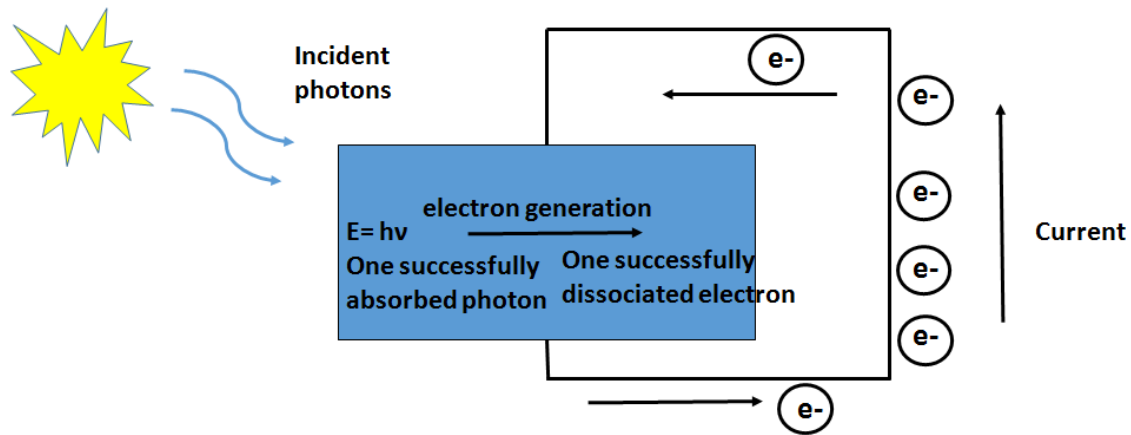


**Fig. 1.2** Charge generation in solar cell after the absorption of the light photons.

### 1.3.1. Fundamentals of parameters of solar cells

In order to quantitatively characterize the photovoltaic performance of the solar cells under the standard operating conditions like AM1.5G standard sunlight of  $100\text{mW}/\text{cm}^2$  also called as one sun, a set of parameters is defined to determine the current-voltage (IV) characterization. As can be seen in the Fig.1.3, the JV characteristic of the solar cells is identical to the diode curve in reverse bias.

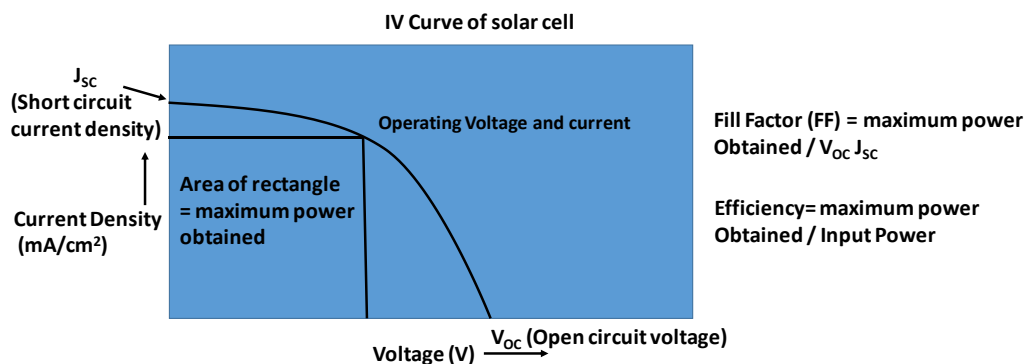


**Fig. 1.3.** Photovoltaic parameters of the solar cells.

The photovoltaic parameters of the solar cells under the current-voltage (JV) characterization are grouped as:

#### **1.3.1.1. Open circuit voltage ( $V_{OC}$ ):**

When no power is derived from the solar cell across the load, a maximum voltage is measured across the electrodes of the solar cells defined as the open circuit voltage. At open circuit configuration, the load resistance circuit is open.

#### **1.3.1.2. Short circuit current density ( $J_{SC}$ ):**

When the load resistance across the electrodes of the solar cells is ideally zero and the circuit is short circuit then a maximum current is measured through it defined as the short circuit current density.

#### **1.3.1.3. Fill Factor (FF):**

At the points open circuit voltage and short circuit current in the JV curve, the power generated is zero because either of the both parameters is zero at those points. However, at one of the points in the JV curve, the power obtained is maximum. Ideally, the power generated across the solar cell is equal to the product of the open circuit voltage and short circuit current. The fill factor is thus defined as the ratio of the maximum power obtained to the product of the open circuit voltage and short circuit current. The fill factor is a quantitative indicator of the effective charge transfer across the solar cell.

$$FF = P_{max}/(V_{OC} * J_{SC}) \quad (1.1)$$

#### **1.3.1.4. Efficiency ( $\eta$ ):**

The efficiency of the solar cell is defined percentage ratio of the maximum power per unit area of the solar cell obtained across it to the input power per unit area incident on it. In standard

conditions the efficiency is calculated under AM 1.5G standard input light intensity of  $100\text{mW}/\text{cm}^2$ .

$$\eta = P_{max}/P_{in} = (V_{oc} * J_{sc} * FF) / P_{in} \quad (1.2)$$

Apart from the JV characterization of the solar cells, the parameters for determining the photon absorption and the subsequent charge generation are defined in terms of the IPCE (Incident Photon to Current Conversion Efficiency) and QE (Quantum Efficiency). IPCE is defined as the ratio of number of the absorbed photons to the number of the incident photons while the QE is defined as the number of the charge carriers (electrons) generated to the number of the photons absorbed.

$$IPCE = \frac{\text{number of absorbed photons}}{\text{number of incident photons}} * 100 = 1240 \frac{\text{nm}}{\text{eV}} * \frac{J_{sc}}{\lambda(\text{nm}) * P_{in}} * 100 \quad (1.3)$$

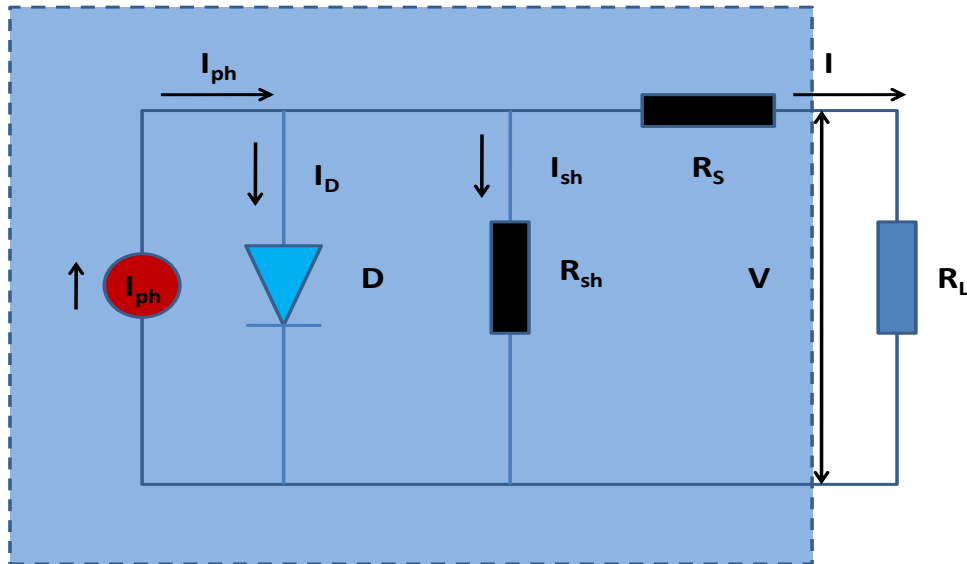


**Fig. 1.4.** Equivalent circuit model of a solar cell.

The current voltage characteristics of the solar cells can be understood using the equivalent circuit diagram (ECD) which can be used to determine the following key parameters of the solar cell.

- **Photocurrent:**

When the input light photons are incident upon the solar cell device then photo electrons are generated in the solar cell device which form an electric current through the device and is called as photocurrent ( $I_{ph}$ ) of the solar cell device. This current is dependent upon the intensity of the light incident on the solar cell and is generated by the dissociations of the excitons into electrons and holes.

- **Diode:**

The diode in the ECD represents the current voltage characteristics of the solar cell.

- **Series resistance:**

The series resistance ( $R_s$ ) represents the resistance to the charge carrier transport across the bulk of the device.

- **Shunt resistance ( $R_{sh}$ ):**

The shunt resistance represents the losses due to the leakage in the bulk and the interfaces of the solar cell device.

- **Load resistance:**

The load resistance ( $R_L$ ) represents the external load resistance across the solar cell device.

The current voltage characteristics of the solar cell can be fitted into the diode equation to obtain the parameters of the solar cells. The parameters obtained from the diode model fitting can then be used to determine factors like charge transfer, series and shunt resistance losses, photoelectron

generation and efficient conversion to current responsible for the reduction in the efficiency of the BHJ solar cells.

In general, the diode equation for the JV characteristics is given by:

$$I = \left( (I_{ph} - \frac{V}{R_{sh}}) / (1 + \frac{R_s}{R_{sh}}) \right) - I_0 / (1 + \frac{R_s}{R_{sh}}) \left( e^{\frac{V-IR_s}{nKT}} - 1 \right) \quad (1.4)$$

where  $I_0$  is the dark current and  $n$  is the diode ideality factor.

In order to fit the JV characteristics with the above diode equation, the series and the shunt resistance values are estimated from the JV characteristics. Under the assumption  $R_s \ll R_{sh}$ , the shunt resistance is calculated from the inverse of the slope of the JV characteristics at the zero bias voltage. At the higher bias voltages, the shunt resistance becomes smaller and can be neglected, the JV characteristics are linearly dependent upon the  $R_s$  and the  $R_s$  can be calculated by the inverse of the slope of the JV characteristics under the assumption that photocurrent is constant and independent of the bias voltage.

Thus, the series and the shunt resistance are given by:

$$R_{sh}(V \approx 0) = \left( \frac{dI}{dV} \right)^{-1} \quad (1.5)$$

$$R_s(V \approx V_{OC}) = \left( \frac{dI}{dV} \right)^{-1} \quad (1.6)$$

From the ECD, it can be seen that the shunt resistance is given by,

$$(I_{ph} - I_D - I)R_{sh} = V + IR_{sh} \quad (1.7)$$

$$I(1 + R_{sh}/R_s) = I_{ph} - I_D - V/R_{sh} \quad (1.8)$$

Using the diode equation given by

$$I_D = I_0 \left( e^{\frac{V-IR_s}{nKT}} - 1 \right) \quad (1.9)$$

Under the assumption that the series resistance is much smaller than the shunt resistance, the equation (1.4) can be modified into

$$I = I_{ph} - \frac{V}{R_{sh}} - I_0 \left( e^{\frac{V-IR_s}{nKT}} - 1 \right) \quad (1.10)$$

In order to take into account the effects of the series and the shunt resistance on the short circuit current and the open circuit voltage, the equation (1.4) can be thus modified under the short circuit condition into

$$I = - (I_{ph} - I_0 \left( e^{\frac{V-IR_s}{nKT}} - 1 \right) ) / \left( 1 + \frac{V}{R_{sh}} \right) \quad (1.11)$$

Thus, the short circuit current is mainly limited by the series resistance  $R_s$ , with higher series resistance leads to the lower current.

Similarly, under the open circuit voltage condition, the equation (1.4) can be thus modified into

$$V_{oc} = \frac{nKT}{e} \ln \left( \left( \frac{I_{ph} - V_{oc}/R_{sh}}{I_0} \right) + 1 \right) \quad (1.12)$$

Under the open circuit voltage condition, the open circuit voltage is nearly independent of the series resistance and increases linearly with decrease in the dark current. This increase in the open circuit voltage with the dark current is negligible. From the equation (1.12), it can be seen that the open circuit voltage increases by 0.058 V with a decrease of decade in the dark current.

#### **1.4. Generations of the solar cells**

The work on the solar cells began in 1959 in Bell Labs. With the subsequent work on it, various types of solar cells have been developed along the duration of its development. These different types of the solar cells are categorized into different generations according to the types of the

materials that are used for their fabrication, their processing technology, their architecture and their typical efficiencies.

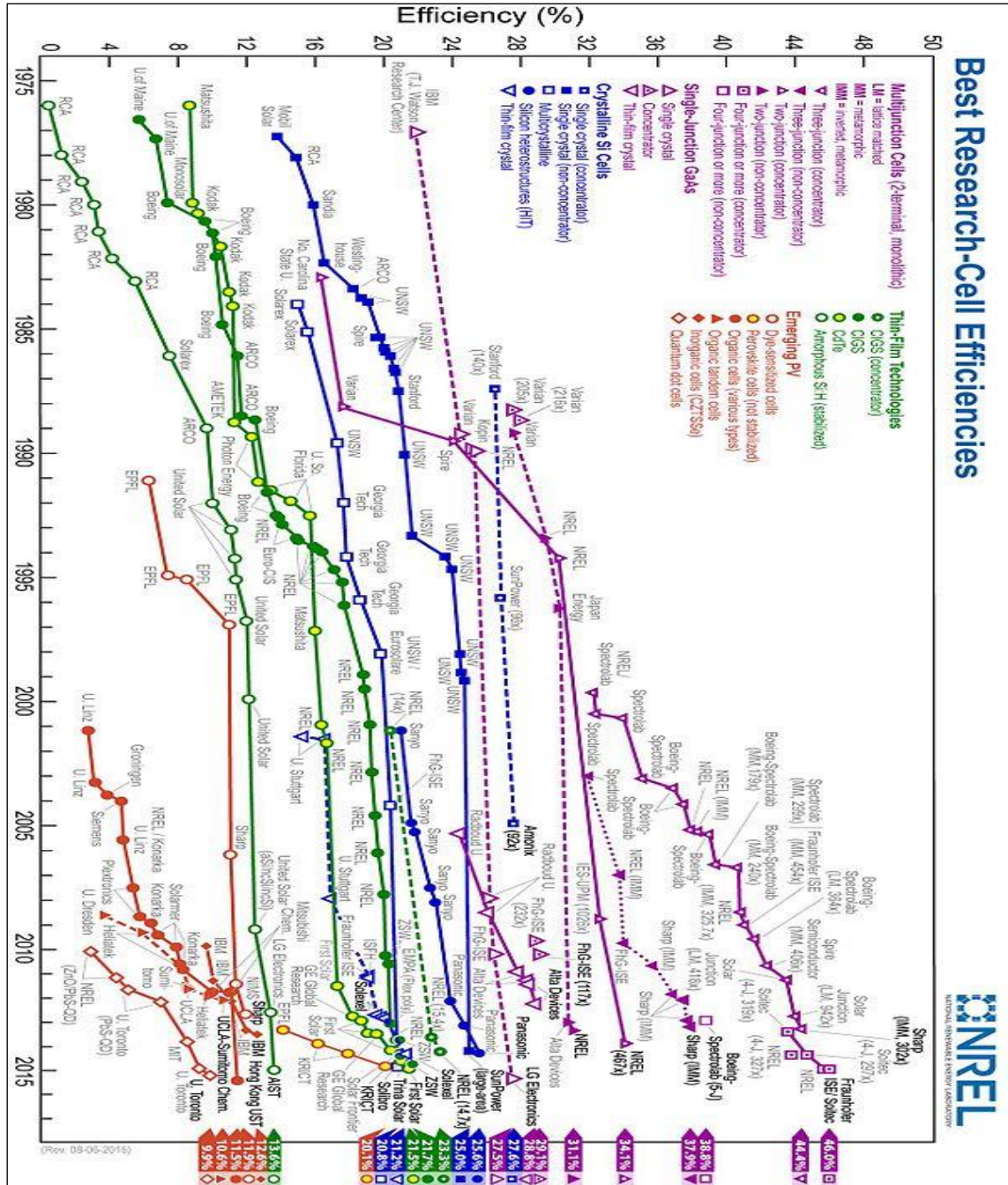
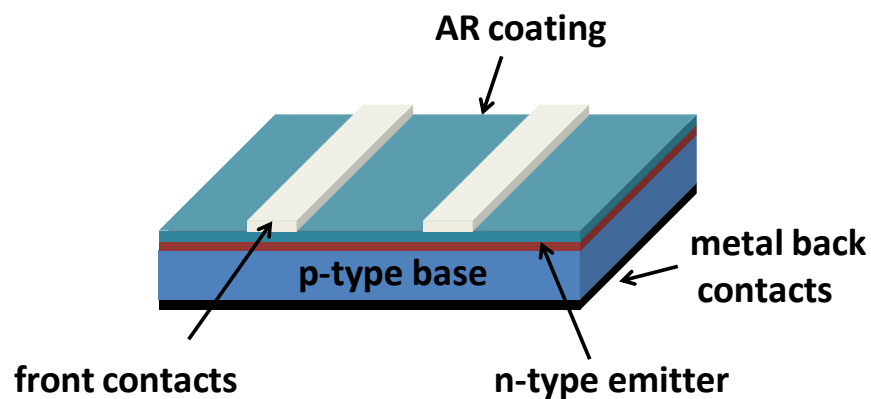


Fig. 1.5. Different generations of solar cells with reported efficiencies.

It can be seen from Fig. 1.5 showing the reported efficiencies of these different generations of the solar cells that efficiencies of the earlier generations of the solar cells of nearly 46% is much higher but even with the reported efficiencies are lower for the subsequent generations, these are been continually developed due to other potential advantages offered by these generations of the solar cells. The different types of these solar cells are categorized into following generations:

#### **1.4.1. First generation monocrystalline and amorphous Si (Silicon) based solar cells:**

Currently, the photovoltaic industry is based on the single junction monocrystalline and amorphous Si wafer based solar cells. These solar cells account for more than 92% of the total production by 2014 with the share of 56% by the multi crystalline solar cells. In this generation of solar cells, efficiencies of 34.1% in the single crystal Si solar cells and 46% with four and more junctions have been achieved. However, even with the higher efficiencies the first generation solar cells lack the advantages of flexibility, low cost of fabrication and fast processibility.



**Fig. 1.6.** Schematic of the first generation single crystal Si solar cell.

### 1.4.2. Second generation monocrystalline and amorphous Si (Silicon) based solar cells:

The second generation of the solar cells employ the use of thin films in order to remove the unnecessary materials during the fabrication of the solar cells. This has been done by depositing the thin layers of amorphous Si (a-Si), CuIn (Ga)Se<sub>2</sub> (CIS), CdTe, CdS and polycrystalline Si solar cells on the low cost glass substrates such as glass.

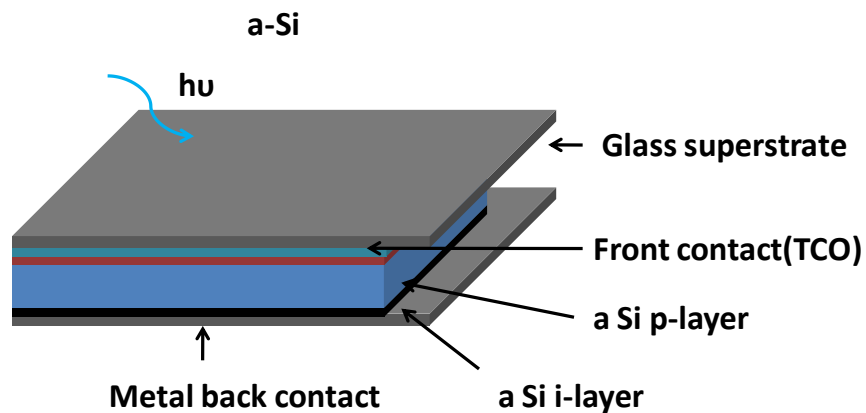
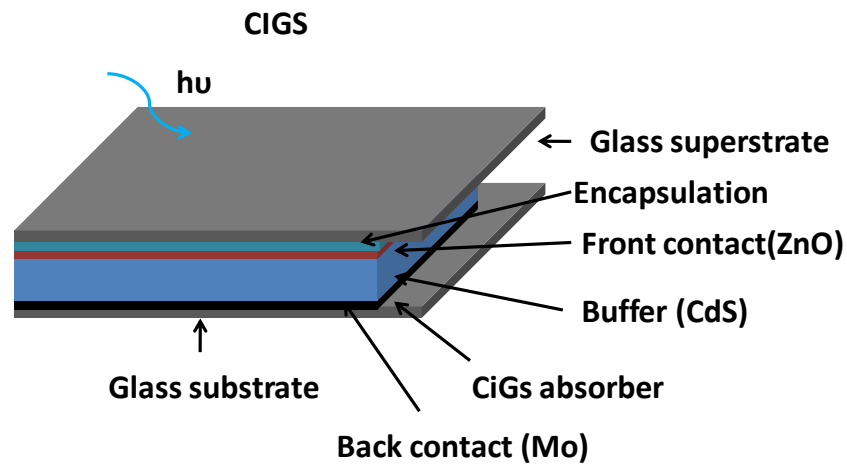
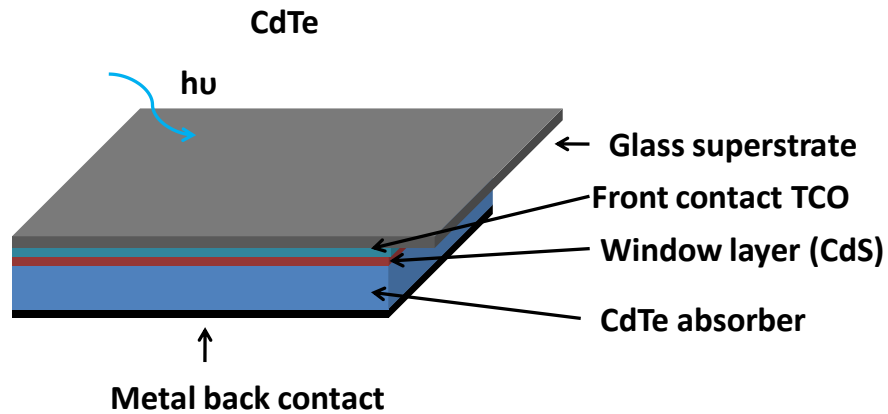


**Fig. 1.7.** Schematic of the second generation thin film CdTe, CiGS and a-Si solar cells.

These solar cells work on the principle that they absorb the solar spectrum more efficiently than the single crystalline and multicrystalline Si solar cells even at low thickness of less than 10 $\mu$ m of the thin films of these materials. The architecture of the solar cell consists of an absorber layer of the active material of CdTe, CiGs and a-Si on the top of which a buffer layer of CdS is deposited. These layers are sandwiched between the encapsulation layer at the top and the metal back contact layer at the bottom of the layers. This is further sandwiched between two layers of the glass substrates at the top and the bottom. The efficiencies with these devices have reached upto 16.5% with CdTe and 18.4% with CiGS. The solar cells based on CdTe, CdSe and GaAs are more efficient than their previous generation having efficiency of nearly 35% but are highly toxic in nature, during the fabrication and waste renewal.

#### **1.4.3. Third generation thin film organic solar cells:**

The inflexibility, high cost of fabrication, longer duration, complex fabrication processes of fabrication, lower power to area of coverage and toxicity has led to development of thin film polymer solar cells.

##### **1.4.3.1. Polymer solar cells**

With the advent of the conducting polymers synthesised in 1977 by Alan J. Heeger, Alan MacDiarmid and Hideki Shirakawa who reported high conductivity in oxidized iodine-doped polyacetylene, the application of the conducting polymers have been established in solar cells [4]. These solar cells based on the conducting polymers are known as polymer solar cells. A polymer solar cell consists of a donor conducting polymer in conjunction with a fullerene molecule which acts as acceptor for the electrons generated during the charge generation process in the solar cell. The donor polymer and the acceptor molecule are mixed together in a solvent to

be deposited as active layer material in the polymer solar cells. The details of the polymer solar cells are describes as below:

**a. Basic structure of the device:**

A typical polymer solar cell consists of a conducting polymer which acts the donor polymer and a fullerene derivative which acts an acceptor of the electrons from the exciton pair generated due to the absorption of the light photons.

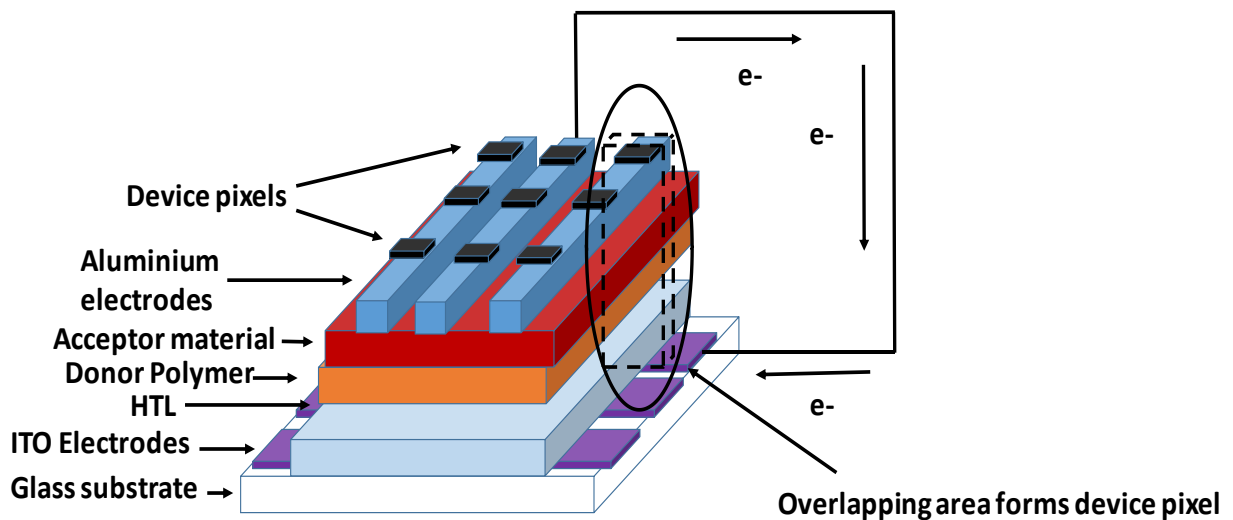


**Fig. 1.8.** Basic structure of polymer solar cell.

The donor polymer and the acceptor derivative form the active layer of the device and are sandwiched between the top layer of the aluminum electrode and the bottom layer of the HTL layer of PEDOT:PSS. The PEDOT:PSS layer is coated on the ITO coated glass substrate. The deposition of HTL and active layers of the device is done through the spin coating technique while the top aluminum layer is deposited through thermal evaporation technique. The details of the working principle of the polymer solar cells are described.

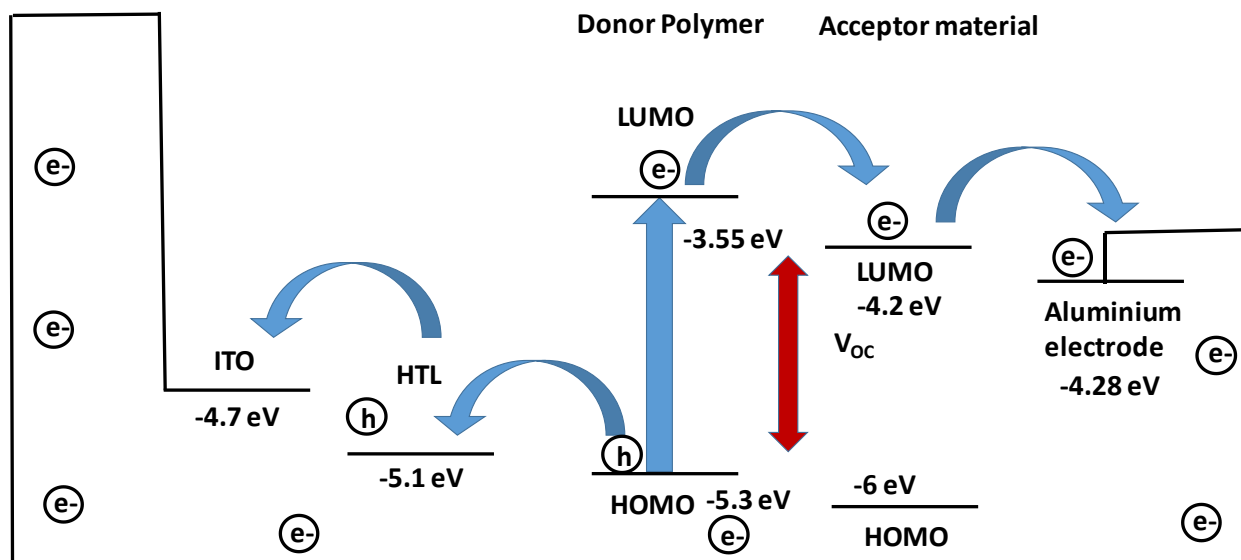


**Fig. 1.9.** Schematic representation underlying the working principle of polymer solar cell.

**b. Working principle:**

The polymer solar cells works on the principle of the exciton formation and its subsequent dissociation at the interface of the donor polymer and acceptor fullerene after the absorption of the photon in the donor polymer. The whole process of the charge carrier generation is divided into four steps:

- **Light absorption:**

The photons incident on the device are absorbed in the donor polymer area of the active layer of the device where the photon energy is used to create a hole-electron pair in the donor.

- **Exciton diffusion:**

The exciton pair created by the absorption of the photon then moves towards the donor/acceptor interface. The hole and the electron in the exciton pair are bounded strongly to each other by the Coulomb force due to the low dielectric constant of donor polymer and have low screening length. The movement of the excitons is due to the diffusion of the excitons towards the interface.

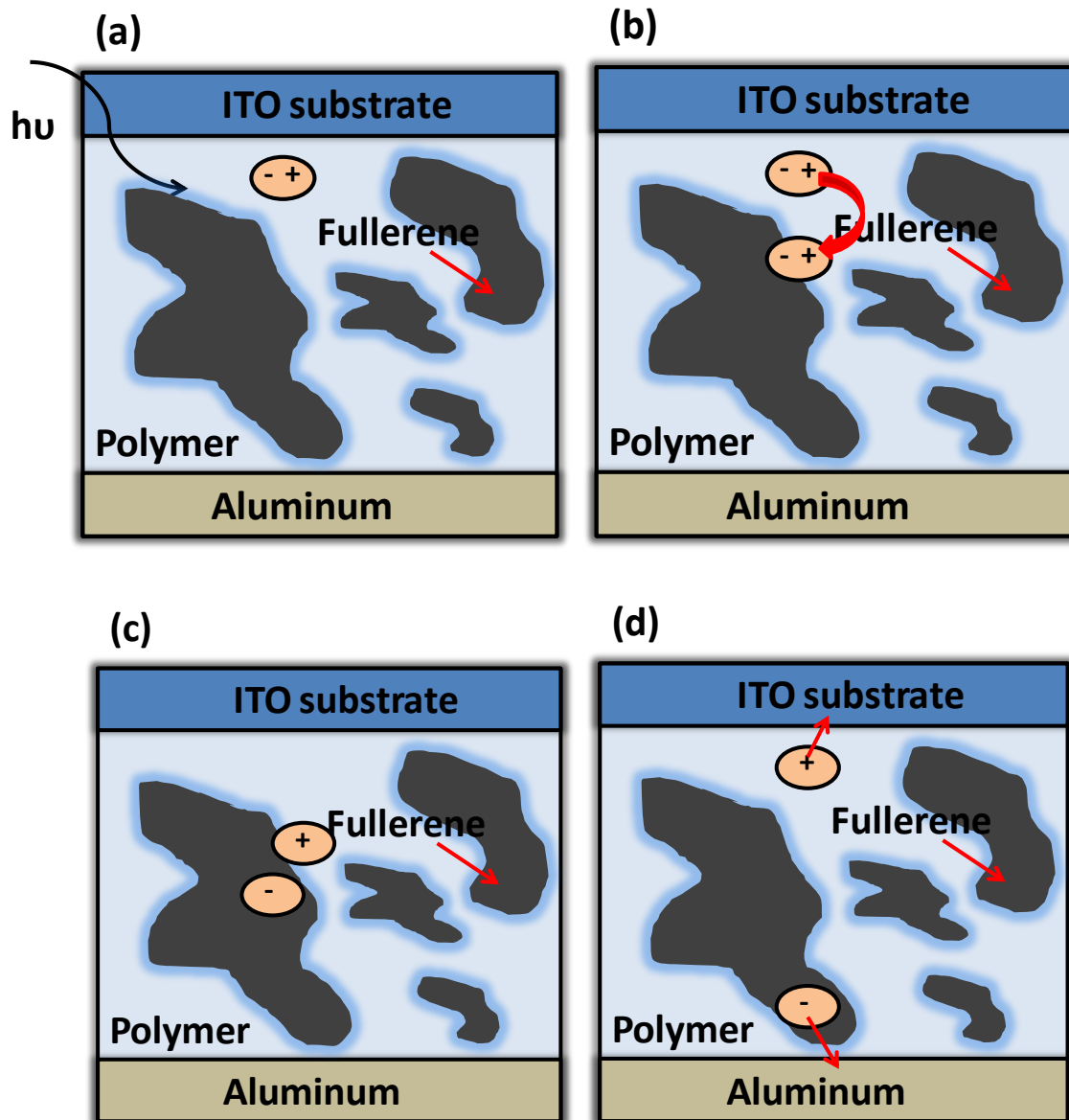


**Fig. 1.10.** Charge carrier generation in polymer solar cell.

- **Exciton dissociation:**

The exciton pair undergoes dissociation at the interface of the donor polymer and the acceptor which is governed by the energetically favorable interface of the donor/acceptor interface. The dissociation is carried out when the difference between the LUMO levels of the donor/acceptor is higher than exciton binding energy. The exciton pair remains bounded and are known as the geminate or polaron pair.

- **Charge transfer to electrodes:**

The charge transfer mechanism, of both holes and electrons in the solar cell is governed by the hopping mechanism, however, with a very low charge mobility which is less than by a factor of 1000 as compared to the crystalline silicon. The geminate pair of the charge is dissociated by the built in potential of the two electrodes and under the influence of the electric field, the charge carriers move towards both the electrodes. The hopping mechanism is thus a slow charge transfer process and is accompanied by a number of losses. These loss mechanisms are further classified as: exciton decay, geminate recombination of the hole-electron pair and bimolecular recombination of the free charge carriers.

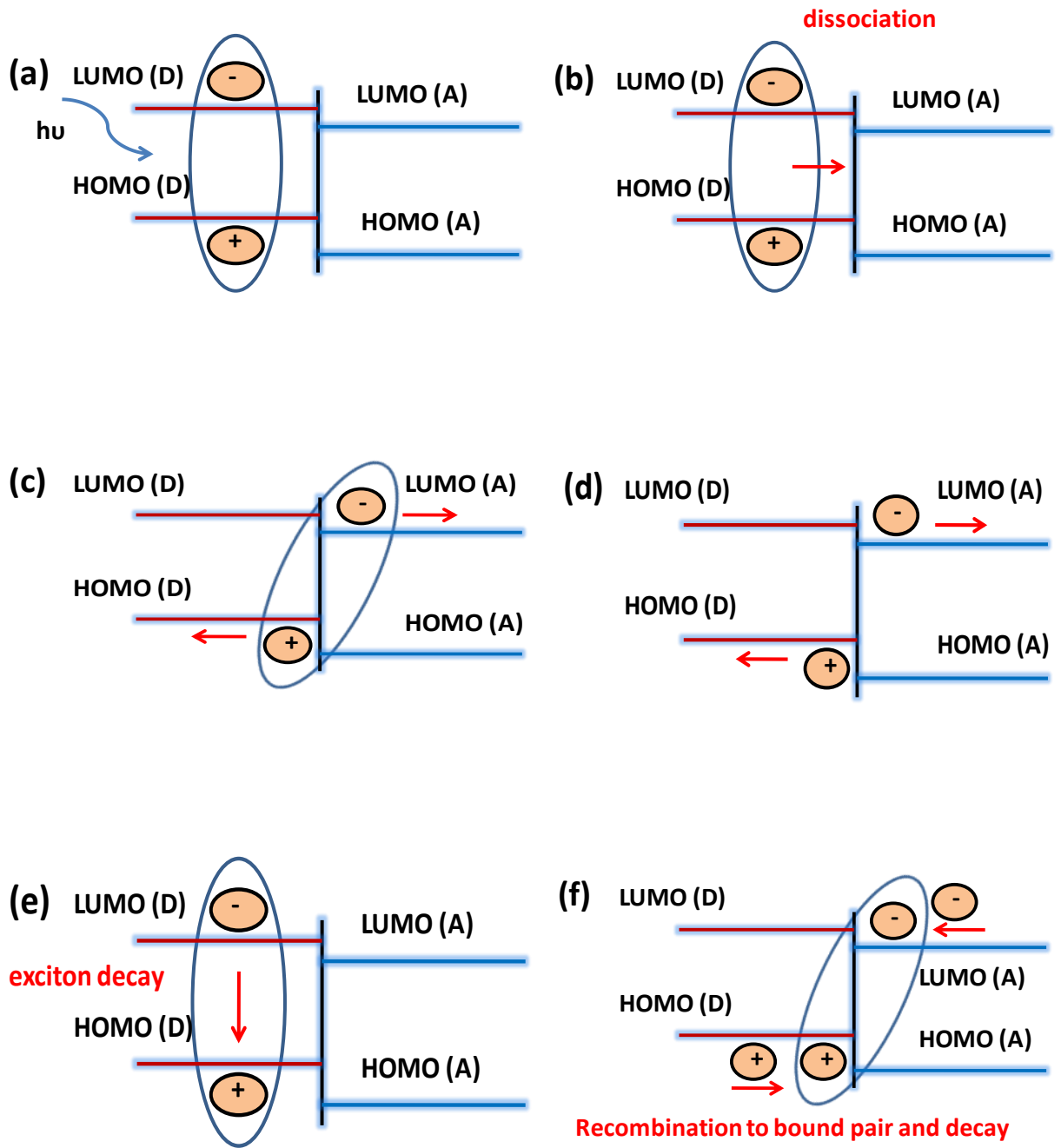


**Fig. 1.11.** Charge carrier diffusion and recombination in polymer solar cell.

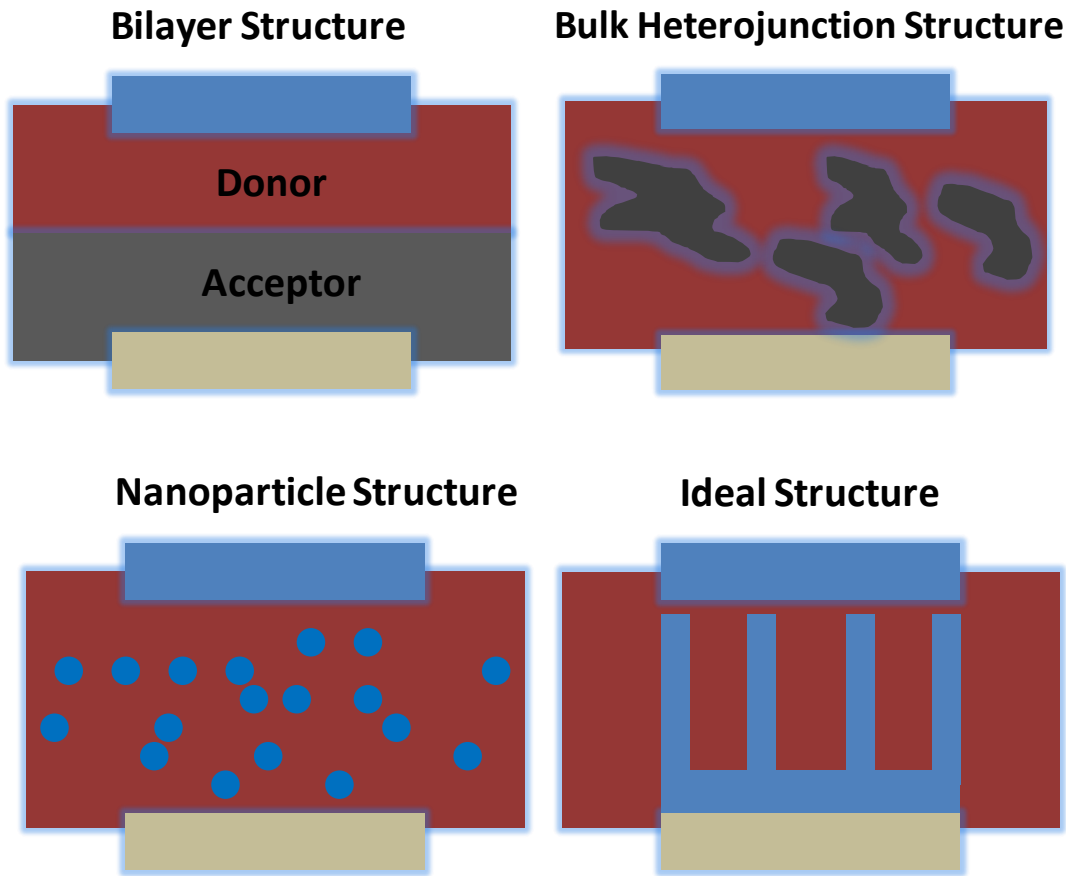


**Fig. 1.12.** Architecture of polymer solar cell.

### c. Architectures

The donor polymer and the acceptor fullerene derivative form the active layer of the polymer solar cells. In the bulk of the active layer the incident light photons are absorbed by the donor polymer and the excited electrons are dissociated at the interface of the donor and acceptor. However, for the effective dissociation of the electrons at the donor/acceptor interface the structure of the donor and acceptor in the bulk of the polymer solar cell must be fabricated. This has led to the development of the different architectures of the polymer solar cells with their advantages and disadvantages depending upon the factors governing the charge generation and

dissociation at the bulk of the active layer and the donor/acceptor interface. The different types of the polymer solar cell architectures are described as:

- **Bilayer Structure:**

This is the basic structure of the polymer solar cells in which a layer of acceptor derivative is deposited on the top of the donor polymer layer. The acceptor derivative and the donor polymer are dissolved separately in the same solvent and are then the donor polymer is deposited on the top of HTL after which the acceptor derivative is deposited on the top of the donor polymer layer. This architecture allows maximum absorption of the incident light photons as the maximum area and large bulk area of the donor polymer is exposed to the incident light photons. However, this architecture leads to the problems of charge recombination and ineffective charge dissociation. This is because when the excitons are generated in the donor polymer, the excitons have to move towards the donor/acceptor interface for effective dissociation at the interface. However, the recombination length for the excitons in the polymer solar cells is of order of 10nm which is very less than the deposited thickness of the donor polymer layer which of order of more than 100nm. This leads to the recombination of more number of generated excitons in the donor polymer layer before the effective dissociation at the donor/acceptor interface. This leads to the generation of effectively less number of the charge carriers which leads to less current across the electrodes. In addition, the ratio of the area of the donor/acceptor interface to the volume of the bulk of the donor polymer layer is less which leads to less number of the excitons dissociation at the donor/acceptor interface which leads to less current across the electrodes.

- **Bulk Heterojunction Structure:**

In order to overcome the problems of the ineffective exciton dissociation in case of the bilayer structure, the bulk heterojunction structure was developed. In BHJ structure, the donor

polymer and the acceptor derivative are mixed in a solvent to form the active layer solution. This solution is then deposited on the top of the HTL layer to form the active layer of the polymer solar cell. The BHJ structure overcomes the problems of the exciton dissociation in two ways. Since the donor polymer and the acceptor derivative are dissolved in the same solvent, the interface area of the donor polymer and the acceptor derivative is significantly increased as compared to that of bilayer structure. Also the donor polymer area in the BHJ are smaller in size and are distributed throughout the bulk of the active layer therefore the effective length to reach to the donor/acceptor interface is less as compared to that of bilayer structure and is even less than the recombination length which is of order of 10nm. Thus due to the more donor/acceptor interface area and less charge carrier distance, the exciton dissociation is significantly increased at the donor/acceptor interface which leads to the generation of the higher current across the electrodes of the polymer solar cells. However with these advantages of the BHJ structure, the absorption of the incident light photons is less as compared to that of the bilayer structure due to less bulk of the donor polymer exposed to the incident light photons for the absorption of the light photons. Also the area of the contact between the acceptor fullerene in the bulk of the active layer with the aluminum electrode is significantly less as compared to that of the bilayer structure which leads to the less number of the electrons transferred to the aluminum electrode and thus less generation of the current across the electrodes.

- **Nanoparticle Structure:**

In this structure, the donor polymer is introduced in the bulk of the active layer in the form of nanoparticles in order to overcome the problems in the bulk heterojunction architecture. Both the donor/acceptor interface area and the charge carrier distance are increased significantly as compared to the bulk heterojunction architecture which significantly increased the charge

dissociation at the donor/acceptor interface. This leads to overall increase in the current across the electrodes. This structure also overcomes the problem of the less area of the contact between the acceptor fullerene derivative and the aluminum electrodes as most of the acceptor derivative forms the bulk of the active layer and thus the contact area between the fullerene derivative and the aluminum electrode is larger as compared to that of the bulk heterojunction architecture. However, in this structure due to small size of the donor polymer in the form of nanoparticles the volume of the donor polymer for the absorption of the incident light photons is significantly less as compared to the bulk heterojunction structure. This leads to the less generation of then excitons in the donor polymer and thus less current across the electrodes.

- **Ideal Structure:**

In this structure, the acceptor derivative is deposited in the form of nanorod structure in the bulk of the active layer. The donor polymer forms most of the bulk of the active layer and is deposited on the top of the rod structure of the acceptor derivative. The acceptor derivative layer is deposited on the top of the HTL layer over the top of which the nanorod structure of the acceptor derivative is grown. This structure overcomes the problems of the bulk heterojunction architecture as both the donor/acceptor interface area and the charge carrier distance is significantly increased in this structure. This structure also overcomes the problem of the less volume of the donor polymer for absorption of the incident light photons as the volume of the donor polymer is also larger as compared to that of the bulk heterojunction structure. The area of the contact between the acceptor derivative and the aluminum electrodes is also larger which increases higher current across the electrodes.

## 1.5. Literature survey

The polymers solar cells have emerged as the potential source for the energy requirements because of the various advantages of flexibility, low cost of fabrication and fast processibility as compared to the silicon based solar cells. However even with these promising advantages, the polymer solar cells lack comparable higher efficiencies compared to the silicon solar cells. For polymer solar cells a world record of 12% efficiency has been reported by HS. Rohr. Heliatek Press Release, <http://www.heliatek.com> [5]. In addition to the problems of low efficiencies, the polymer solar cells also suffer from the problems of the stability and degradation. The problem of the lower efficiencies in the polymer solar cells has been attributed to the different issues related to the factors like device architecture, materials used for the fabrication of the solar cells including the properties like molecular weight of the donor polymer, purity of the materials, energy level alignments of the these material and band gap of the materials and the processing parameters and conditions like thickness of the various layers, thermal and solvent annealing treatment and duration of the treatments during the fabrication of the solar cells. The stability and the degradation of the polymer solar cells during the period of their operation has been attributed to the material properties which make them prone to undergo structural changes after reaction with the ambient oxygen and moisture when they are exposed to them. Different types of conjugated polymers and fullerene derivatives have been reported to be used as donor and acceptor type material with varying range of the efficiencies obtained with them [6]. Some of these materials are PTPTB, copolymer PFDTBT, PEOPT:PCBM and MDMO-PPV [6]. The absorption spectrum of the polymer solar cells depends upon the bandgap which is difference between the HOMO of the donor polymer and the LUMO of the acceptor material while the open circuit voltage depends upon the HOMO level of the donor polymer. Thus higher energy

solar spectrum is absorbed by the donor type polymer with a lower band gap and the open circuit voltage is higher for the deeper lying HOMO levels of the donor polymer as shown in the Fig. 1.13. But for a deeper lying HOMO level and lower band gap, the LUMO level of the donor material is also reduced which leads to the mismatch of the energy levels alignments at the donor/acceptor interface for the efficient dissociation of the charge carriers at the interface. Thus the band gap as well as the HOMO level of the polymer solar cells must optimized in order to obtain improvement of the efficiency in the polymer solar cells. In case of PEOPT even with a tunable bandgap (2.1 to 1.75 eV) depending upon the non-ordered to ordered phase, the reported efficiency achieved has been 0.02% [7]. The PEOPT polymers are categorized under the polythiophenes type conjugated polymer. In order to achieve higher energy solar spectrum absorption, a conjugated electron rich donor polymer PTPTB was introduced with a lower band gap of 1.7 eV. With a lower band gap of 1.7 eV, the peaks of the spectral photocurrents have been obtained at absorption maximum of 600 nm and increased contributions upto 750 nm which resulted in an increased IPCE. However even with lower bandgap, the efficiency reported with PTPTB polymer is around 1% [6]. However, with band gap tunability other factors like external quantum efficiency and the absorption band of the donor polymer is also taken into account for further improvement in the efficiency. Another polyfluorene copolymer PFDTBT was synthesized with an absorption onset around 650 nm which is higher than that of other polymers. Even with a larger bandgap, higher fill factor of 46%, higher open circuit voltage of more than 1V and higher efficiency of 2.2% has been reported with PFDTBT.

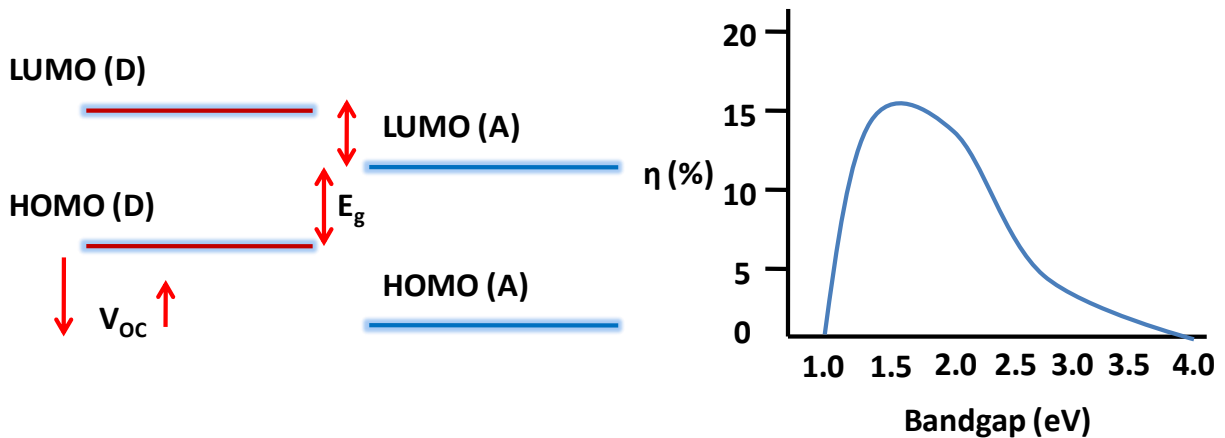


**Fig. 1.13.** Variation in the efficiency with bandgap of polymer solar cell.

In order to overcome the problem of the higher bandgap in the donor polymer materials and the thermal losses of the photons between the bandgap and open circuit voltage, tandem device architecture has been developed which also enhances the absorption of the solar spectrum for improvement in the efficiency of the solar cells. With a tandem architecture of P3HT:ICBA/PDTP-DFBT:PC<sub>71</sub>BM, efficiency upto 10.6% has been achieved with two different donor/acceptor configurations of P3HT:ICBA and PDTP-DFBT:PC<sub>71</sub>BM deposited in tandem with each other [16]. This tandem structure enhances the absorption of the solar spectrum due to the different parts of the solar spectrum ranging from 400 to 900 nm are absorbed by both the polymers P3HT and PDTP-DFBT. With the same tandem structure using the thin films of ZnO nanoparticles in the architecture of PTB7-Th:PC<sub>71</sub>BM and ZnO/CPEs ICLs reported efficiency of 11.3% has been achieved [10]. This increment in the efficiency has been attributed to the total absorption of the solar spectrum by the tandem structure. In addition to the tandem structure, introduction of the electron transport layer has also been reported which leads to the enhancement of the charge transport with the reported efficiency of 9.2% [7]. However, similar range of efficiency of 9.94% has also been reported with the single junction devices [8]. This

was done by reducing the tail state density below the conduction band of the acceptor material using the donor polymer PTB7-Th having a deeper HOMO level of -5.22 eV and a lower optical bandgap of 1.6 eV. Similar efficiency of 10.08% has been reported with single junction polymer solar cell using a high mobility conjugate polymer PDVT-10 with mobility of  $8.2 \text{ cm}^2\text{V}^{-1}\text{s}^{-1}$  along with the donor polymer PBDTTT-EFT [11]. This has been attributed to the deeper lying HOMO levels of -5.28 eV and -5.24 eV of both polymers PDVT-10 and PBDTTT-EFT and more absorption of the solar spectrum by both the polymers. Table 1.1 indicates the huge variation in the efficiencies reported across the literature for the same as well as different materials under the same fabrication conditions. This clearly points towards the lack of the reproducibility of the efficiencies under similar conditions.

**Table 1.1.** Summary of efficiencies of different polymer BHJ solar cells.

<b>Donor Polymer</b>	<b>Architecture</b>	<b>Bandgap (eV)</b>	<b>Efficiency (%)</b>
PTPTB [6]	Single junction	1.7 - 2.1	1
PEOPT [6]	Single junction	1.75	0.02
PFDTBT [6]	Single junction	1.9	2
P3HT /PDTP-DFBT [9]	Tandem junction	1.24	10.6
PTB7-Th ZnO/CPEs [10]	Tandem junction	1.6	11.3
PDVT-10 PBDTTT-EFT [11]	Single junction	1.84	10.08
PCDTBT:PC <sub>70</sub> BM [12]	Single junction	1.8	7.20
PCDTBT/PC <sub>70</sub> BM [13]	Single junction	1.8	7.1

P3HT/PC <sub>61</sub> BM [14]	Single junction	2.1	4.24
PTB7 / PC <sub>70</sub> BM [15]	Single junction	1.6	8.67
PBDTP-DTBT/PC <sub>71</sub> BM [16]	Single junction	1.70	8.07
PTB7 / PC <sub>70</sub> BM [17]	Single junction	1.6	7.9
P3HT/PC <sub>61</sub> BM [17]	Single junction	2.1	4.24
P3HT/PC <sub>61</sub> BM [18]	Single junction	2.1	4.4
PCPDTBT:PC <sub>71</sub> BM [19]	Single junction	1.70	3.2
P3HT/PC <sub>61</sub> BM [20]	Single junction	2.1	2.8
P3HT/PC <sub>61</sub> BM [21]	Single junction	2.1	3.9
PCPDTBT:PC <sub>70</sub> BM [21]	Single junction	1.70	6.16
PCPDTBT:PC <sub>70</sub> BM [22]	Single junction	1.70	5.1
P3HT/PC <sub>61</sub> BM [21]	Single junction	2.1	3.37
P3HT/PC <sub>61</sub> BM [23]	Single junction	2.1	3.68
PCDTBT:PC <sub>70</sub> BM [24]	Single junction	1.8	6.1

However even with different techniques have been developed for the enhancement in the efficiencies of the polymer solar cells, the issues with the stability of these solar cells in the ambient atmosphere are not addressed with the same methodology. In order to prevent the degradation of the solar cells in the ambient atmosphere, the factors responsible for the degradation must be understood in detail. It has been reported that the materials used in the fabrication of the polymer solar cells undergo chemical interactions with the oxygen and moisture present in the ambient atmosphere [25]. These chemical interactions then produce structural changes in these materials which make them unsuitable for solar cells.<sup>25</sup> The

degradation of the solar cells has been further classified broadly into two types: chemical degradation and physical or mechanical degradation [25]. The chemical degradation of the materials occurs when the small amounts of the oxygen and moisture are diffused in the active layer of the solar cell. There are different ways in which the oxygen and the moisture can react with the active layer materials. It has been reported that the oxygen is converted into superoxides or hydrogen peroxides in the presence of the UV illumination which then react readily with these materials [25]. The path of the diffusion of the oxygen and moisture is occurs through the top aluminum electrode to the bottom ITO electrode [26]. This diffusion is possible through pinholes in the electrodes which form microscopic path to oxygen and moisture for diffusion into the active layer of the solar cell. The oxygen diffuses through the various layers of the solar cell and reacts with all the materials reaching to the ITO surface where it is accumulated on the interface between the ITO and the HTL of the solar cell. Apart from the degradation by the oxygen and moisture, the polymers used in the fabrication of the solar cells undergo photo-oxidation upon exposure to the incident light. In case of certain polymers it has been reported that there is formation of singlet oxygen after the energy transfer from the photo excited polymer to the adsorbed ground state oxygen molecules [27]. This singlet oxygen then reacts with polymer resulting in the degradation of the polymer [27]. The mechanism by which the oxygen and moisture react with the donor polymer is different for these polymers. In case of the donor polymer P3HT, it has been reported that oxygen reacts with P3HT to form charge transfer complexes which form the singlet oxygen when these charge transfer complexes are dissociated from the excited state [28]. It has also been reported that oxygen reacts with thiophenes at the low temperature under irradiation to form thioozonides [28]. However at the room temperature the rate of the degradation of the polymer increases. The formation of these charge complexes is

a reversible and the formation of the metastable oxygen species which causes the irreversible degradation of the polymer. In addition to the degradation of the polymers in the solar cells, the PEDOT:PSS layer also undergoes degradation due to the reaction of PEDOT:PSS with other materials present in the solar cells. It has been found that the amount of PSS is higher as compared to the PEDOT in the PEDOT:PSS which diffuses into different layers and reacts with these layers of the solar cell [29]. This degradation is further increased by the formation of the phenolate in the PEDOT:PSS which further reacts with the PSS which results in the formation of PSS in the PEDOT:PSS. Apart from the degradation of the polymer material in the solar cell, the electrode materials are also prone to the degradation. The aluminum electrode deposited on the top of the active layer has been reported to undergo degradation after reaction with the active layer [25]. It has been reported that aluminum forms Al-C bonds after reaction with the donor polymer of the active layer [30]. The degradation of the aluminum electrode is also caused by the acceptor fullerene derivative PCBM which has high affinity for the electrons which makes them prone to react with the metal electrodes. This degradation of the aluminum electrodes occurs at the interface of the aluminum and the active layer and leads to the ineffective charge transfer across the interface of the aluminum and the active layer. In addition to the degradation of the aluminum electrode, the ITO electrode also undergoes chemical degradation after reaction with the HTL layer deposited on the top of the ITO electrodes. It has been reported that this reaction between the ITO and the PEDOT:PSS occurs due to the hygroscopic PSS which leads to the etching of the ITO layer and further increases the resistance of the ITO layer [31]. The other type of the degradation that the solar cells undergo is the mechanical degradation which includes the degradation of the device structure along with the morphological stability of the materials in the various layers of the device. The materials used in the fabrication of the solar cells undergo

morphological changes at the room temperature during the period of their operation. It has been reported that in case of the P3HT:PCBM solar cells, both P3HT and PCBM undergo a nanophase segregation due to the slow diffusion which leads to the change in the structure of the device [32]. This change in the nanostructure of the device leads to the degradation in the performance of the solar cell. However these changes in the device structure are dependent on the process and the method of the fabrication of the solar cells. This is because of the dependence of the device structure on the various parameters of the process of fabrication including materials used for fabrication, purity of the materials, concentration of the materials, ratio of the donor and acceptor, thickness of the layers deposited and annealing temperature of the device. It has been reported that this mechanical degradation can be prevented by optimizing the device architecture in order to improve the morphological stability of the materials in the solar cells [25]. However, the device performance is not only reduced by the chemical and the mechanical degradation of the device but is also dependent upon several other factors. The different mechanisms of these processes are reported for the different device structures and materials [23]. One of the factors responsible for the reduced performance of the polymer solar cells is ineffective charge transfer across the interfaces between the various layers of the device. This ineffective charge transfer reduces the device parameters like open circuit voltage, short circuit current density and the fill factor and thus the efficiency of the device. This ineffective charge transfer is governed by the quality of various interfaces between the layers of the solar cell. The charge transfer across the interface occurs due to the built-in voltage developed between the interfaces of the layers of the solar cell. The built-in voltage drives photogenerated holes to anode and electrons to cathode. Appearance of an S-kink in the J-V characteristics is well established that strongly reduces the fill factors (FF) and hence the efficiency of the BHJ solar cell. S-kink has been observed in many

of the organic BHJ devices and has been attributed to interface morphology as well as mismatched injection and extraction barriers across the interface [45, 50]. Apart from poor quality of the interfaces, other factors responsible for the appearance of S-kink include oxygen doping, presence of organic impurities, vertical phase segregation, reduced surface recombination, formation of charge dipole etc.

It has been shown that BHJ devices based on PCDTBT and PCBM exhibit S-kinks when annealed at moderate temperatures of 100°C for few hours, and similar results have been obtained by others [58]. The spectroscopic studies have shown that the properties of the PCDTBT:PCBM active layer almost remained unaffected at such a low annealing temperatures, [58] and therefore, the appearance of S-kink could be associated with the degradation of interfaces. Therefore, preparation of high-quality BHJ solar cells requires robust characterization to ensure that key physical parameters, such as, layer thickness, interfacial quality, and density are well controlled.

### **1.6. Objectives of the present thesis**

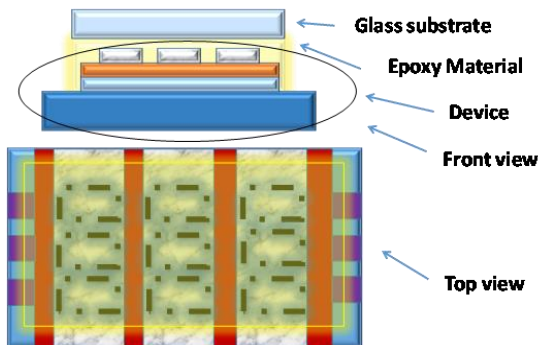
It can thus be seen that even with the development of different materials for the fabrication of the polymer solar cells, architectures and techniques to improve the efficiency of the polymer solar cells, these solar cells show a large variation in the reported efficiencies and lack reproducibility of these efficiencies under the similar fabrication conditions. In addition, one of the key challenges of the polymer solar cells is the chemical and morphological stability over the period of the operation of these solar cells. The various factors control the morphology of the interfaces between the various layers and bulk of the layers which is responsible for the ineffective charge transfer across the interface and bulk of the devices. This inefficient charge transfer is responsible for the lower efficiency in the polymer solar cells. Even with the techniques of

encapsulation of the devices, the diffusion of the ambient oxygen and moisture into the device layers cannot be effectively prevented through the encapsulation of the device. Keeping all the above mentioned issues in view, this thesis thus aims at;

- The development of BHJ polymer solar cells based on PCDTBT and P3HT donor polymers.
- Understanding the effects of factors like thickness of the layers in the solar cells, nature of the interfaces and morphology on the low efficiency in BHJs,
- Adoption of the novel techniques for the improvement of the efficiency and
- Investigation of the stability of the developed solar cells under ambient condition over time.

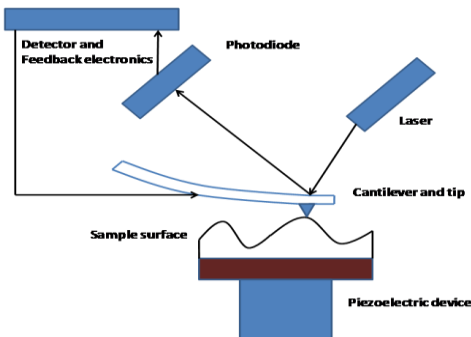
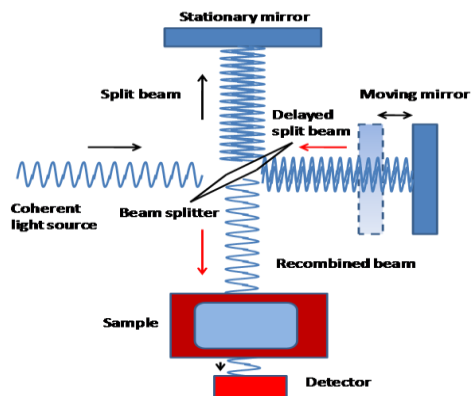
# Chapter 2

## Experimental Techniques



### Highlights

1. Introduction to the different types of the materials used for the fabrication of the polymer solar cells.
2. Introduction to the different types of the methods and their steps for the fabrication of the polymer solar cells.
3. Introduction to the different types of the instruments used in the fabrication steps of the polymer solar cells.
4. Introduction to the different types of the instruments used in the different types of the characterization of the polymer solar cells.



This chapter presents a number of materials and methods that have been employed for the fabrication of the polymer solar cells with different configurations (single/multi layers) and characterization tools and techniques for the measurement of the photovoltaic performance as well as other properties of the devices like surface morphology (roughness), thickness, roughness and electron density profiles etc. of the various constituent layers. A number of instruments that are used for the fabrication of the devices and the characterization of the BHJ solar cells are also described.

## **2.1. Materials used**

The key materials used for the fabrication of the BHJ solar cells are grouped into two categories

- (i) materials used for the fabrication of the operating device and
- (ii) materials used for the encapsulation of the operating devices.

These materials are described as follows:

### **2.1.1. Materials used for the device fabrication**

The materials which form the various constituent layers of the BHJ solar cells along with the base substrates on the top of which they are deposited are presented as:

#### **2.1.1.1. ITO base substrates:**

ITO glass consists of a thin layer of Tin doped Indium oxide, a conducting and transparent oxide material, on the top of a glass substrate. The ITO glass substrates used for the fabrication of the devices were purchased from Vision tek systems. Ltd U.K. The sheet resistivity of the ITO layer is 6- 12 ohm/sq with a transmittance of more than 80% at 550 nm, measured through the four probe technique and UV-Visible spectroscopy. The ITO substrate is actually a soda-lime-silica glass coated with two continuous layers of SiO<sub>2</sub>, acting as a barrier layer and an ITO layer of nearly thickness of 150 nm. These ITO coated glass substrates are having the roughness of 0.4

nm measured by atomic force microscopy thus making it suitable for the deposition of the subsequent layers of HTL and active layers with smooth morphology.

#### **2.1.1.2. PEDOT:PSS:**

The PEDOT:PSS to be deposited on the top of the ITO substrate acting as the HTL is directly purchased from the Ossila® U.K. of make Heraeus Clevios™ (PH 1000). The PEDOT:PSS solution is in the base of water and propanol solvents and is further filtered using 0.45 µm PTFE filter before its application for the device fabrication. The conductivity measurements done using the four probe method on the PEDOT:PSS films deposited on the top of ITO substrates have revealed the conductivity of the films to be of order of 100 S/cm. The UV-Visible spectroscopy measurements have shown the transmittance of the films of thickness 70 nm at 550nm to be more than 80%. The work function of the PEDOT:PSS was measured using Kelvin probe technique and has been found to be nearly 5.1 eV which lies between the HOMO of the ITO (4.7 eV) and HOMO of the donor polymer (5.3 eV) used in active layer. This energy level alignment favors the efficient charge transfer of holes across these layers, thus enhancing the device performance.

#### **2.1.1.3. Donor polymers:**

For the fabrication of the BHJ solar cells, two types of conducting polymers PCDTBT and P3HT were used as donor type material. The PCDTBT polymer of make M134 - R3 purchased from Ossila® with the average molecular weight  $M_w$ , of 36,700 Da (by weight fraction) purified through Soxhlet solvent purification was used. The other polymer P3HT of electronic grade was purchased from Sigma Aldrich having the average molecular weight  $M_n$  of 54-75 kDa, ultra high purity (less than 25 ppm of trace metals) and 98% regioregularity of the donor polymer.

#### **2.1.1.4. Acceptor Fullerene:**

For the acceptor material used in the active layer of the BHJ solar cells, PC<sub>71</sub>BM was used. The acceptor fullerene was purchased from the Sigma Aldrich. The acceptor fullerene is a derivative of the fullerene molecule and is functionalized further which enhances the solubility of the acceptor in the solvents for the preparation of active layer solution as well as the absorption of the light photons in the visible range.

#### **2.1.1.4. Aluminum:**

For the deposition of the anode metal top contacts for the extraction of the electrons from the active layer, aluminum material is used deposited through the thermal evaporation. The aluminum material is purchased from Sigma Aldrich and is having ultra purity of 99.99% of trace metals basis with high conductivity.

#### **2.1.2. Kelvin clips:**

For the JV characterization of the fabricated and encapsulated devices, gold coated Kelvin clips purchased from SynkeraTechnologies Ltd. were used. The clips are connected to the top and the bottom contact electrodes of the devices for measurements.

#### **2.1.3. Solvent materials:**

Different types of ultra high purity grade solvents for the cleaning of the ITO glass substrates and for the preparation of the active layer solution were used. For cleaning of the substrates methanol (anhydrous) and propanol (anhydrous) were used. For the preparation of the active layer solvents 1,2-dichloro benzene (anhydrous) and chloroform (anhydrous) were used. During the cleaning procedure of the ITO glass substrates a soap solution purchased from Hellmanex, ultra pure milli-Q deionized water and semiconductor grade solvents acetone and propanol were used.

#### **2.1.4. Materials used for the device encapsulation**

The devices fabricated inside the MBraun Glove Box are prone to degradation by the oxygen and moisture present in the ambient environment. Thus for the encapsulation of these devices, an epoxy sealant material purchased from Ossila® is used.

### **2.2. Fabrication of BHJ solar cells**

The fabrication of the BHJ solar cells requires a number of steps along with instruments used in these different steps. The different types of the instruments used for the fabrication of the devices are described as follows:

#### **2.2.1. MBraunglove box**

The materials used for the fabrication of the BHJ solar cells are prone to the degradation by the oxygen and the moisture present in the ambient environment. This requires the fabrication of the BHJ solar cells inside MBraunglove box with an inert atmosphere of less than 0.1 ppm of oxygen and water. All the fabrication steps of the BHJ solar cells as well as the sealing of the devices are carried out inside the glove box. The MBraunglove box consists of two boxes – box 1 which consists of a spin coater (Delta6 BM/TT, SussMicrotec Lithography GmbH) used for the deposition of different layers of the HTL and active layer and box 2 which consists of a thermal evaporator (BOC Edwards Inc.) for the deposition of the top layer of aluminum electrode. The inert atmosphere inside the glove box is maintained through the circulation of a gas between the glove box and gas purifier system. The gas removes the oxygen and moisture inside the glove box and is circulated to the gas purifier system where the oxygen and the moisture are absorbed by the reactive reagent. The encapsulation of the solar cell devices is also carried out inside the glove box for the further measurements of JV characterization.

### **2.2.2. Fabrication steps**

For the fabrication of the BHJ solar cells two types of donor polymers were used: PCDTBT and P3HT. The fabrication steps for both of these types of solar cells remain same, however, for the procedure steps like thermal annealing for the improvement in the photovoltaic performance of the solar cells vary in both cases. The polymer solar cells fabrication followed the device architecture of ITO/PEDOT:PSS/PCDTBT:PCBM/Al. All the fabrication steps were carried out inside the Glove Box. The fabrication steps are described as follows:

#### **2.2.2.1. Patterning**

ITO coated glass substrates were first cut into size of 2.5cm X 2.5cm. For the patterning procedure, thin adhesive stripes of 2 mm width and 2.5 cm length were masked onto the top surface of the substrates. These masked substrates were then put in the etchant solution of HCl:H<sub>2</sub>O:HNO<sub>3</sub> in ratio of 10:1:10 for 30 minutes. The etchant solution removes the unmasked ITP films from the surface of the substrates while the masked film stripes are obtained after patterning.

#### **2.2.2.2. Cleaning steps**

The patterned substrates are cleaned in various solvents to remove the impurities from the ITO substrates. The substrates are cleaned using the Hellmanex soap solution for 15 minutes through ultrasonication process. After this, the substrates are further cleaned using deionized water, acetone and propanol each for 15 minutes using the ultrasonication process. The substrates are dried under N<sub>2</sub> gas for further fabrication steps.

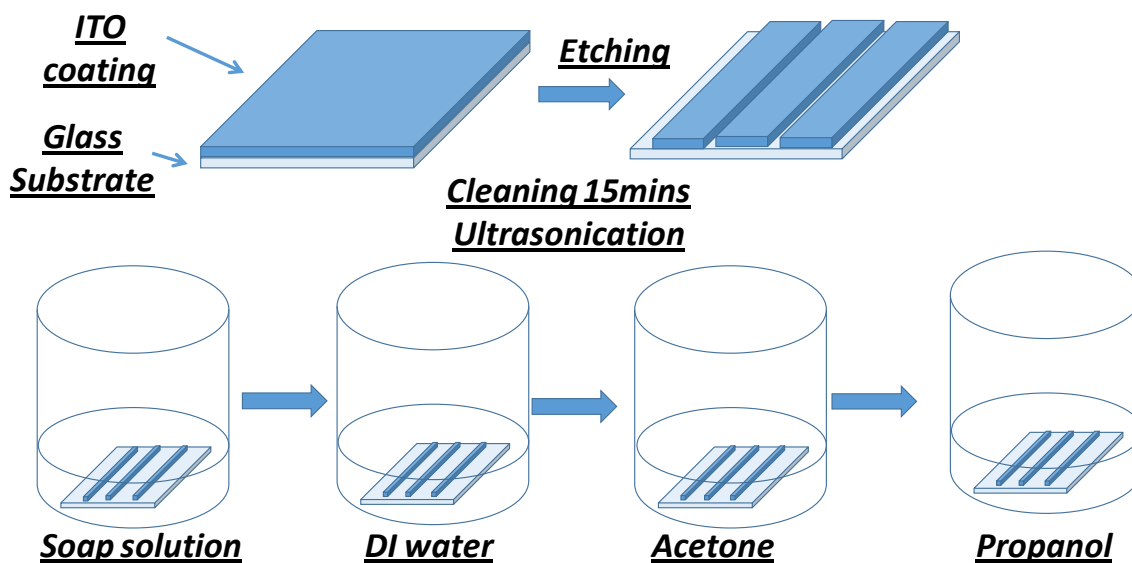


**Fig. 2.1.** Cleaning procedure of the ITO substrates.

### 2.2.2.3. Deposition of the PEDOT:PSS

The HTL layer of PEDOT:PSS is deposited on the top surface of the cleaned ITO substrates using the spin coating technique. The PEDOT:PSS used for the deposition is first filtered through the  $0.45\mu$  PTFE filter and is then deposited through spin coating with the thickness of 70 nm of the PEDOT:PSS layer. The substrates are then thermally annealed at the temperature of  $130^{\circ}\text{C}$  for 30 minutes.

### 2.2.2.4. Deposition of PCDTBT:PCBM

The PCDTBT:PCBM solution is first prepared in 1,2-dichlorobenzene or chloroform in a ratio of 1:4 with a concentration of 10 mg/ml. The solution is then left for stirring for 60 hrs after which it is filtered using  $0.25\mu$  PTFE filter.

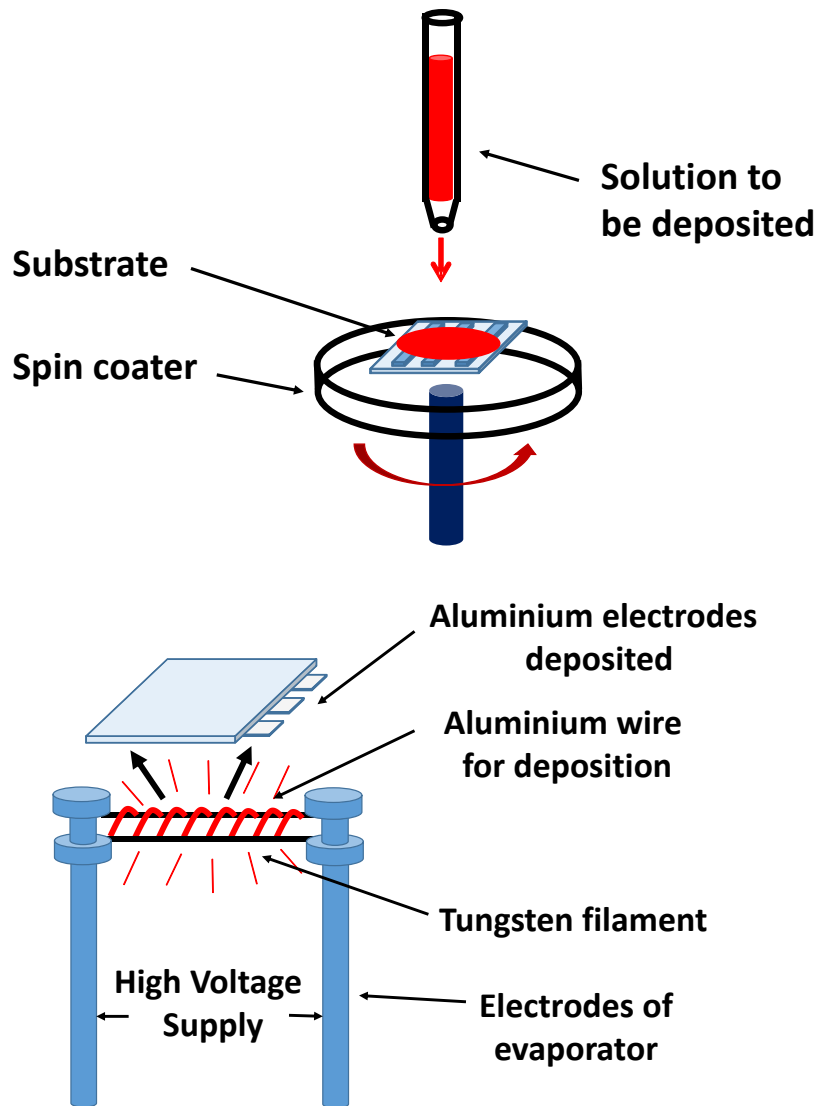


**Fig. 2.2.** Deposition of the PCDTBT:PCBM active layer and thermal evaporation of the aluminum electrodes.

The PCDTBT:PCBM solution is then deposited on the top of the PEDOT:PSS layer using spin coating with the thickness of 70 to 200 nm of the PCDTBT:PCBM.

#### 2.2.2.5. Deposition of Aluminum electrode

For the deposition of the aluminum electrodes, the PCDTBT:PCBM coated substrates are masked and using the thermal evaporation under the vacuum of  $10^{-6}$ Torr, aluminum electrodes

are deposited on the top of the PCDTBT:PCBM layer with the thickness of 100 nm. The device area of a solar cell on the substrate obtained is 4mm<sup>2</sup>.

### 2.2.2.6. Encapsulation of the solar cells device

After the aluminum electrodes are deposited on the top of the device, the encapsulation of these devices is carried out. The devices fabricated are characterized under one sun and are to be used for operation in the ambient environmental conditions. The materials used for the fabrication of the solar cells are prone to the degradation by the oxygen and moisture present in the environment, thus it is necessary to prevent the exposure of the device to the ambient oxygen and moisture through the encapsulation procedure. An epoxy material is dropped on the top surface of the device and is then covered and pressed with a thin glass plate to cover the surface of the device. The deposited epoxy material is then treated under UV light for 30 minutes which hardens the epoxy material and prevents the exposure of the device to the ambient environmental conditions.

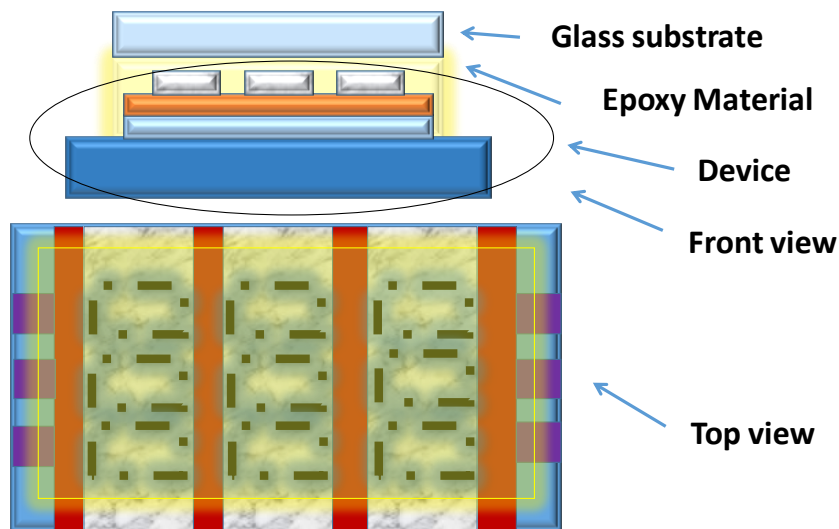


**Fig. 2.3.** Encapsulated polymer solar cell.

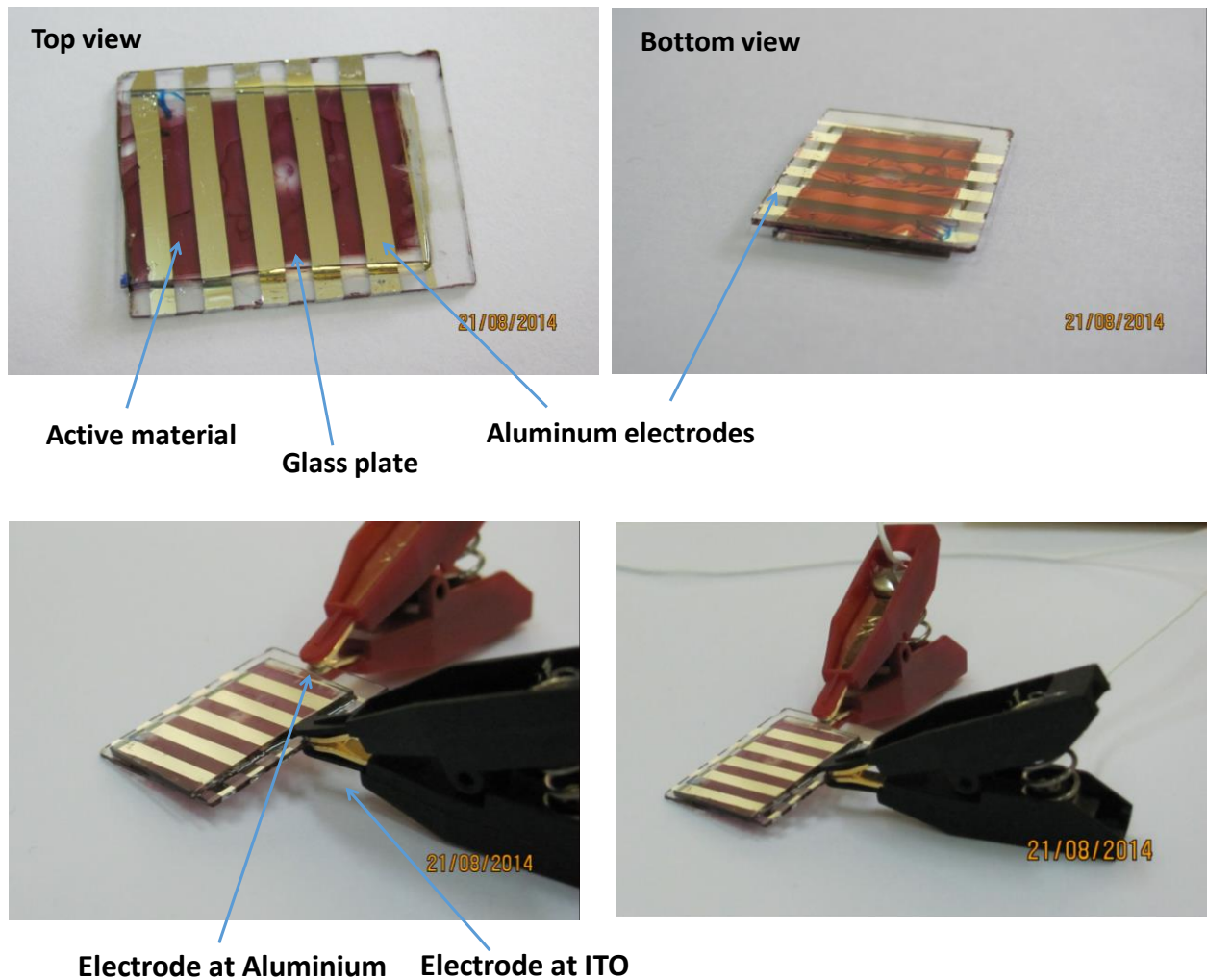


**Fig. 2.4.** Encapsulated PCDTBT:PCBM solar cells.

### 2.3. Characterization techniques

The different characterization techniques and tools used for the different types of the characterization of the solar cells are described as follows:

#### 2.3.1. UV-Visible spectroscopy

The molecules in any material undergo different types of transitions when energy is supplied to them. In order to determine the electronic transitions in the molecules which absorb the light in the UV-Visible spectrum of the electromagnetic spectrum a type of absorption/reflectance type

spectroscopy called as UV-Visible spectroscopy is used where a plot between the band of absorption or wavelength and the absorbance is recorded. The UV-Visible spectrophotometer instrument of Jasco V-530 make was used for the measurement of different data in various experiments:

1. The transmittance of ITO coated glass, PEDOT:PSS coated ITO glass, PCDTBT/PCBM/PCDTBT:PCBM coated ITO glass.
2. The absorbance of the conducting polymers, PCBM, active layer of PCDTBT:PCBM coated on the ITO substrates.
3. The thickness of the different layers of the PCDTBT:PCBM deposited through spin coating on the ITO substrates.
4. The direct band gap of the P3HT:graphene and PCBM:graphene after dissolving the P3HT and PCBM with graphene nanosheets.

### **2.3.2. Fourier Transform Infrared Spectroscopy**

In order to determine the vibrational transitions corresponding to the chemical bonds and the chemical functional groups that the molecules undergo when they are supplied the energy, Fourier Transform Infrared Spectroscopy is used. The FTIR generates an interferogram which is constructed between the interference pattern of the direct infra red beam from the source and each unit of the path difference the transmitted light has to undergo. This interferogram is further Fourier transformed to generate the plot between the spectrum of interference pattern and the wave number corresponding to different wavelengths of the infrared light from source ranging from  $400\text{ cm}^{-1}$  to  $4000\text{ cm}^{-1}$ . The FTIR spectrometer of Bruker Vertex 80 V at the resolution of  $4\text{ cm}^{-1}$  make was used for the recording the following data:

1. The change in the FTIR spectrum peaks of PCDTBT, PCBM and PCDTBT:PCBM films after annealing the films for 4, 8, 12, 16 and 20 hrs of annealing time, in order to determine the thermal stability of the polymer materials.
2. The change in the FTIR spectrum of unfiltered and filtered PEDOT:PSS films in order to determine the structural changes between the two types of the PEDOT:PSS.

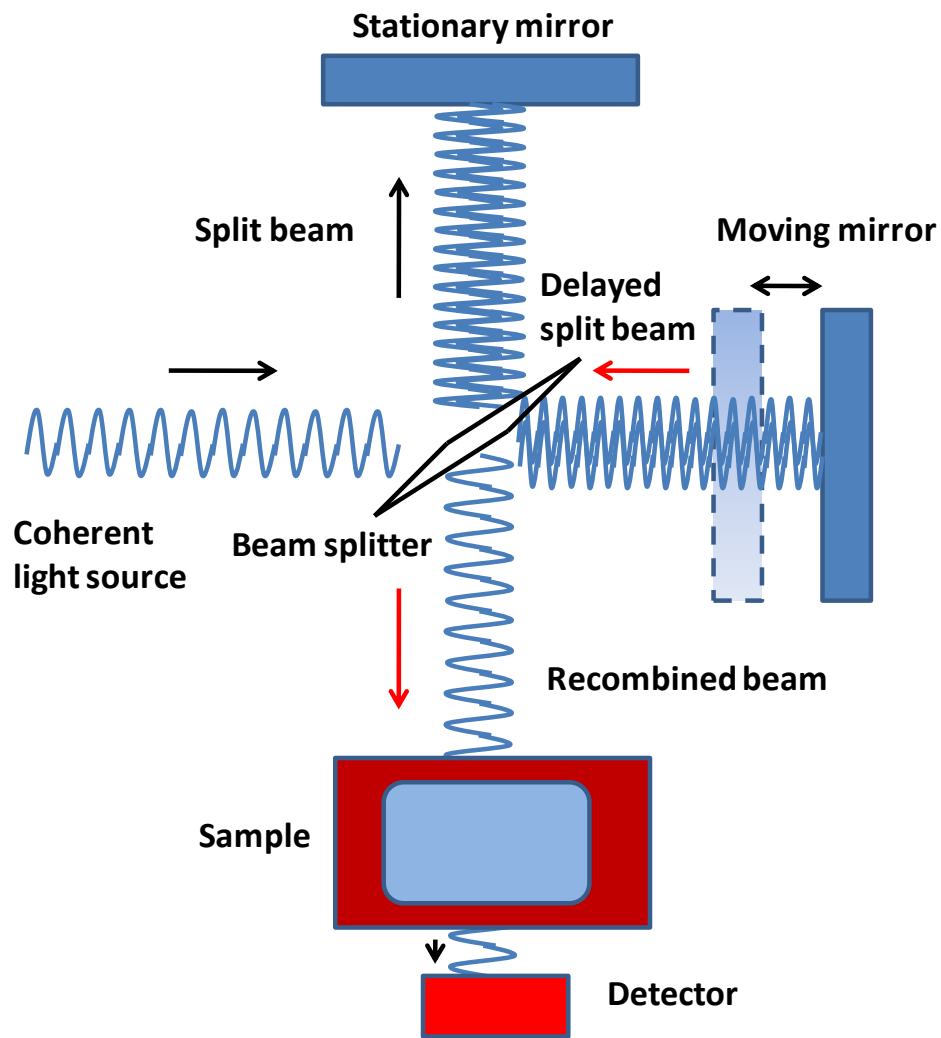


**Fig. 2.5.** Schematic representation of the FTIR spectrophotometer set up.

### **2.3.3. Atomic force microscopy**

For the morphological characterization of the thin films of the materials deposited, AFM was carried out using the Nanonics (Multiview 4000) atomic force microscopy. The AFM works on the principle where a probe consisting of a glass fiber tip of diameter 10 nm is moved on the top surface of the film and motion of the tip on the surface of the film is sent by a feedback to the controller for controlling the motion of the probe. This is done by using a piezoelectric crystal attached to tuning fork to which the tip of the probe is attached. The tuning fork oscillates at the resonance frequency of 25-50 kHz in the tapping mode. The scans of the AFM are recorded in the phase mode. According to the morphology of the surface of the film, the tip of the probe interacts with the surface and this interaction produced difference signal called as error signal. The error signal is then sent to the proportional - integral- differential (PID) controller, which further sends a feedback signal through a high piezo driver to make the constant phase and moves the piezo driver in x, y and z direction to generate a morphological image of the surface of the film. The AFM was used to determine the morphology and roughness of the surface of the ITO substrates, PEDOT:PSS films coated on the ITO substrates and P3HT, P3HT:PCBM and P3HT:PCBM:graphene films coated on the surface of the ITO substrates.

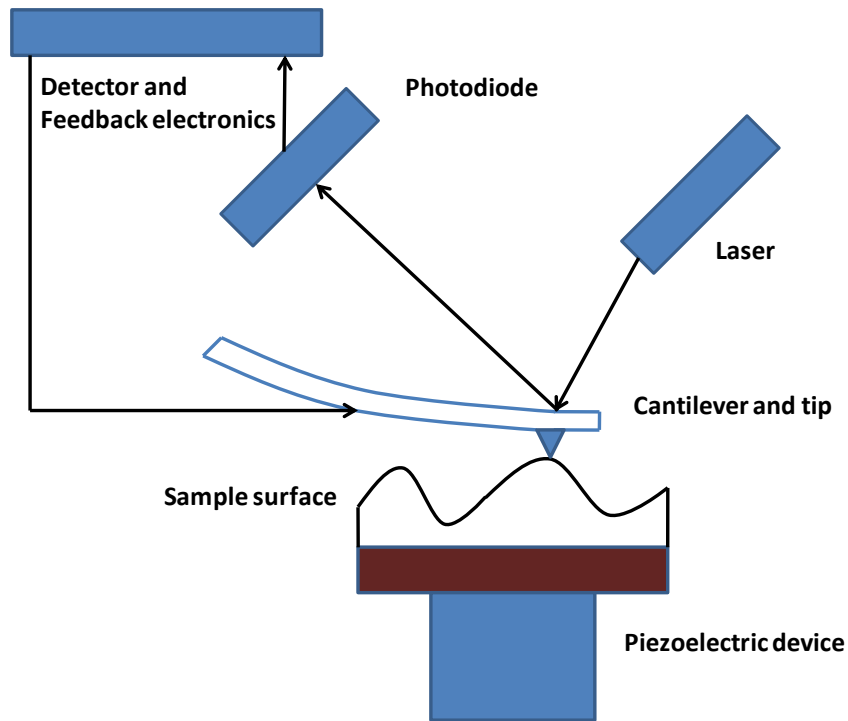


**Fig. 2.6.** Schematic representation of the Atomic Force Microscopy set up.

#### 2.3.4. Kelvin probe microscopy

The Kelvin probe microscopy technique is used to determine the work function of the materials deposited in the form of thin films on the surface of the substrates. The Kelvin probe technique consists of a gold coated tip mounted just above the surface of the sample kept at ground potential. The tip is oscillated at the frequency of 27 kHz. At a proximal distance above the sample the tip experiences an electric force, which is used to provide a feedback signal to determine the work function of the sample. The gold tip used for work function measurements has the diameter of 2 nm and the measurements are carried out at the room temperature. The Kelvin probe instrument of KP technology (SKP 5050) make was used to determine the work function of the filtered and the unfiltered PEDOT:PSS films deposited on the surface of the ITO substrates.

### **2.3.5. Raman spectroscopy**

In order to determine the structural information of the materials, Raman Spectroscopy was used. The Raman spectra was recorded for the thermally annealed films of PCDTBT:PCBM deposited on the ITO substrates, P3HT films and P3HT:PCBM:graphene films. The spectra were recorded in the 180° backscattering geometry using the Ar<sup>+</sup> laser (514 nm) as excitation source. The Raman spectrometer Jobin-Vyon (LabRAM HR 800) was used for recording the Raman spectra.

### **2.3.6. X-ray reflectometry**

The X-ray reflectometry is a non-destructive tool to determine the roughness, thickness, electron scattering length density and electron density of the various layers and thin films in the BHJ solar cell device. The XRR is based on the working principle that because of the refractive index of materials for the x-rays is less than 1, x-rays undergo total internal reflection when they enter the surface of a material at grazing angle. The x-ray beam from the source is made incident on the top surface of the BHJ device and the incident angle is varied after measurement of the total internal reflection intensity corresponding to this angle. The measurement of the total internal reflection intensity of the x-rays at the surface of the thin films provides the profile of the reflectivity patterns from the various layers of the BHJ solar cell device. This profile is a plot between the reflectivity and the incident angle of the x-ray. By fitting the reflectivity profile, the thickness, roughness and electron density of the various layers of the BHJ solar cell is calculated. The Rigaku MFM310 make instrument was used to carry out the XRR measurements on the various layers of the PCDTBT:PCBM solar cells to determine the thickness, roughness and electron density at the various layers.

### **2.3.7. X-ray photoelectron spectroscopy**

The X-ray photoelectron spectroscopy is a tool to measure the elemental composition at parts per thousand amounts, empirical formula, chemical state and electronic state of the elements composing a material. It is surface sensitive technique which is based on the principle that when high energy x-ray beam is made incident on the surface of a material, the photons of the x-ray knock out the electrons from the outer orbital of the elements composing the material. The energy of the photon is used in the ionization energy and the kinetic energy of the electrons of the elements. The ionization energy of the electrons of the elements is calculated by difference of the total energy of the incident photons of the x-ray beam and the measured kinetic energy of the electrons knocked out from the surface of the material. From the measured ionization energy and the number of the electrons, the corresponding element and its amount in the material is determined. The XPS measurements on the PEDOT:PSS films deposited on the surface of the ITO substrates are carried out using Mg K $\alpha$  source (RIBER MBE system). The binding energy scale was calibrated to the Au 4f<sub>7/2</sub> line of 83.95 eV. X-ray reflectivity (XRR) measurements were carried out using 18 kW rotating anode X-ray laboratory source with Cu K $\alpha$ -radiation (wavelength,  $\lambda = 1.542\text{\AA}$ ).

### **2.3.8. Photovoltaic characterization**

#### **2.3.8.1. Current-voltage characterization:**

The JV characteristics of the fabricated BHJ solar cells were carried out using solar simulator (Sciencetech Canada) under one sun (AM 1.5G) of the incident light. The measurements of the current and the voltage were carried out using the Keithley 2400 digital source meter and PARSTAT potentiostat/galvanostat. The solar simulator was calibrated using a standard silicon

solar cell before measurements. In some of the experiments, the JV characterization was carried out under the different intensities of the incident light.

#### **2.3.8.2. Incident photon to current conversion efficiency (IPCE):**

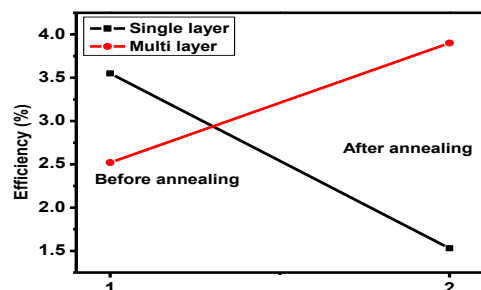
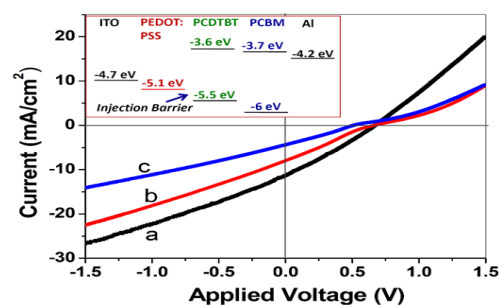
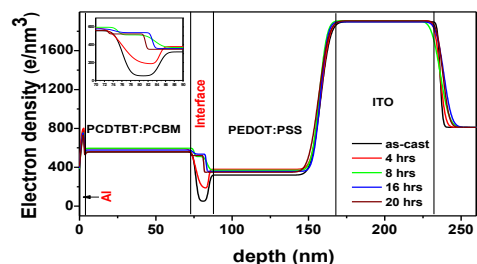
The measurement of the spectral response of the BHJ solar cells was carried out using solar simulator (Sciencetech Canada).

#### **2.3.8.3. Electrochemical impedance spectroscopy:**

The electrochemical impedance spectroscopy is carried out to measure the series resistance through the bulk of the solar cell and shunt resistance across the various interfaces of the solar cell. The series and shunt resistance measurements are used to determine the effective charge transfer across the bulk and the interfaces of the solar cell. The electrochemical impedance spectroscopy was carried out using the PARSTAT potentiostat/galvanostat at the open circuit potential and AC amplitude of 10mV under the one sun of incident light intensity.

## Chapter 3

### *S-kinks in BHJs and efficiency enhancement by solvent annealing*



#### *Highlights*

1. Study on the effects of thermal annealing of PCDTBT:PCBM on the device performance has revealed the degradation of the photovoltaic performance with temperature and annealing durations. The observation of the S-kink in the JV curve of the devices shows the degradation of the device.
2. The XRR technique has effectively predicted the possible degradation mechanism to be the higher electron density at the interfaces.
3. The Raman and UV-Vis studies have shown that the degradation of the device is not in the bulk of the device but at the interfaces between the HTL and the active layer.
4. The solvent annealing approach has been effectively used to enhance the performance of the devices with S-kink.

*\*part of the work has been published in AIP Conf. Proc. 1512, 776 (2013), Chem. Phys. Lett. 6–11, 646 (2016) and AIP Advances 6, 095012 (2016).*

### 3.1 Introduction

This chapter is focused on the organic solar cells based on the conducting polymer PCDTBT and experiments on understanding the factors like charge transfer and electron density profiles at the interfaces which inhibit the efficiencies of PCDTBT:PCBM solar cells. Also experiments using novel approach of layer by layer deposition in PCDTBT:PCBM solar cells along with the solvent annealing of these devices for improving the efficiency of the solar cells have also been carried out and the results and analysis of the experiments is also presented.

In order to fabricate the bulk heterojunction solar cells, the donor polymers PCDTBT, chemical structure shown in Fig. 3.1. (a), and P3HT, chemical structure shown in Fig. 3.1. (b), have been used because both of these donor polymers have been reported to be better in the efficiencies of the BHJs fabricated using these as compared to other donor polymers[33, 34, 35, 36, 37, 38]. The higher efficiencies in the BHJs based on the P3HT and PCDTBT are attributed, in case of P3HT, to the long absorption wavelength upto 650nm [39](near visible end), deep HOMO level of -5.1 eV and low band gap of 1.9 eV and higher solubility of 84.1 mg/ml with bromobenzene and 14.7 mg/ml with 1,2-dichlorobenzene [40], a most commonly used solvent while in case of PCDTBT to the higher internal quantum efficiency of nearly 100% [64], longer operating times at 250°C under 1 sun [41], low band gap of 1.8 eV [42]and deeper HOMO level of -5.4 eV [42]. During the fabrication of the BHJs based on PCDTBT and P3HT, the thermal annealing of the various layers like HTL and the active layer consisting of PCDTBT:PCBM or P3HT:PCBM, is carried out. The thermal annealing of the PEDOT:PSS is done in order to remove the remaining water in the thin layer of PEDOT:PSS coated on the ITO substrate which can degrade the photovoltaic performance of the solar cell. However in case of P3HT, it has been found that P3HT shows an increase in crystallinity with thermal annealing temperature below

melting point of P3HT. But due to limited crystallite growth of PCBM makes the enhancing effects of thermal annealing limited upto 130 to 155°C [43]. This improvement in the crystallinity of the P3HT with thermal annealing improves the charge transfer across the bulk of the active layer and thus the efficiency of the solar cell. In order to understand the effects of the thermal annealing on the PCDTBT:PCBM solar cells, experiments were carried out. The PCDTBT:PCBM solar cells were fabricated as described. After the fabrication of the solar cells, a set of the devices were characterized under one sun input light intensity while the thermal annealing of other set of devices was carried out at the temperature of 130°C for 30 min. It has been found that the thermally annealed devices undergo degradation in their photovoltaic performance and showed the appearance of S-kink in their current-voltage characteristics with reduced fill factor, open circuit voltage and short circuit current density and thus reduced efficiency [58].

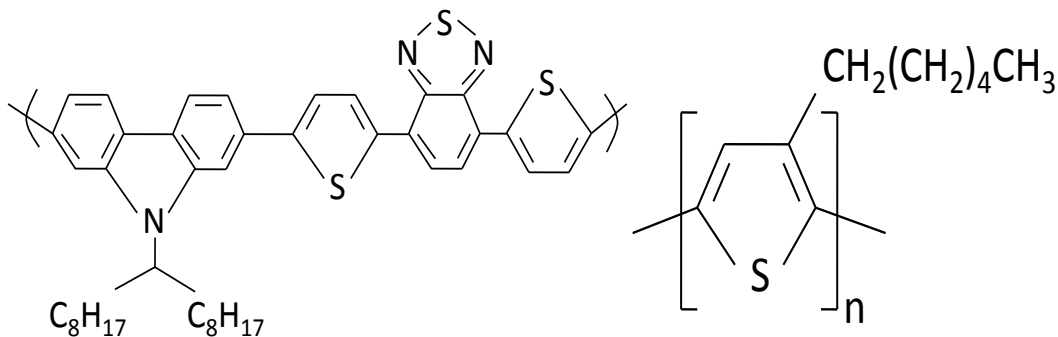


**Fig. 3.1.**(a) Chemical structure of PCDTBT and (b) P3HT.

In order to determine the possible reasons for the degradation of the thermally annealed devices, UV-Vis and Raman spectroscopy measurements were carried out on PCDTBT, PCBM and PCDTBT:PCBM blend as shown in Fig. 3.2. It has been found that there is modification in the intensity of the UV-Vis absorption spectra peaks of PCDTBT:PCBM with respect to the PCDTBT and PCBM. This modification shows the interaction between the polymer and the

PCBM molecules. There are two band transitions at 450 and 578 nm for PCDTBT corresponding to  $\pi$ - $\pi^*$  transition and two peaks at 345 and 520 nm corresponding to  $\pi$ - $\pi^*$  transition and asymmetry of the  $C_{60}$  molecules. The absorption intensity in the spectra does not change with the thermal annealing suggesting no crystallization or disordering in the PCDTBT:PCBM. There is slight increase in the intensity of the C-C intra stretch ( $1374\text{cm}^{-1}$ ) relative to in-plane skeleton mode ( $1445$  and  $1538\text{ cm}^{-1}$ ) after the thermal annealing. This change can be attributed to the increase in the degree of the molecular ordering of the PCDTBT:PCBM after thermal annealing which can improve the device performance.

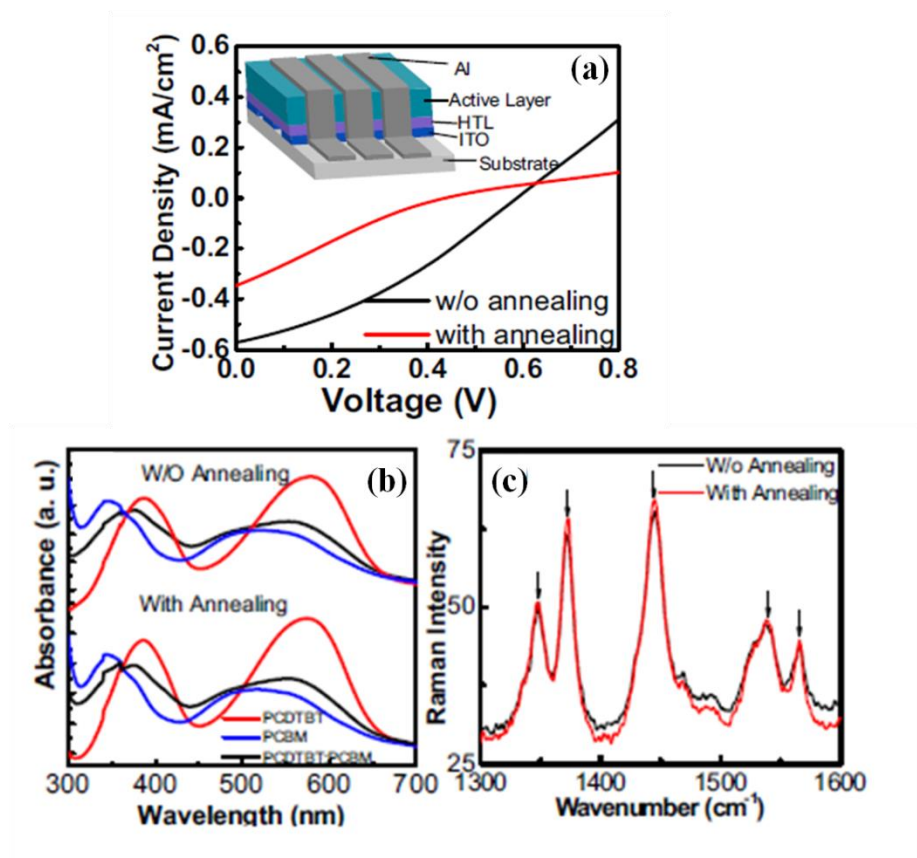


**Fig. 3.2.** (a) JV characteristics, (b) UV-Vis and (c) Raman spectrum of PCDTBT:PCBM solar cells before and after thermal annealing.

But the devices have shown degradation in the photovoltaic performance after thermal annealing with the appearance of the S-kinks in the current-voltage characteristics of the devices. Such degradation in the photovoltaic performance of the PCDTBT:PCBM devices after thermal annealing can be attributed to the degradation of the interfaces between the various layers of the PCDTBT:PCBM based BHJs.

Thus, the efficiency of a BHJ solar cell critically depends upon quality of its interfaces. The imperfect interfaces can lead to S-kink in the current-voltage characteristics that reduce the efficiency of BHJ solar cells. In order to further determine the possible reasons of the degradation of the device performance, using PCDTBT:PCBM based BHJ solar cells, we used a powerful non-destructive X-ray reflectivity technique to estimate the electron density profile across the BHJ solar cells. A direct correlation is observed between the enhanced electron density at PEDOT:PSS/PCDTBT:PCBM interface and appearance of S-kink in J-V characteristics, which is also supported by x-ray photoelectron spectroscopy and Kelvin probe measurements.

In the BHJ solar cell consists of a blended donor-acceptor active layer, e.g. PCDTBT and phenyl C<sub>61</sub>-butyricmethyl ester (PCBM) etc., which is sandwiched between a hole-collecting anode (e.g. PEDOT-PSS/ITO) and an electron-collecting cathode (e.g. Au, Al etc.) there is a built-in voltage ( $V_{bi}$ ) that drives photo-generated holes to anode and electrons to cathode. The efficiency of BHJ solar cell is directly associated with the current-voltage (J-V) characteristics under illumination, which is governed by the quality of various layers and interfaces involved in devices. However, in some cases instead of diode-like J-V characteristics under 1 sun, S-shaped characteristics are observed i.e. with increasing bias voltage, current levels off and again increases as voltages approaches to open circuit voltage ( $V_{OC}$ ). The observation of S-kink in the

J-V characteristics leads to decrease in fill factor (FF),  $V_{oc}$  and, in turn the lowering of overall device efficiency. Generally, the S-kink is observed due to following reasons:

(i) ***Injection and extraction barriers:*** The injection and extraction barriers across the hole transport layer (HTL)/donor interface can arise either due to mismatched electrode work functions or presence of interface defects and traps. Shaheen et al studied the effect of several cathode materials such as Al, Ag, Mg:Ag/Ag, LiF/Al, Ca/Al, and Ba/Al on the device efficiency and stability [44]. They observed S-kink in low work function cathode material. Tress et al suggested  $V_{oc}$  does not get affected by the extraction barrier but reduces in case of injection barrier. When the barrier exceeds 0.2 eV, S-kink is observed [45]. Wagenpfahl et al suggested that the injection barrier change the charge- carrier density at the contacts and therefore affects the  $V_{oc}$  [46]. However, numerical device simulation attributed the appearance of S-kink in case of reduced surface recombination velocity occurring in the device. By choosing an hole injection layer with high work function or doped buffer layers, the energetic barrier between donor and anode can be reduced resulting in normal device characteristics[47,48]. Similarly, the choice of bathocuproine (BCP) as an exciton blocking layer (EBL) or resulted in elimination of S-shape as a result of improved charge extraction [49].

(ii) ***Interface dipoles:*** The presence of defects and traps can result in interfacial dipoles causing barrier formation for carrier extraction [50]. It is observed by Hany et al that isolated Al clusters formed during cathode evaporation lead to defect states close to interface and thereby changing the electric field distribution in the device [51]. The presence of strong interfacial dipoles results in the charge blockage, leading to an S-kink in J-V characteristics of device under illumination.

**(iii) Unbalanced mobility of charge carriers:** Unbalanced mobility of hole and electrons results in accumulation of charge carriers of lower mobility at the electrode surface causing an additional electric field in the device. Riede et al carried out electrical simulation based on drift-diffusion model and predicted that the S-kink is observed if mobility mismatch factor is larger than 100 [52]. The theory was verified by combining low mobility material with acceptor having different electron motilities. S-kink has also been eliminated by improving the hole mobility of donor material [53].

**(iv) Interfacial Morphology:** Interfacial morphology of the donor/acceptor blends also causes S-shape in the J-V characteristics due to oxygen doping during processing or ambient air operation [5]. An efficient device operation for normal structure requires vertical phase separation of donor and acceptor at anode and cathode, respectively. It was found that fullerene localization at the anode interface leads to S-kink [54]. Further, the morphology was also varied depending upon the processing using a mixture of solvents. Low surface energy of P3HT results in a thin P3HT enriched layer on top surface causing the S-kink. Usage of high boiling point solvent such as p-xylene suppresses the P3HT enrichment and thereby eliminating the S-kink [55].

It is to be noted that though there may be several reasons for the appearance of S-kink in the J- V characteristics, the effect remains the same i.e. charge accumulation in the device leading to additional electric field and therefore reduced FF and device efficiency. In order to identify the causes of the S-shaped J-V characteristics, measurements have been carried out either as a function of temperature/light intensity or transient photocurrent measurements, which reveal redistribution of the electric field [56,57]. Earlier we have shown that BHJ devices based on PCDTBT and PCBM exhibit S-kink when annealed at moderate temperatures of 130°C for few

hours [58] and similar results have recently been obtained by others [59]. The spectroscopic studies have shown that the properties of the PCDTBT:PCBM active layer almost remained unaffected at such low annealing temperatures [18], and hence, the appearance of S-kink could be associated with the degradation of interfaces. Therefore, a robust characterization technique, preferably using a nondestructive technique, is required to prepare high-quality BHJ solar cells so that the key physical parameters, such as, layer thickness, interfacial quality and density are well controlled. In addition, high efficient tandem BHJ solar cells require a proper nondestructive tool to characterize various layers and interfaces beforehand.

X-ray reflectivity (XRR) is an efficient and powerful nondestructive technique for the measurements of layer thickness, surface roughness and electron density profile in multilayers [60, 61], and therefore, is suitable for investigating the origin of S-kink in BHJ solar cells. In this paper, for the first time, we investigate the PCDTBT:PCBM based BHJ solar cells using XRR and demonstrate a correlation between the electron density at the interface and presence of S-kink in the J-V characteristics. This correlation has further been supported using x-ray photoelectron spectroscopy (XPS) and Kelvin probe (KP) measurements.

### **3.2. XRR experiments**

The ITO-coated (resistivity: 8-12  $\Omega$ /sq) glass slides were first cleaned with detergent, ultrasonicated in deionized water, acetone and isopropyl alcohol for 15 min each followed by an ozone treatment for 20 min. In different experiments, 70 nm thick layer of PEDOT:PSS (obtained from Ossila® and filtered through 0.45  $\mu$ m PTFE filter) was spin-coated onto ITO substrates. These samples were then transferred to glove box (MB 200G, MBraun Inc. Germany) having moisture and oxygen <0.1 ppm and annealed at 130°C for 30 min. The active layer (thickness: 70 nm) of PCDTBT:PCBM (1:4 W/W, 10 mg/ml in 1,2-dichlorobenzene) was spin-

coated on the PEDOT:PSS/ITO anodes. Finally, Al cathode (thickness:100 nm) was thermally evaporated through a shadow mask on the active layer to obtain BHJ solar cells with an active area of 4mm<sup>2</sup>. These solar cells were encapsulated using UV curable epoxy inside the glove box and taken out for the photovoltaic characterization. More than 100 devices were fabricated and characterized. The current-voltage (J-V) characteristics of the devices were measured using a solar simulator (Sciencetech, Canada) under 1 sun (AM 1.5 G), 100 mW/cm<sup>2</sup> illumination. The intensity was calibrated using a standard silicon reference diode. A non-contact, non-destructive vibrating capacitor device, known as Kelvin Probe (KP) scanning microscopy, was employed to measure the work function of PEDOT:PSS surface having resolution of ~ 3meV (model: KP Technology). XPS was carried out using Mg K $\alpha$  source (RIBER MBE system). The binding energy scale was calibrated to the Au 4f<sub>7/2</sub> line of 83.95 eV. X-ray reflectivity (XRR) measurements were carried out using 18 kW rotating anode X-ray laboratory source with Cu K $\alpha$ -radiation ( $\lambda = 1.542\text{\AA}$ ).

### 3.3 Results and Discussion

Majority of the fabricated PCDTBT:PCBM BHJ solar cells exhibited nice diode-like J-V characteristics under the illumination of 1 sun (Fig. 3.3.(a)), whereas ~20% of them exhibited S-kink in their J-V characteristics (Fig. 3.3. (b)). The photovoltaic parameters of these devices are summarized in Table 3.1. Devices without S-kinks exhibited efficiency in the range of 2.1-3.1%, whereas the devices with S-kinks exhibited poor efficiency (0.5-1.3%) owing to poor V<sub>OC</sub>, current density (J<sub>SC</sub>) and FF. It is to be noted that devices were fabricated with basic cell design without any kind of post or pre-treatment as well as buffer layers in order to identify the cause of S-kink. In literature, the efficiency of PCDTBT:PCBM BHJ solar cells is found to depend upon several factors, including molecular weight of the donor material, pre- and/or post-treatments,

thickness of active layer, buffer layers, device structure etc. [19, 62, 63, 64]. The best efficiency of ~3.1 % observed in our case is comparable to the efficiencies reported for PCDTBT:PCBM BHJ solar cells fabricated under identical processing conditions [42, 65, 66].

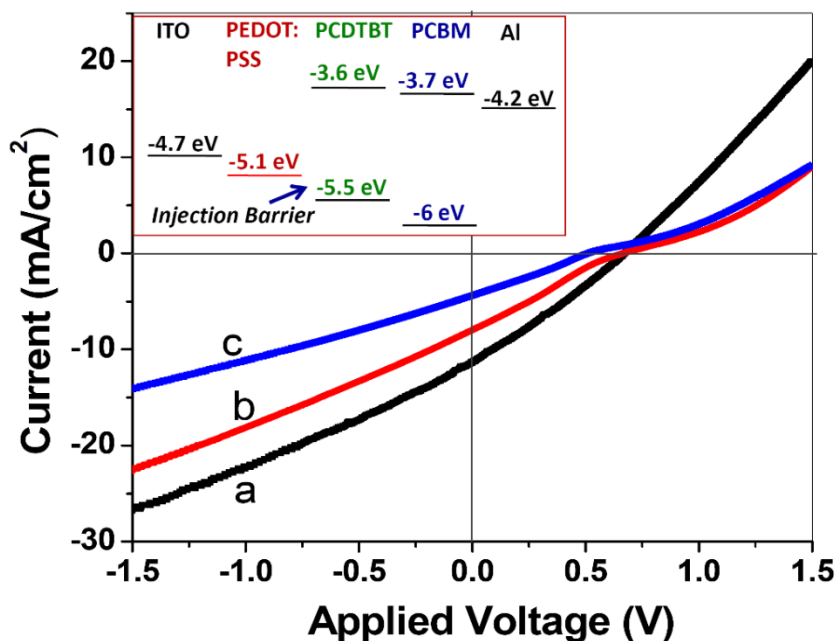


**Fig. 3.3.** Typical experimental J–V curves recorded for devices under 1 sun (AM 1.5 G), 100 mW/cm<sup>2</sup> illumination for (a) devices without S-kink, (b) devices with S-kink and (c) appearance of S-kink after annealing (100°C for 4 h) the devices representing (a). The inset shows the energy levels of the materials employed in device fabrication, and represents the injection barrier for holes.

However, the efficiency can be further improved to ~5% if one employs appropriate buffer layers and solvent/thermal treatments. The main purpose of this work is to investigate why some of the BHJ solar cells (fabricated under identical conditions), exhibit S-kink. Therefore, we have neither added buffer layer nor subjected the devices for any kind of treatments as it would lead to additional parameters for the investigations.

One of the possibilities envisaged for the observation of S-kink in some of the devices was if the quality of the deposited PEDOT:PSS layer is varying from sample to sample, which in turn may lead to a poor quality of (PCDTBT:PCBM)/(PEDOT:PSS) interface. To investigate the role of PEDOT:PSS layer on the S-kink, the work function of several freshly-prepared PEDOT:PSS samples were measured using Kelvin Probe method. As shown in Fig. 3.4., majority of PEDOT:PSS layers have an average work function of 5.1 eV (Fig. 3.4.(a)), while few of them exhibited an average work function of 5.3 eV, (see Fig. 3.4.(b)) that is significantly higher by 0.2 eV. The values obtained using this method may be different from those obtained from ultraviolet photoelectron spectroscopy (UPS) since KP gives an average value over a sample while UPS is a localized measurement [67]. The increase in the work function of the PEDOT:PSS may be associated with the presence of surface states or dipoles which might be created either due to chemisorbed oxygen or excess PSS at the surface. It has been reported that the charges of  $\text{PEDOT}^+$  and  $\text{PSS}^-$  cause formation of local dipoles [68]. The orientation of these dipoles with sulphate groups towards surface leads to an increase in the work function. Therefore, an increase in the work function of PEDOT:PSS films could be due to a the top layer of PEDOT:PSS which may contain excess of PSS owing to thermal treatment. Other reason for the increment in the work function may be due to chemisorbed oxygen.

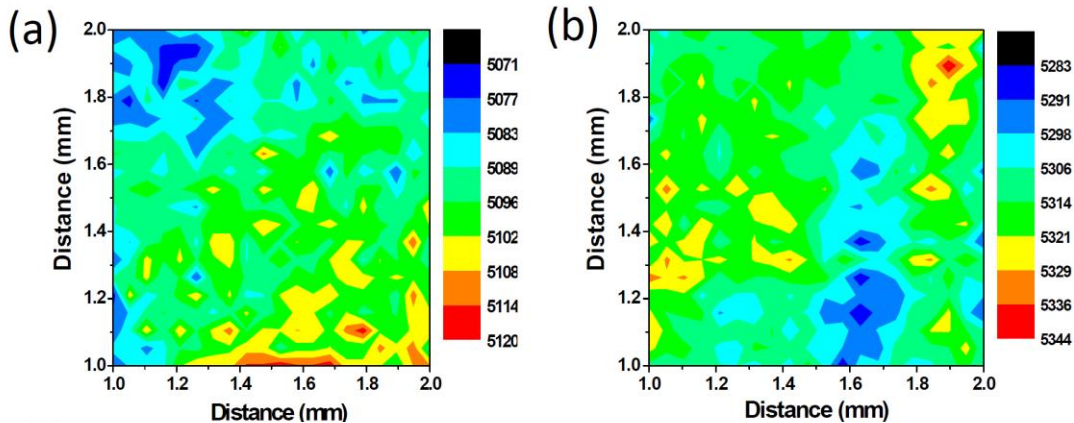


**Fig. 3.4.** Work function mapping of (a) filtered and (b) unfiltered PEDOT:PSS layers recorded using Kelvin Probe exhibiting average work function value of 5.1 and 5.3 eV, respectively.

The work function of PEDOT:PSS affects the energy barrier height at the interface of PEDOT:PSS with the active layer as shown in inset Fig. 3.4., and therefore, determines the hole injection at this interface leading to S-kink observed in J-V characteristics.

In order to further investigate why some of the PEDOT:PSS layers exhibit higher work functions, core level S2p and O1s XPS spectra were recorded for PEDOT:PSS layers exhibiting different work functions (Fig. 3.5.). The low binding energy peak corresponds to S atoms in the thiophene ring while high binding energy peak is attributable to sulphur atoms in PSS [69]. A single spin-orbit doublet having ratio of  $2p_{3/2}$  and  $2p_{1/2} \sim 2:1$  and splitting of 1.2 eV was used for all deconvolutions. A doublet at 169.7 (S  $2p_{3/2}$ ) and 168.5 eV (S  $2p_{1/2}$ ) was attributable to PSSH, and that at 165.9 (S  $2p_{3/2}$ ) and 164.5 (S  $2p_{1/2}$ ) was assigned to sulphur of PEDOT. As shown in the Fig. 3.5.(b) and (c), the S 2p spectra were found to be identical for all the samples with PSS/PEDOT ratio of 1:2.5, confirming that there is no loss or degradation of the material. However, the O1s spectrum of PEDOT:PSS layer having higher work function exhibited a broader and asymmetric peak as shown in Fig. 3.5.(c) and (d). In the case of PEDOT:PSS layer with lower work function (i.e. 5.1 eV), the O1s spectrum could be deconvoluted into oxygen component corresponding to the various bonds in PEDOT:PSS i.e. 534.1 eV from the oxygen atoms in the dioxyethylene bridge of PEDOT ( $O_{PEDOT}$ ), and 533 and 532.2 eV from the oxygen atoms bound to the sulfur sites in the sulfonic acid groups of PSS ( $O_{PSS}$ ) [70]. The peak at 531.7 eV is attributed to the presence of physisorbed oxygen in PEDOT:PSS films, which is due to the fact that the films got exposed to ambient during their loading into XPS chamber. The

PEDOT:PSS ratio as derived from the  $O_{\text{PEDOT}}:O_{\text{PSS}}$  ratio is found to be 1:2.5, which is consistent with the ratio measure from S 2p data. In the case of PEDOT:PSS layers with higher work function, the ratio  $O_{\text{PEDOT}}:O_{\text{PSS}}$  is increased to 1:3. It is seen from the deconvoluted curves that relative intensity of the peak at 532.3 eV corresponding to PSS is enhanced significantly as compared to the other component of PSS. The enhanced intensity at 532.3 eV can arise due to the presence of chemisorbed oxygen in PEDOT:PSS sample which overlaps with the peak of PSS. The presence of chemisorbed oxygen is attributed to the possible reaction of PEDOT:PSS with molecular oxygen and/or water. It has been known that even small amounts of water in the anode results in deterioration of device properties [71,72]. PEDOT/PSS in air contains a significant amount of water because of the hygroscopic properties of PSS. In fact this effect was predominantly observed, when PEDOT:PSS film was subject to an UV–ozone treatment [73]. It is therefore anticipated that due to slight unintended variations in the processing conditions (e.g. concentration of solution, extra exposure to the ambient etc.) chemisorbed oxygen can be present at the PEDOT:PSS surface, which could be the responsible factor for the observed S-kink in the devices. It may further be noted that devices exhibiting nice diode-like J-V characteristics started showing S-kink when they were annealed at 100°C for more than 4 h (Fig. 3.3.(a)). It is seen that the annealing the devices at 100°C for 4 h results in a drastic reduction of the efficiency (0.6-2.1%). As the annealing temperature is low, the efficiency reduction cannot be attributed to the segregation and crystallization of PCBM that often takes place at temperatures >140°C[74, 75]. In order to gain insight into why some of the devices show S-kink and why annealing converts diode-like behavior into S-kink behavior, we have performed the XRR measurements as a function of wave vector transfer (i.e., the difference between the outgoing and incoming wave vectors),  $Q = 4\pi\sin\theta/\lambda$  (where,  $\theta$  is angle of incidence and  $\lambda$  is x-ray wavelength). In order to

correlate the XRR data with J-V characteristics, we mimicked the BHJ solar cell by depositing only 5nm Al layer so as to allow penetration of X-rays through the sample depth. The XRR data is qualitatively related to the Fourier transform of the electron density depth profile (EDP)  $\rho(z)$  averaged over the whole sample area [36, 76]. The EDP as a function of vertical depth was then inferred from the XRR data by fitting a model  $\rho(z)$  whose reflectivity best fits the XRR data. A model consisted of layers included layer thickness, interface (or surface) roughness and EDP [36]. Typical experimental specular reflectivity data measured for a device as a function of wave vector transfer  $Q$  is shown in Fig. 3.6. (a). The experimental reflectivity data were fitted using the dynamical formalism of Parratt [77], as shown in the inset of Fig. 3.6. (a). The method employs the application of the X-rays to determine the EDP profiles at the various depths within the deposited layers of the device. The X-rays are allowed to penetrate through the top surface of the layer of aluminum. The X-rays are reflected and refracted at the interfaces between the various layers of the device. The interference pattern of the reflected and the refracted X-rays is recorded by a detector. The angle of the incidence of the X-rays is kept very small and is only changed slightly to get the interference pattern at these different angles. The interference pattern varies with the change in the EDP profiles at the interfaces which can be used to determine the EDP profiles at these interfaces. By fitting the XRR data of samples without s-kink to the assumed model, we obtained the EDP profiles of various layers. However, for the samples showing the S-kink in J-V characteristics, the best fit of experimental data is obtained only when an additional interface of thickness  $\sim 7-9$  nm was considered between PCDTBT:PCBM and PEDOT:PSS. The fitting of GXRR data for the devices with and without S-kink are shown in Fig. 3.6. (b). The resultant EDP profiles across the ITO/PEDO:PSS/PCDTBT/Al was constructed from this data as shown in Fig. 3.6. (c). Various fitting parameters of

(PCDTBT:PCBM)/(PEDOT:PSS) interface are also summarized in Table 3.1. It is seen from the Fig. 3.6. (c) that the EDP profiles for the both samples are identical except at the few nm interface of (PCDTBT:PCBM)/(PEDOT:PSS). The electron density at the (PCDTBT:PCBM)/(PEDOT:PSS) interface increases substantially from 50 to 874  $e/nm^3$  for devices without S-kink and with s-kink, respectively. The EDP values obtained here are within reasonable range of values reported in literature [78]. The formation of a thin high electron density layer of thickness  $\sim 7-9$  nm at the interface between (PCDTBT:PCBM)/(PEDOT:PSS), for samples showing S-kink in J-V characteristics, could be associated with the interfacial dipoles form as a result of chemisorbed oxygen. It is to be noted that such a significant change in the EDP cannot result from the segregation of either PSS or PCDTBT owing to small contrast in their mass density.

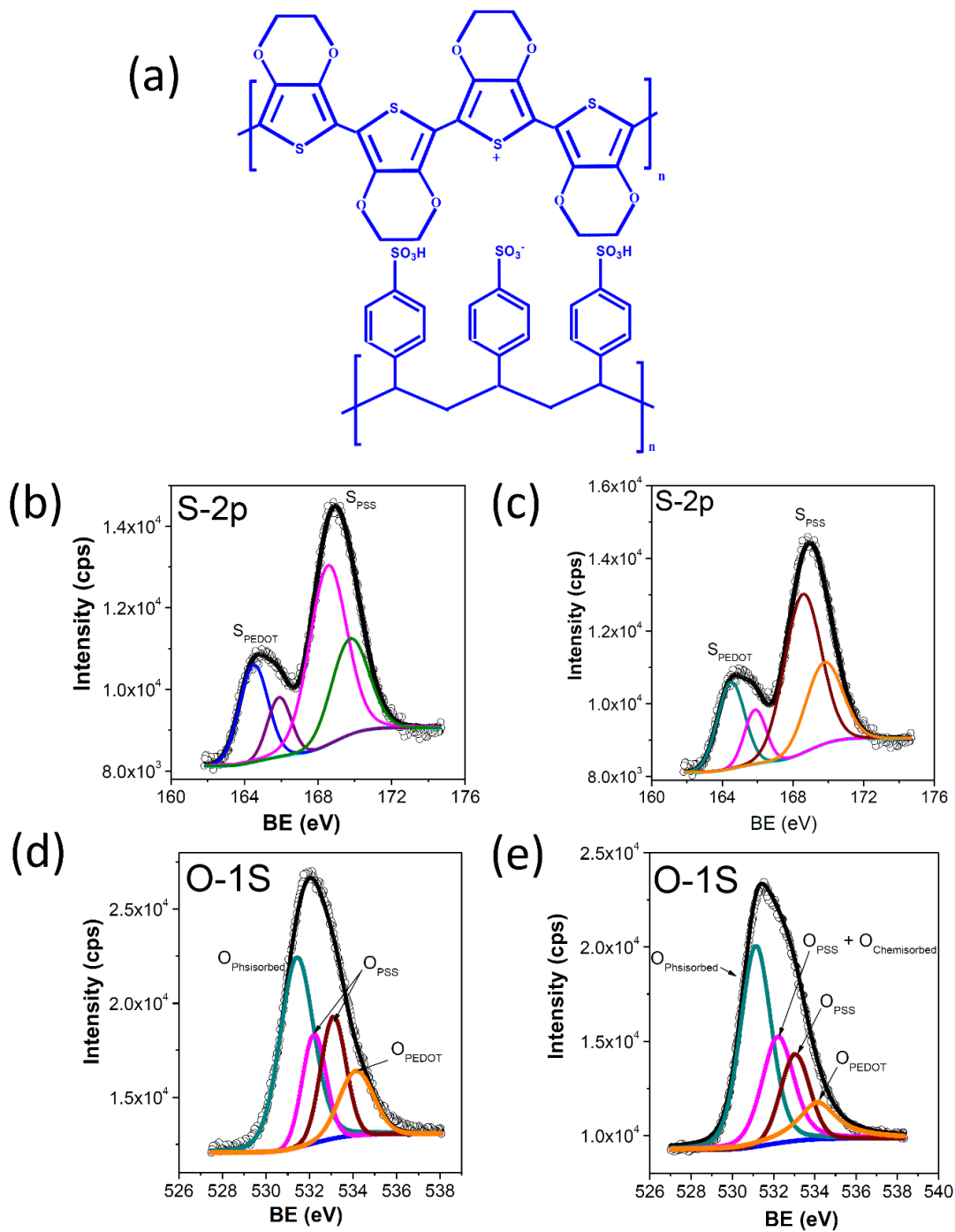


**Fig. 3.5.**(a) Structure of PEDOT:PSS and (b) S2p and O1s XPS spectra of the PEDOT:PSS samples (b) and (d), and (c) and (e) corresponding to average work function value of (a) 5.1 and (b) 5.3 eV for the samples, respectively.

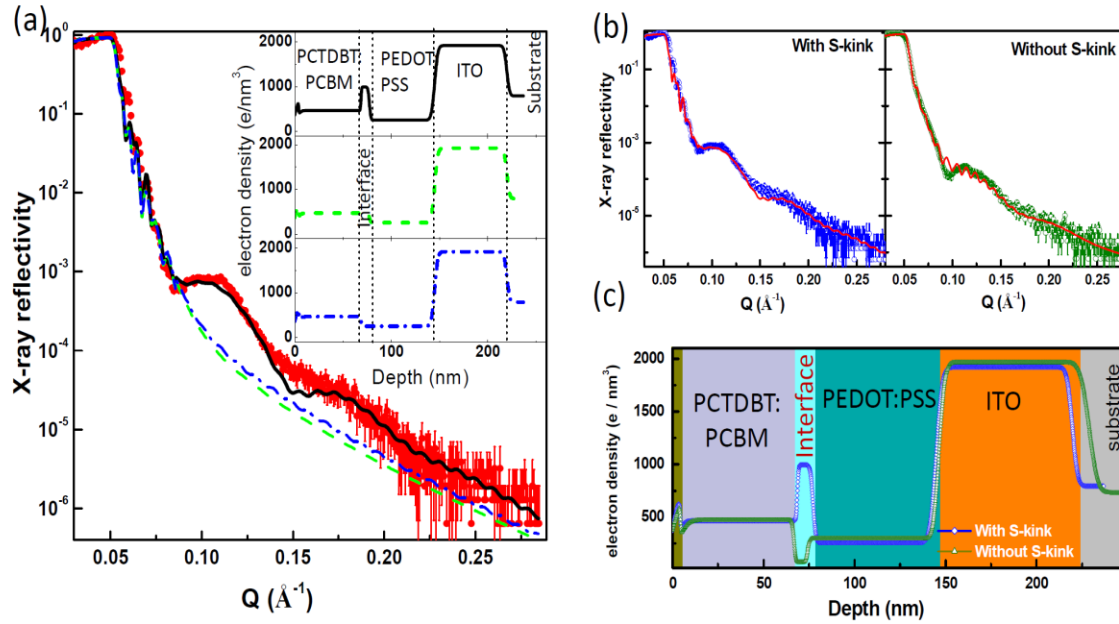


**Fig. 3.6.** (a) Fitting of GXRR data for a typical ITO/PEDOT:PSS/PCDTBT:PCBM/Al bulk heterojunction solar cell using the different electron density profiles shown in the inset. It is seen that the best fitting is observed only when an additional interface between PCDTBT:PCBM and PEDOT:PSS is taken into account. (b) Fitting of GXRR data for devices with and without S-kink in their J-V characteristics and (c) the resultant electron density profile.

In addition to this, we also observed S-kink in normal devices when they were annealed at 100°C for more than 4 h as discussed above. The EDP profiles for these samples were also constructed under abovementioned model and are shown in Fig. 3.7. The resultant parameters of the interface are also summarized in Table 3.1. It is seen from the Fig. 3.7 that annealing significantly changes the EDP profiles at the (PCDTBT:PCBM)/(PEDOT:PSS). This change is observed for samples which are annealed at 100°C for 4h and further increment in annealing time does not change the EDP profile much. The similar kind of behavior is reflected where a drastic decrease in efficiency is observed for devices when annealed at 100°C for 4h.

In addition to this there is also significant increase in the surface roughness of all the interfaces of BHJ solar cells. This is in contrast to the EDP parameters obtained for devices showing S-kink when normal devices were fabricated. Our earlier observation rules out any degradation of the donor material, i.e. PCDTBT [36]. We also rule out the segregation of PCBM as it requires high annealing temperature. The increased EDP at the (PCDTBT:PCBM)/(PEDOT:PSS) interface in this case could be attributed to segregation of PSS at 100°C as well as diffusion of oxygen at the (PCDTBT:PCBM)/(PEDOT:PSS) interface. This may lead to roughened interfaces and S-kink observed in the J-V characteristics [79]. The space charge at the (PCDTBT:PCBM)/(PEDOT:PSS) interface contributes to a negative field at donor/acceptor interface, and therefore, the hole extraction is driven by diffusion against this field[5]. A competition between the diffusion and drift current (due to applied bias) is responsible for the appearance of the S-kink. The enhanced roughness of interfaces upon annealing, in addition to injection barrier, is the result of accumulation or reorganization of material at the interface.

We thus demonstrated a direct correlation between the electron density profile at the interface and observed S-kink in the J-V characteristics of the PCDTBT:PCBM based BHJ solar cells. The Kelvin Probe and XPS analyses suggest that the chemisorbed oxygen ( $O_2^-$ ) in PEDOT:PSS layer is responsible for the enhanced electron density at the interface and give rise to S-shape in J-V characteristics upon light illumination. In addition, it was also observed that annealing of the devices causes increase in the surface roughness and electron density of the interfaces owing to re-organization of materials at the interface and therefore lead to S-kink in devices. As the XRR is a non-destructive technique for identification of electron density profiles

of multilayers, it can be utilized to predict the quality of multilayer thin-film solar cells as well as for their process optimization, especially in tandem structures.

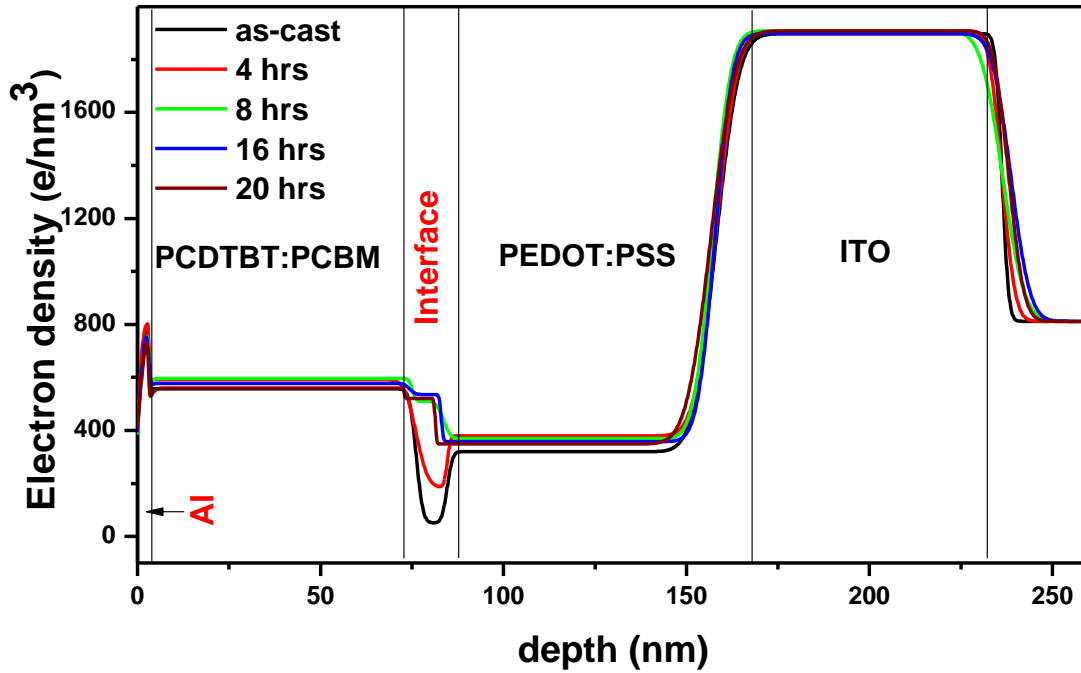


**Fig. 3.7.** The electron density profile of the device with diode-like J-V characteristics annealed at 100°C for different period of time. Annealing leads to increase in the electron density at the PCDTBT:PCBM/ PEDOT:PSS as well as increase in the roughness of all the interfaces.

**Table 3.1.** Summary of photovoltaic parameters of different BHJ solar cells and estimated parameters of the (PCDTBT:PCBM)/(PEDOT:PSS) interface using GXRR measurements.

BHJ solar cell	Photovoltaic parameters				Parameters of PCDTBT:PCBM/PEDOT:PS S Interface		
	V <sub>OC</sub> (V)	J <sub>SC</sub> (mA/cm <sup>2</sup> )	FF (%)	η (%)	Thickness (nm)	Electron density (e/nm <sup>3</sup> )	Roughness (nm)
Without S-kink	0.52-0.67	11.3-15.5	28-39	2.1-3.1	7.5±0.5	50±15	1.2±0.3
With S-kink	0.41-0.66	4.1-8	25-30	0.5-1.3	8.5±0.3	874±24	1.0±0.2
Annealed@100°C/4h	0.51-0.52	4.5-12.2	27-34	0.6-2.1	7.5±0.5	189±15	1.4±0.2
Annealed@100°C/8h	0.49-0.54	4.5-8.4	22-34	0.6-1.1	8.0±0.5	370±16	2.4±0.2
Annealed@100°C/16h	0.45-0.50	5.6-6.1	22-30	0.4-0.8	8.5±0.5	359±17	4.5±0.3
Annealed@100°C/20h	0.40-0.42	3.6-4.9	18.2-25	0.5-0.6	8.5±0.5	349±18	4.5±0.2

### 3.4. Efficiency enhancement by solvent annealing

As the thermal annealing cannot be used for the PCDTBT:PCBM based BHJs, a novel approach must be adopted the improvement in the photovoltaic performance of the devices. One of the important factors which determine the overall efficiency of the polymer solar cells is the amount of the light absorbed by the active layer of the solar cell. The higher is the amount of the light absorbed, the more is number of excitons created. With higher number of the excitons created, higher of number of charge carriers are generated if these excitons are dissociated across the donor-acceptor interface. This leads to higher current being generated by the device and thus higher efficiency is achieved with such devices. The absorption of more amount of the light photons in the active layer of the polymer solar cells can be achieved by increasing the thickness

of the active layer. However increasing the thickness of the active layer also causes the problem of recombination of the excitons as the diffusion length of the excitons has been found out to be order of 10 nm which is very low as compared to the higher thickness of the active layer. This recombination of the excitons decreases the efficient dissociation and thus charge transfer across the donor-acceptor interface resulting in the decreased current density and thus decreased efficiency of the solar cells.

### 3.4.1. Adoption of a new approach for fabrication of the PCDTBT:PCBM solar cells with higher thickness

In order to fabricate the polymer solar cells based on PCDTBT:PCBM with higher thicknesses, we have developed a novel approach of layer by layer deposition of the active layer. The conventional (Fig. 3.8) and more widely used approach for the deposition of the active layer is though spin coating of the active layer on the substrate. But this approach provides with the problems of limited thickness of the active layer as it is not possible to achieve a thickness below certain value due to low rpm speed of the spin coating and even with the highest achievable thickness with such method the morphology of the layer is not uniform throughout the deposited layer.

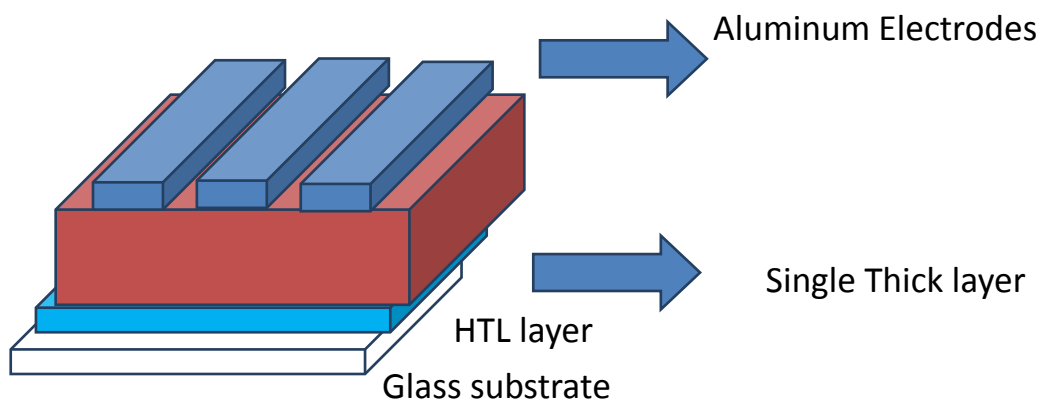


**Fig. 3.8.** Conventional approach of deposition of the single thick active layer on substrate through spin coating.

Such non uniform morphology reduces the efficient charge transfer across the active layer and electrode interfaces. Thus it becomes very important to adopt a new approach to achieve higher thickness of active layer with the uniform morphology throughout the deposited layer. In order to achieve higher active layer thickness, we adopted a layer by layer deposition approach as shown in Fig. 3.8, in which thinner layers of active layers are deposited individually over each other through spin coating. In order to achieve this, we speculated that thinner layers of active layers can be deposited on the substrate at higher rpm speeds of the spin coating. At such higher rpm speeds the morphology of the active layer deposited on the substrate is highly uniform and smooth across the deposited active layer. Another thinner layer of active layer material can be deposited in the similar fashion at the same rpm speed on the top of this deposited layer. However if the active layer material PCDTBT:PCBM is prepared in the solvent of 1,2-dichlorobenzene, it is not possible to achieve another thinner layer on the top of the previously deposited active layer with uniform and smooth morphology. This is because of the fact that the boiling point of 1,2-dichlorobenzene is very high 180.5°C and its takes a longer duration for the solvent to completely evaporate from the previously deposited active layer before the next layer could be deposited on the top of this layer. As a result depositing next layer on the top of previous layer will dissolve the previous layer and a single non uniform active layer will be achieved. However if the use of 1,2-dichlorobenzene is replaced with the use of chloroform, having lower boiling point of nearly 60°C, as a solvent in the active layer, it will give uniform layers of active layers deposited over each other. This is because of the fact that chloroform with lower boiling point will evaporate immediately as the deposition of previous layer is completed. As next layer is deposited over the previous layer, chloroform will again evaporate immediately before dissolving the previous layer. This will give us two distinct layers

of active layers with uniform morphology across the layer but with an interface between them. In similar fashion, a number of layers of active layer material can be deposited over each other to give desired higher thickness of the active layer without compromising with the morphology of the active layer.

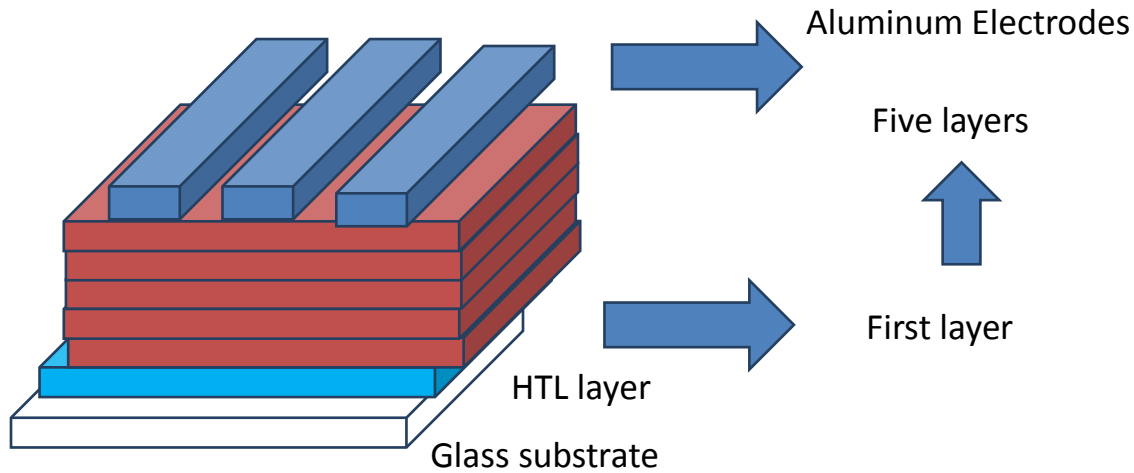


**Fig. 3.9.** New layer by layer deposition approach of deposition of the thick active layer on substrate through spin coating.

### 3.4.2 Advantages offered by layer by layer deposition

The layer by layer deposition approach offers following advantages as compared to the deposition of the single thick layer through spin coating:

1. Layer by layer deposition approach gives advantage of control of thickness as compared to direct deposition.
2. The absorptivity is approximately linearly proportional to the number of layers and hence thickness.
3. At higher thicknesses ( $>200\text{nm}$ ) the morphology as a result of layer by layer deposition is better as compared to direct deposition.

4. Device performance can be studied, optimized and controlled with layer by layer deposition approach which is not possible with direct deposition.
5. Thermal annealing studies have shown improvement in layer by layer devices in PCDTBT:PCBM which is not possible with direct deposition.

### 3.4.3. Fabrication of the PCDTBT:PCBM solar cells

In order to study the photovoltaic performance of the PCDTBT:PCBM solar cells at different thicknesses, we fabricated the PCDTBT:PCBM solar cells with varying thicknesses with deposition of single layer upto five layers of the active layer material on different substrates each as shown in Fig. 3.9. We fabricated two substrates of each thickness, from single to five layers, with each substrate consisting of nine devices giving a total of 90 devices in all the substrates.

### PCDTBT:PCBM Bulk Heterojunction Solar Cells

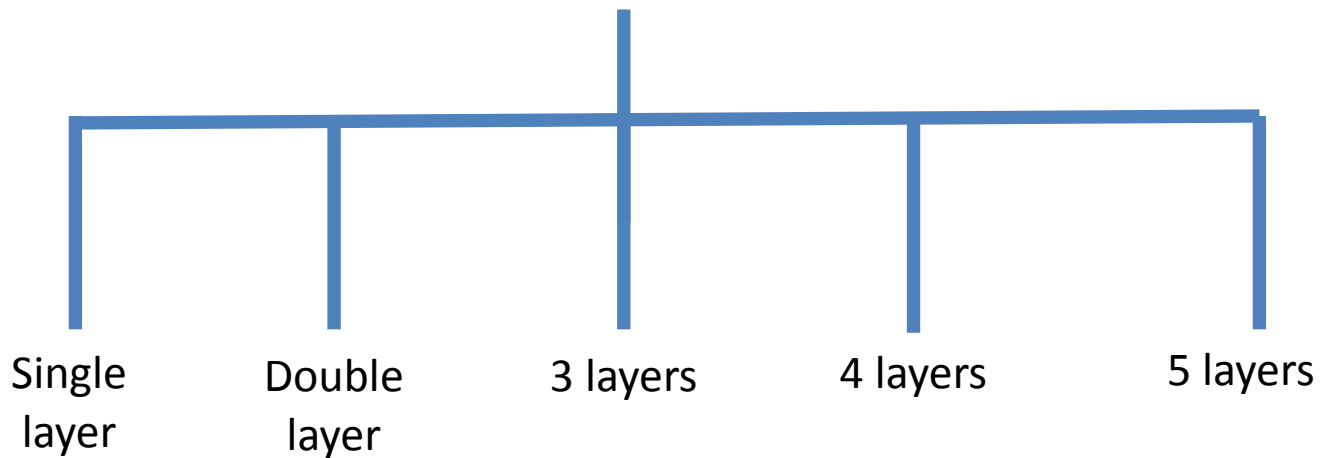


**Fig. 3.10.** Two substrates of each layer with nine devices each were fabricated and characterized.

The structure for the fabrication of the solar cells consists of ITO/PEDOT:PSS/PCDTBT:PCBM/Al where each layer of the material is deposited on each other through spin coating. The thicknesses of these layers are optimized, with PEDOT:PSS having thickness of 40 nm, PCDTBT:PCBM of thickness 70 nm and aluminum of thickness 100

nm. The PCDTBT:PCBM devices are fabricated with the same procedure as described earlier. After the fabrication, the devices are characterized for JV characteristics inside the Glove Box under incident light intensity of  $5\text{mW}/\text{cm}^2$ . After this, the devices are encapsulated with special epoxy seal in order to prevent the devices from getting exposed to the oxygen and moisture when these devices will be characterized in the ambient atmosphere. This encapsulation is done by placing a small drop of the epoxy on the substrate and placing a thoroughly cleaned thin glass plate on top of it, gently pressing the glass plate so that epoxy is distributed uniformly across the substrate. After this, the substrate is given light treatment for 30 -40 minutes during the epoxy gets hardened. The devices are again characterized inside the Glove Box under the same light intensity to ensure that the devices do not undergo any degradation in their photovoltaic performance due to the sealing procedure. It has been confirmed that sealing of the devices with epoxy does not cause any degradation in the photovoltaic performance of the devices. After the encapsulation procedure, the substrates are taken out from the Glove Box for further characterization under the AM 1.5G or one sun standard of input light intensity using AAA Solar simulator.

### **3.4.2. JV Results**

The JV results of the PCDTBT:PCBM solar cells with different thicknesses from single to five layers under one sun incident light are shown in Table 3.2.

From the Table 3.2., it can be seen that as the thickness of the layers is increased from single to five layers the open circuit voltage increase monotonously from 0.52 to 0.80 V. This enhancement in the open circuit voltage leads to improvement of the overall efficiency of the solar cells which directly depends on the open circuit voltage. However, the JV results (Fig. 3.11) also show that the short circuit current density and fill factor show opposite behaviour to

that of open circuit voltage when the thickness of the layers is increased from single to five layers. For the single the devices have shown a maximum current density of  $17.33 \text{ mA/cm}^2$  which continuously decreases to a lower value of  $7.51 \text{ mA/cm}^2$  for five layer devices. Similarly the fill factor shows decrement from 39.26 to 25.39% as the active layer thickness is increased.

**Table 3.2.** Variation of Photovoltaic Parameters under AM1.5G with thickness

Parameters	Single layer	Double layer	Three layers	Four layers	Five layers
$V_{OC}$ (V)	0.52	0.67	0.76	0.78	0.80
$J_{SC}$ ( $\text{mA/cm}^2$ )	17.33	13.49	10.35	10.24	7.51
FF (%)	39.26	35.14	35.06	32.61	25.39
Efficiency (%)	3.55	3.18	2.78	2.61	1.53

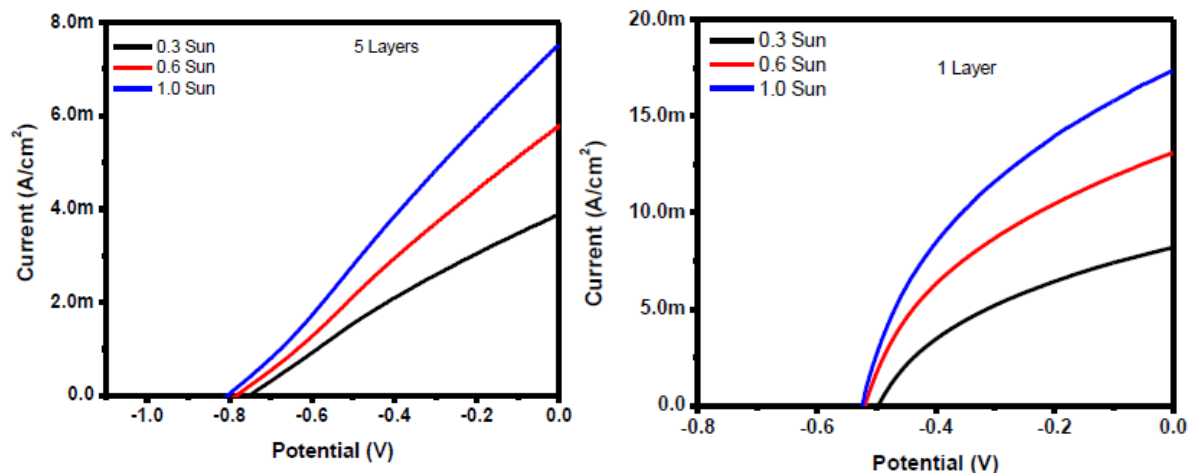


**Fig. 3.11** JV characteristics of single-layer and five-layer cells under varying input intensity.

### 3.4.4 Encapsulation and stability studies on PCDTBT:PCBM solar cells

One of the most important factors determining the performance of the polymer solar cells is their stability in performance over longer period of times. As the active layer materials used in

the fabrication of the solar cells are prone to degradation in the ambient atmosphere due to oxygen and moisture, these devices must be encapsulated in order to prevent their exposure to the atmosphere. Thus the encapsulation of the devices of the different layers and the comparison in the stability in the performance of the encapsulated and unencapsulated devices with time was done. For the encapsulation of the devices a thin glass plate was placed on the device array of the substrate with a drop of special epoxy adhesive was kept between the glass plate and device array. The glass plate is gently pressed so that the adhesive spread across uniformly across the device array. The substrate is then given light treatment of 30-40 minutes during which epoxy gets hardened.

Prior and after the encapsulation procedure, the devices are characterized inside the Glove Box to ensure that encapsulation procedure does not cause any degradation of the photovoltaic performance of the solar cells. Devices do not undergo any degradation after encapsulation. The devices are then taken out of the Glove Box and JV characterization of these devices is done under 1 sun input light intensity. In order to study the comparison of the stability in the performance of the encapsulated devices with nonencapsulated devices, a set of devices with no encapsulation is also fabricated and characterized outside Glove Box under 1 sun input light intensity. It has been observed that the nonencapsulated devices undergo degradation in their photovoltaic performance in 120 minutes while the encapsulated show nearly the same photovoltaic performance for a testing period upto 45 days as shown in the Fig. 3.12. Thus the studies on the encapsulation of the polymer solar cells confirm the importance of the encapsulation of the devices for their stable operation for longer period of times.

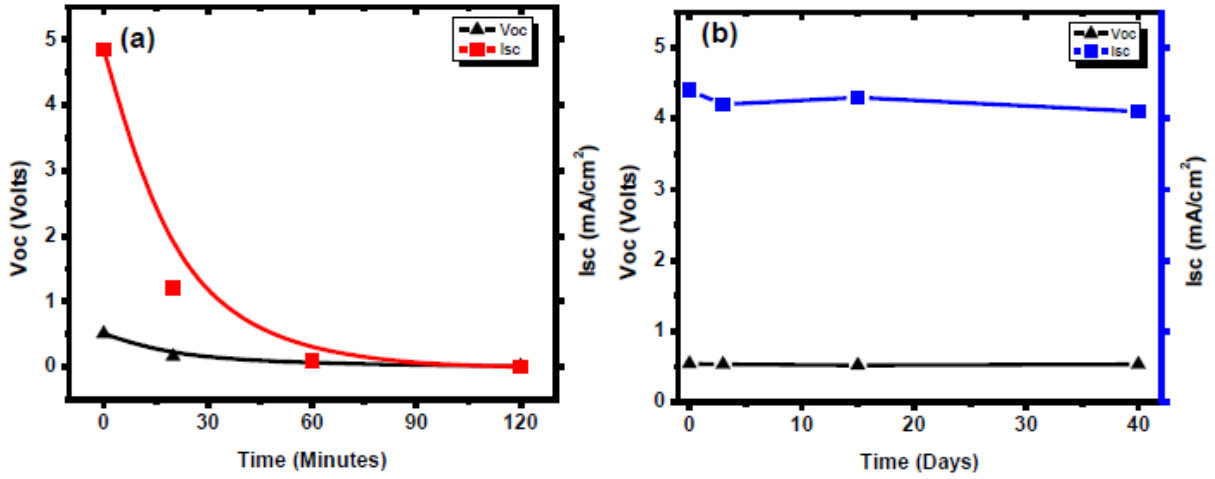


**Fig. 3.12.** Variation of open circuit voltage and short circuit current density with time for (a) unsealed and (b) encapsulated devices.

### 3.4.5 Effect of interface on the photovoltaic performance

The variation in the photovoltaic parameters with the variation in the thickness of the active layer can be attributed to the effects produced by the interfaces between the layers. As evident from the Fig. 3.13, the presence of the interface causes an accumulation of the charge across it because of the resistance offered by the interface to the flow of the charge. Thus even after the formation and dissociation of the excitons across the donor-acceptor interface, the charge transfer is reduced because of the interface between layers which prevents this charge from flowing into next layer. As the number of layers is increased from single to five layers, the trapping of the charge carriers across the interface also increases as the number of interfaces increases with the number of layers. Thus the short circuit current density decreases steadily with the number of layers. On the other hand, the maximum open circuit voltage is achieved with five layers, the reduction of which with decreasing the number of layers can be understood as the internal losses increases with decreasing the number of layers. This has been confirmed by the impedance

spectroscopy measurements which have shown that the internal capacitances, responsible for higher voltage, across the interfaces decrease with decrement in the number of layers. In order to further improve the photovoltaic performance of the PCDTBT:PCBM solar cells at higher thickness we speculated to use thermal annealing or solvent annealing approach. We carried out systematic studies on the variation in the photovoltaic performance of the PCDTBT:PCBM solar cells of different thicknesses with change in the parameters of the thermal annealing and solvent annealing procedure.

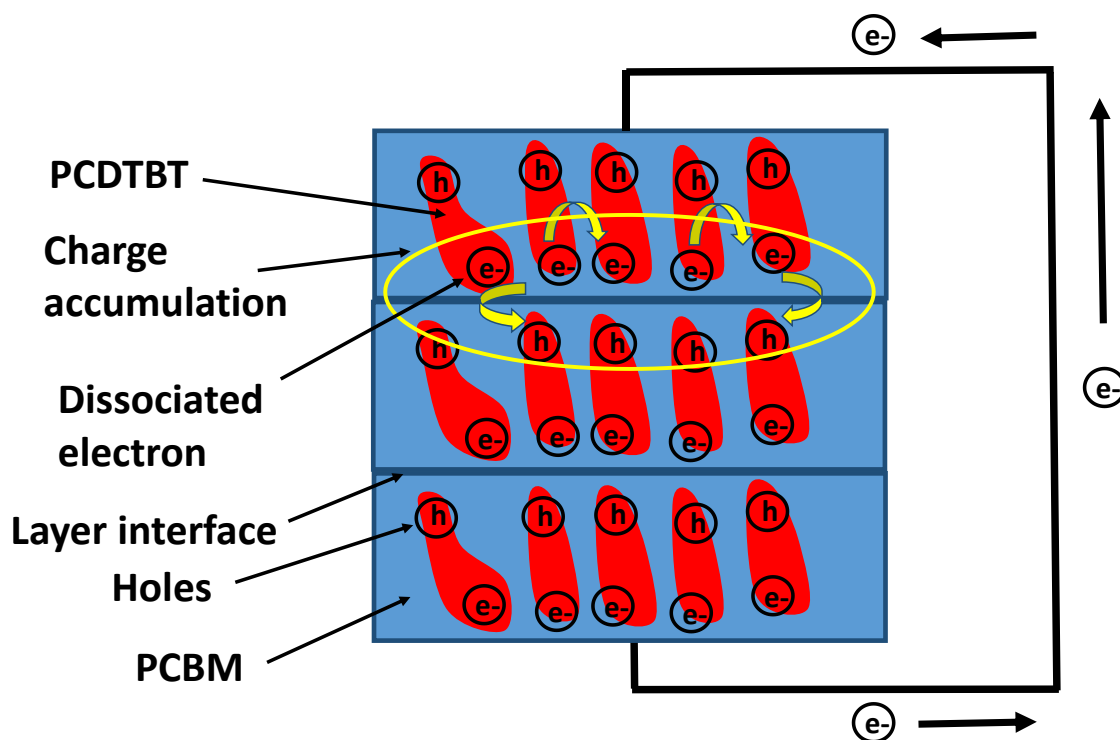


**Fig. 3.13.** Charge accumulation across the interfaces in the various layers of the device.

### 3.4.6 Thermal and solvent annealing of the different layer PCDTBT:PCBM devices

As the number of layers is increased, to further improve the charge transfer across the interfaces and thus the short circuit current density, we carried out thermal annealing in all the set of the

devices with different thicknesses. The earlier studies have already shown that the thermal annealing results in the degradation of the photovoltaic performance of the solar cells. However in order to further study the effects of the thermal annealing on the devices with different layers with different interfaces between these layers, annealing of these devices was carried out for each set of the devices for 4 hours and after each annealing period JV characterization was done. This was done for different number times. As the thermal annealing is increased, the devices with different layers undergo degradation in their JV characteristics. The devices with layers undergo further degradation in their photovoltaic performance has been observed after 16 hours of annealing. The annealing treatment was carried out for a total period of nearly 160 hours. The mechanism for such degradation of the devices with the thermal annealing treatment is already been studied earlier. Thus, in order to improve the performance of the devices, a different approach must be adopted.

In order to improve the short circuit current density in the different layer devices it was speculated that such an improvement can be achieved by dissolving the interfaces between the various layers of the different devices which are speculated to be responsible for the charge accumulation across the interface. For solvent annealing treatment, we again fabricated the different layer devices by the same procedure and carried out the JV characterization of these devices. After the characterization, each substrate was kept in a holder inside a glass beaker consisting of 1 ml of 1,2 -dichlorobenzene at room temperature. The devices were then kept there for 30 s and then JV characterization of the devices was carried out. This procedure was carried out number of times until the devices did not undergo degradation. We observed improvements in JV characteristics of certain devices while other did not show any improvement. The reason of the degradation of the devices, which showed improvement, when

annealing was carried out many number of times was the dissolving of the active layer by the solvent vapours. We also carried similar experiments with chloroform and at different temperatures but due to low boiling point of chloroform the devices showed degradation in their performance as the active layer was dissolved quickly by chloroform even at room temperatures. The experiments and result analysis on solvent annealing of the different layer devices are undergoing.

### 3.4.7 Intensity variation of the input light on the different layer devices

We also carried out the studies on the effects of the variation of the input light intensity on the JV characteristics of the different layer devices. This has been done to determine the injection and the extraction barriers between the HTL and the active layer of the devices. It has been reported that the shape of the S-kink in the JV characteristics of the solar cells is related to the injection and extraction barriers [45]. If the short circuit current density increases with the input light intensity with no change in the increase of the open circuit voltage then it shows the presence of the injection barrier between the HTL and the active layer. However, if there is an increase in the open circuit voltage with the increase in the input light intensity, it shows the presence of an extraction barrier. The presence of these barriers can be related to the shifts in the energy levels of the HTL with the thermal annealing.

**Table 3.3.** Short circuit current density values under the different input light intensities.

<b>Input light intensity</b>	<b>J<sub>sc</sub> (mA/cm<sup>2</sup>)</b>	<b>J<sub>sc</sub> (mA/cm<sup>2</sup>)</b>	<b>J<sub>sc</sub> (mA/cm<sup>2</sup>)</b>	<b>J<sub>sc</sub> (mA/cm<sup>2</sup>)</b>	<b>J<sub>sc</sub> (mA/cm<sup>2</sup>)</b>
------------------------------	---	---	---	---	---

<b>(in sun)</b>	<b>1 layer</b>	<b>2 layer</b>	<b>3 layer</b>	<b>4 layer</b>	<b>5 layer</b>
0.66	4.12	9.58	9.47	7.76	4.35
0.73	4.34	10.25	10.2	8.38	4.59
0.83	5.18	10.87	11.76	9.47	5.18
0.93	5.96	13	12.63	10.35	5.57
1	5.99	13.52	13.57	10.41	5.63
1.1	6.4	13.73	13.88	11.6	5.96
1.2	7.14	14.66	15.23	12.17	6.13
1.4	8.54	14.71	16.12	13.62	6.61
1.5	8.98	15.49	19.28	13.94	6.86
1.8	11.6	20.52	21.2	17.15	7.27
2	12.5	22.45	22.5	18.2	10.2
2.5	14.8	27.5	28.9	24.6	14.2

The input intensities of the incident light were varied from 0.66 sun to 2.5 sun using the AAA solar simulator. All the devices of the different layers have shown an increment in their short circuit current densities as the intensity of the input light is increased as can be seen in Table 3.3. However in all the devices the open circuit voltage has shown a slight improvement with increasing intensity of the input light. It has been observed that for the lower values of the input light intensities the rate of the increment in the short circuit density is high and then improvement in the current density saturates as the input light intensity is increased further beyond 1 sun upto 2.5 sun. Similar effects are been observed for open circuit voltage of all the devices. This effect can be attributed to the recombination of the excitons getting dominant at higher input light intensities due to the formation of more excitons at higher input intensities.

However at lower intensities the exciton dissociation is more dominant than the recombination as less number of excitons are being generated at lower intensities which could undergo recombination with same diffusion path length in the active layer. The other reason that can be speculated for this effect could be the lesser availability of charge carrier generating active layer units due to which as the input intensity goes beyond 1 sun the generation of the charge carriers becomes saturated and there are no charge carrier generating active layer units for charge carrier generation. However this reason can be discarded as the saturation in the rate of increment of the current density occurs at the nearly same point beyond 1 sun input intensity, which should be different for the different layers devices due to their different thickness.

### **3.4.8 Approach for efficiency enhancement in multilayer devices using solvent annealing**

As the efficiency of PCDTBT:PCBM based bulk heterojunction (BHJ) solar cell is limited by the thickness of the active layer and due to the degradation effects of the thermal annealing on the photovoltaic performance, the efficiency enhancement of the BHJ solar cell can be achieved by adopting a mixed approach of use of thicker active layer as well as solvent annealing. The performance of a BHJ solar cell depends upon two crucial parameters i.e. absorption of incident radiation and collection of separated charge carriers. Although the absorption coefficient is material specific, the thickness of active layer can be increased for the better absorption of light[80]. The usual method of layer deposition is spin coating which usually renders imperfect morphologies with aggregations for higher thickness. That is a major reason for the non-uniform absorption of light, charge trapping, Langevin recombination, limited carrier mobilities of the extracted charges, which result in reduced number of photo-generated charge carriers and fill factor and hence, overall reduced device efficiency Therefore, lower thickness values for active layers have been preferred and optimized [81, 82]. In view of this, the mechanisms of charge

generation and charge trapping are a topic of intense research in most of the third-generation solar cell materials. Thus a study was required for the charge trappings at imperfect interfaces in solar cells and their possible remedies.

As PCDTBT has emerged as promising donor material for the fabrication of bulk heterojunction solar cells owing to its low lying highest occupied molecular orbital (HOMO) position which impart high open circuit potential ( $V_{OC}$ ) as well as air-stability to devices [83]. By the use of PCDTBT and appropriate acceptor PCBM, an efficiency >6% has been achieved [84] and further improvement in the efficiency towards theoretical limit is desirable [85]. As discussed earlier, in contrast to P3HT:PCBM based devices, further improvement on PCDTBT based BHJ devices by either thermal annealing or employing thicker active layer has not been successful [86,58]. This is due to amorphous nature of PCDTBT owing to weak  $\pi$ - $\pi$  interaction, which does not get affected by thermal annealing [33, 87]. In addition, this amorphous nature of PCDTBT give rise to intercalated structure when blended with PCBM, which occupy available open spaces between the side chains of the polymer before forming the pure electron transporting PCBM phase [88]. This intercalated structure results in reduced  $\pi$ - $\pi$  interaction in PCDTBT molecules and hinders the phase separation [89]. In order to address the issue, solvent additives have been introduced in blending solutions to control the blend intermixing and morphology during the spin-coating process. This resulted in reduced number of interfaces for recombination of charges and thereby structural ordering in polymer dominating regions, leading to fast charge transport and extraction [90]. In addition to this mixed-solvent, vapor annealing has also been adopted to inhibit intercalation thereby increasing the probability of charged-transfer state dissociation, as well as lifetime and mobility of the carriers [91].

Therefore, an intuitive approach for the layer by layer growth in PCDTBT:PCBM polymer solar cells followed by solvent vapor annealing is attempted for a better understanding of charge trapping and its implications on device efficiency. The results of this approach leads to better understanding of the charge trapping, radiation absorption, and efficiency of PCDTBT:PCBM solar cells using a tandem layered deposition of the photo active blend followed by solvent annealing.

### **3.4.9. Experimental**

As discussed earlier, for fabrication of devices, ITO coated glass having 10  $\Omega$ /square resistivity was taken and patterned (into three linear strips size 3 mm x 25 mm separated by ~4 mm) using chemical treatment by masking with tape and etching the exposed area in an optimized solution of (HCl+HNO<sub>3</sub>+H<sub>2</sub>O) for 30 minutes at room temperature. The etched substrate was cleaned using doubly distilled deionized water, acetone, iso-propanol and dried by blowing pressurized nitrogen. The substrate was then treated with UV-Ozone for 20 minutes prior to deposition of hole transport layer (HTL). 50 nm layer of PEDOT:PSS (Ossila-PH-1000) was spin casted on the substrate at 2500 rpm followed by its annealing for 2 h at 120°C. After annealing the PEDOT:PSS deposited substrate were transferred inside a glove box where oxygen and moisture were controlled within 0.1 ppm level. Each batch of the active layer blend was prepared by mixing of PCDTBT and of PCBM in 1:2 weight ratio in chloroform solvent. The solution was stirred at room temperature using magnetic stirrer for 48 h under dark, this blend was raised to 60°C for 6 h and again stirred for 48 h. The blend was filtered using a 0.45 micron filter. The active layer blend was spin casted on already deposited PEDOT:PSS layer at a spinning speed of 2000 rpm in glove box. The chloroform was preferred as a solvent over dichlorobenzene due to its high vapor pressure and low boiling point, the deposition procedure was quick and the solvent

almost entirely evaporated during the spin casting process. The films were left for about a minute before another layer was deposited with the same spinning speed and solvent concentration. Upto 5 layers were deposited one after another on the substrate. Finally, 100 nm Aluminum electrode were deposited by thermal evaporation (vacuum:  $1 \times 10^{-6}$ Torr) using a shadow mask to yield 3x3 array of devices on a single substrate. The final device configuration was ITO/PEDOT:PSS/PCDTBT:PC<sub>71</sub>BM/Al and the area of each cell was 6 mm<sup>2</sup>. The typical device structure is shown in Fig 3.13. (b). Prior to transferring the device outside glove box, it was sealed using a special epoxy which was cured by UV treatment.

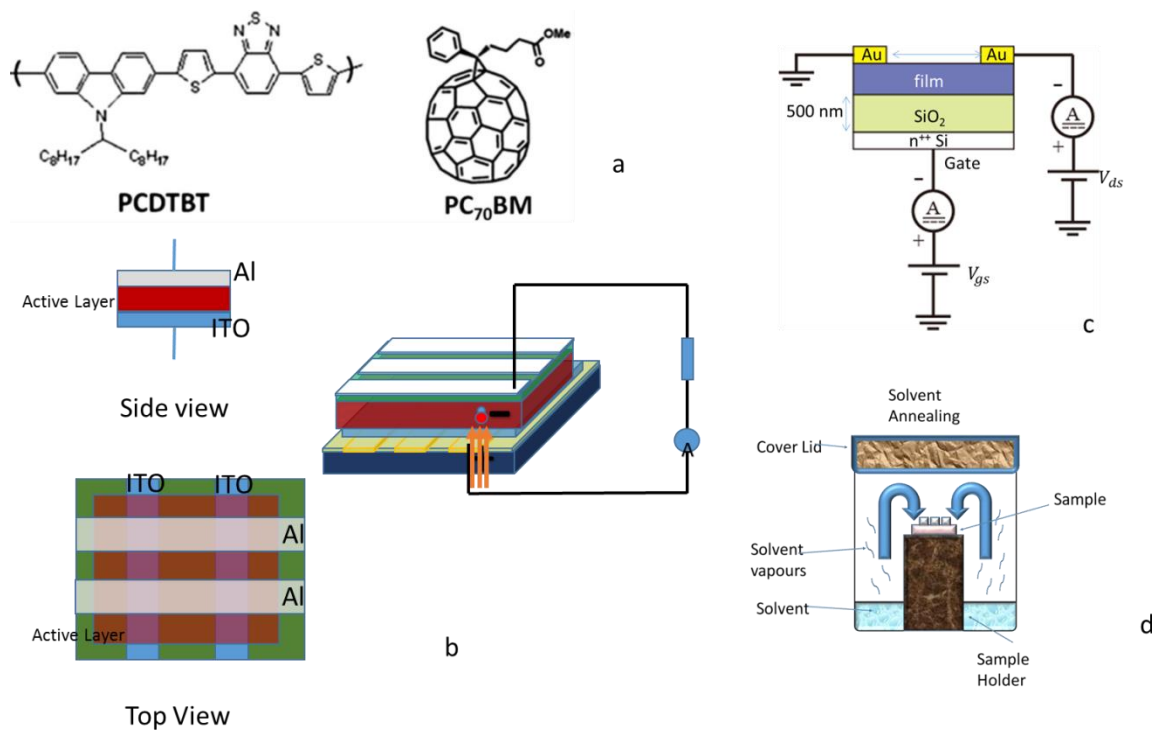


**Fig 3.14.** (a) Chemical structure of PCDTBT and PCBM (b) Typical device structure (c) Bottom Gate Top Contact FET configuration of mobility measurements (d) solvent annealing setup.

For measurement of charge carrier mobilities, the devices were fabricated in Field Effect Transistor (FET) bottom gate top contact geometry. For this purpose, commercially available Si

substrate having 500 nm of thermally grown SiO<sub>2</sub> were taken and cleaned. Then 1-5 layers of active material blend were deposited following method as described above. The typical schematic is shown in Fig 3.13 (c). The transfer (I<sub>DS</sub> vs V<sub>GS</sub> at constant V<sub>DS</sub>) characteristics of the fabricated were measured using standard FET measurement setup using two Keithley 2400 source and in-house developed software. The recorded characteristics are presented in Fig. 5. Field effect hole mobility values (in saturation region) were calculated from the transfer characteristics using the following expression [92]:

$$\mu = \frac{2L}{WC_i} \left( \frac{\partial \sqrt{I_{DS}}}{\partial V_{GS}} \right)^2 \quad (3.1)$$

Where C<sub>i</sub> is the specific capacitance, W is the channel width and L is the channel length and  $\partial \sqrt{I_{DS}} / \partial V_{GS}$  is the slope of the  $\sqrt{I_{DS}}$  vs V<sub>GS</sub> plot.

The UV-Vis spectra were recorded in the range of 300-1000 nm using a JASCO spectrophotometer. The thickness for each layer was estimated using absorption data and re-confirmed by stylus profilometer. Photovoltaic measurements were carried out on AAA Solar Simulator Sciencetech SS 150 calibrated using NREL certified standard Si solar cell. For the impedance spectroscopy measurements, the solar cell were kept at open circuit potential and AC amplitude of 10 mV was applied using PARSTAT impedance analyzer. The spectrum was recorded in 100 mHz to 500 kHz range and analyzed using an equivalent circuit model fitted with ZSimpWin 3.22 software. Some of the films were also subjected to solvent annealing using a set-up shown in Fig. 3.14 (d). The set-up consists of a sample holder inside a lid-covered beaker. The devices were kept in a sample holder and exposed to vapors of 1 ml tetrahydrofuran (THF) at room temperature for 30 s.

### 3.4.10. Results and Discussion

In order to verify the layer by layer deposition of PCDTBT:PCBM blend, UV-Vis spectra were recorded and presented in Fig. 3.15. The typical spectrum consists of four peaks. It is clear from the plots that no significant change is observed in any of the peak positions. All the peaks could be successfully de-convoluted into pristine peaks belongs to each constituent. The similar band features for all plots suggest that there is no aggregation of either PCDTBT or PCBM. A broad band observed at 400 and 550 nm is attributable to the  $\pi$ - $\pi^*$  transition of carbazole moiety and the intra-molecular charge transfer interaction from the carbazole unit to the benzo-thiadiazole unit in PCDTBT, respectively [93]. On the other hand, maxima observed at 380 and 476 nm is assigned to PCBM. These bands are overlapped in the PCDTBT:PCBM blend. Nevertheless, the evolution of 476 nm band may be related to PCBM rich regions whereas that of 550 nm is related to PCDTBT. As expected, the absorbance is increasing linearly and proportionately with the thickness of active layer, suggesting multilayer deposition of blend films resulted in thicker films and therefore absorbs more amount of light as compared with blend films using single layer.

The estimated thickness data obtained is presented in Table 3.4. which was also confirmed independently by stylus profilometer. The first layer of active material, which was deposited over the hole transport layer of PEDOT:PSS, was found to have ~70 nm thickness. The thicknesses for next successive layers were observed to in the range of 52-62 nm. The total thickness for a five layer device was measured to be ~290 nm. The larger thickness of first layer can be attributed to the surface energy difference of the PEDOT:PSS and PCDTBT:PCBM blend. However, the thickness of next layers have been effected due to the deposition using same solvent, as this might tried to dissolve some part of earlier deposited layer.

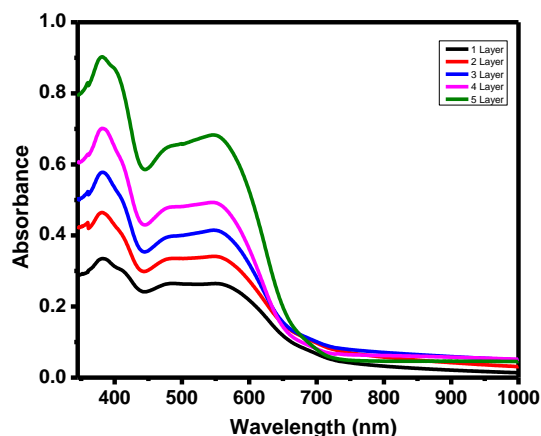


**Fig 3.15.** Optical absorption spectra of single and multilayer films.

**Table 3.4.** Thickness of different layers estimated using optical absorption and profilometry.

Layers	Thickness ( $\pm 5$ nm)
PEDOT:PSS	50
Layer 1	74
Layer 2	56
Layer 3	52
Layer 4	56
Layer 5	62

In order to investigate whether the increment in the thickness indeed aids in light harvesting in BHI solar cell, we recorded the J-V characteristics of various devices under illumination of 1 sun intensity. The recorded curves are presented in Fig. 3.16. and photovoltaic parameters of these devices are summarized in Table 3.5. The best efficiency of  $\sim 3.55\%$  obtained for the devices using single layer is comparable to the efficiencies reported for PCDTBT:PCBM BHI solar cells

fabricated under identical processing conditions [42, 65,66]. It is also inferred from the table that open circuit voltage ( $V_{OC}$ ) increases and, short circuit current density ( $J_{SC}$ ) and fill factor (FF) decreases for devices having higher thickness as compared with single layer devices. The overall effect of this is a monotonous decrease in the efficiency of the device with the thickness.

Though  $J_{SC}$  is expected to increase when the blend layer thickness is increased, we observed a significant decrease in the  $J_{SC}$  for higher thickness films. On the other hand, the  $V_{OC}$  is enhanced when the thickness is increased. The  $V_{OC}$  is determined by the generation rate of the excitons as well density of the defect states according to following equation [94]:

$$V_{OC} = \frac{E_g}{q} - \frac{K_B T}{q} \ln \left( \frac{(1-P(B_L-B_{SRH}))N_{CV}^2}{PG} \right) \frac{n_c}{K_B T} \quad (3.2)$$

where P and G is the dissociation probability and generation rate of the exciton, respectively and  $E_g$  is the effective energy gap,  $N_{CV}$  is the effective density of states, and  $B_L$  and  $B_{SRH}$  are the Langevin and Shockley– Read–Hall (SRH) recombination strengths, respectively .

The increased thickness of the film leads to generation of more charge carriers, which may be one of the reasons behind improved  $V_{OC}$ . In addition, the enhancement in the  $V_{OC}$  may be related to enhanced recombination into the triplet states, resulting in increment in the energy of the charge transfer states [95]. The one possible reason for reduction in short circuit current for higher thickness devices could be the trapping of charges at the interfaces which would act as traps for the photo-generated carriers. Solvent annealing experiments were performed to study the charge trapping and THF solvent was used for this purpose. The photovoltaic parameters of all solvent annealed films are presented in Table 3.6. The J-V characteristics for two extreme cases (1 and 5 layers) are presented in Fig 3.15. (b) It is evident on comparison that when the

films of higher thickness were solvent annealed in THF vapors an improvement in all photovoltaic parameters was observed. An enhanced device efficiency~3.9% of devices from 1.53% is observed for 290 nm thicker device. This may arise due to improved morphology of the blend which reduces the recombination and therefore results in improvement in enhanced  $J_{SC}$  and FF and therefore, an overall improvement in the efficiency.

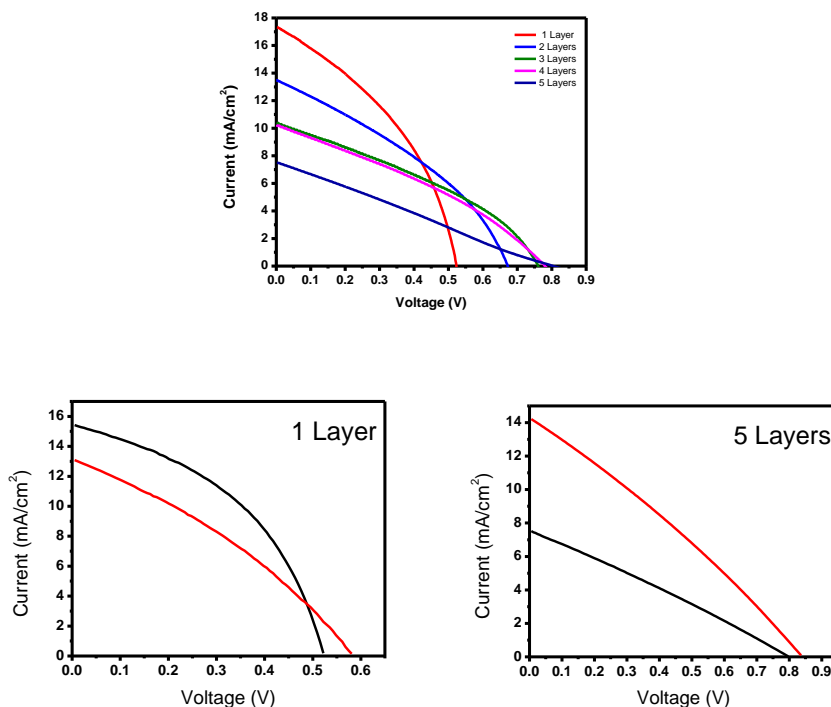


**Fig 3.16.** J-V characteristics of (a) different layers devices under 1 sun (b) for single layer device before and after solvent annealing (c) for multilayer device before and after solvent annealing (red plots for solvent annealed films).

**Table 3.5.** Summary of photovoltaic parameters of BHJ solar cells with different layers under input intensity of 100 mW/cm<sup>2</sup>.

Thickness	Composition	$V_{OC}$	$J_{SC}$	$V_p$	$I_p$	FF	Efficiency
-----------	-------------	----------	----------	-------	-------	----	------------

(±10) nm		(V)	(mA/cm <sup>2</sup> )	(V)	(mA/cm <sup>2</sup> )	(%)	(%)
70	1 Layer	0.52	17.33	0.33	10.84	39.26	3.55
130	2 Layer	0.67	13.49	0.42	7.63	35.14	3.18
180	3 Layer	0.76	10.35	0.53	5.22	35.06	2.78
230	4 Layer	0.78	10.24	0.47	5.58	32.61	2.61
290	5 Layer	0.80	7.51	0.39	3.98	25.39	1.53

**Table 3.6.** Device parameters for different layer devices at input intensity of 100 mW/cm<sup>2</sup> (after solvent annealing).

Thickness (±10) nm	Composition	V <sub>oc</sub> (V)	J <sub>sc</sub> (mA/cm <sup>2</sup> )	V <sub>p</sub> (V)	I <sub>p</sub> (mA/cm <sup>2</sup> )	FF (%)	Efficiency (%)
70	1 Layer	0.58	13.08	0.35	10.06	44	2.52
130	2 Layer	0.73	10.21	0.46	6.22	38	2.84
180	3 Layer	0.75	11.78	0.43	6.15	36	3.18
230	4 Layer	0.79	14.24	0.42	7.68	29	3.23
290	5 Layer	0.83	14.21	0.45	7.64	29	3.9

**Table 3.7.** Impedance Spectroscopy of different layered devices.

	As deposited		After solvent annealing
	Single Layer	Five Layers	Five Layers
<b>R<sub>0</sub>(Ω cm<sup>2</sup>)</b>	37.94	85.87	96.9
<b>R<sub>1</sub>(Ω cm<sup>2</sup>)</b>	2783	2539	5169
<b>C<sub>1</sub> (nF cm<sup>2</sup>)</b>	17	63	7.99
<b>n</b>	0.94	0.91	0.885
<b>R<sub>2</sub>(Ω cm<sup>2</sup>)</b>	-	2700	-

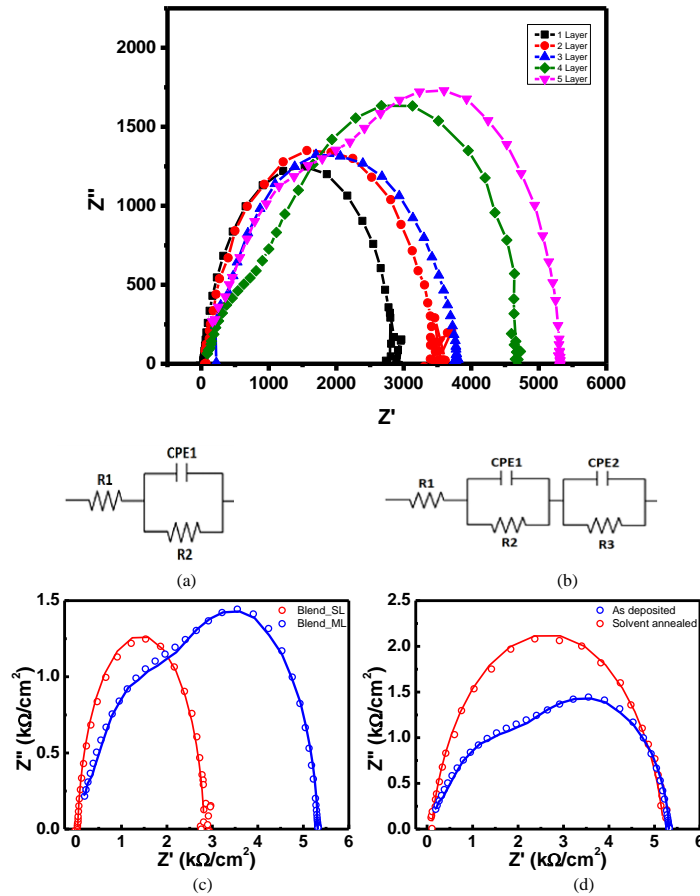


**Fig. 3.17.** Impedance spectra of BHJ solar cells for 1- 5 layer devices, equivalent circuit models used for fitting the impedance spectra for (a) thin and (b) thick active layer, respectively. Impedance spectra of devices having (c) active layer of different thickness and (d) thick active layer after solvent annealing, under illumination of 1 sun intensity.

To further understand the improvement in efficiency in higher thickness devices after solvent annealing, we have carried out impedance spectroscopy at 1 sun illumination. The Nyquist plots of devices under illuminated conditions are shown in Fig. 3.17. The Nyquist plots are complex plane representations of the imaginary part of the impedance  $Z''$ , and the real part of

the impedance,  $Z'$ . Devices exhibited a single semi-circle in the complex plane for single active layer, whereas a second partial arc gradually appeared at high frequencies in devices with higher thickness of active layers. In addition, the intersection of the semicircle with  $Z'$  axis occurs at increased resistance at low frequency and approximately similar resistance value  $\sim 85 \Omega$  at low frequency. The gradual appearance of second semicircle corresponding to additional time constant (capacitance) emphasized the charge holding capacities of the multilayer devices at the interface layers. We have modeled these data using a simple equivalent circuit, consisting of a resistor ( $R$ ) in series with a resistor  $R_1$  and capacitor  $C_1$  in parallel, and various parameters derived from this model are represented in Table 3.7. The value of resistance  $R$  represents the resistive losses occurring in ITO, PEDOT:PSS whereas the resistance  $R_1$  in parallel with constant phase element  $Q_1$  is attributable to recombination process occurring at the interface of donor and acceptor. Correspondingly,  $R_1$  is attributable to the bulk resistance of the active layer i.e. recombination resistance and is a measure of whether the photo-generated charge carriers will be efficiently collected at the electrodes or be lost to bimolecular recombination [96] and the value of CPE, on the other hand related to a chemical capacitance owing to photo generated charge carriers accumulated in the fullerene phase within the active layer and provides information about DOS in fullerene LUMO states ( $E_{Fn}$ ) [97]:

$$C_{\mu} = e^2 \frac{\partial n}{\partial E_{Fn}} = e^2 \frac{n_c}{k_B T} \quad (3.3)$$

where  $C_{\mu}$ ,  $n_c$  and  $E_{Fn}$  is the chemical capacitance per unit volume, electron concentration, and quasi-Fermi level due to the rise of the electron Fermi level in the acceptor LUMO. Since Fermi level of donor HOMO ( $E_{Fp}$ ) remains almost unchanged under 1 sun illumination,  $C_{\mu}$  influences the final value of  $V_{OC}$  in the device.

As evident by the table, the value of  $R_0$  for devices having thicker active layer and could arise due to resistive losses occurring at various interfaces. On the other hand,  $R_1$  is slightly increased when the thickness of the active layer is increased, suggesting the resistive losses in thicker active layer. Owing to this enhanced bulk resistance, the effective number of collected photo-generated charge carriers is reduced and thereby contributing to decreased short circuit current. On the other hand, the value of  $C_1$  is increased due to more occupancy of photo-generated charge carriers, which effectively raises the Fermi level of PCBM and therefore results in enhanced  $V_{OC}$ . Other than this, an additional feature that consists of a small arc appears when thicker active layers are used for device fabrication and therefore, two additional elements  $R_2$  and  $C_2$  are required to fit these spectra. The high frequency resistor  $R_2$  represents an absolute loss of the photo-generated power owing to this additional resistance, reciprocal of  $\partial J/\partial V$  increases and therefore FF reduces [98]. The extra component of capacitance  $C_2$  has emerged due to trapping (holding) of the photo-generated carriers at the interfaces. This fact has been proven as after solvent annealing the extra capacitance has been removed.

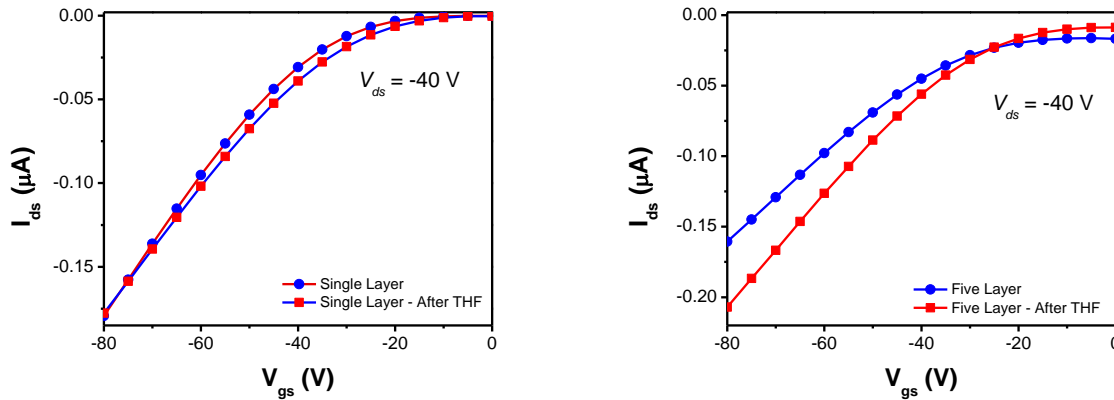


**Fig 3.18.** FET transfer characteristics of single layer and 5-layer PCDTBT:PCBM films.

The charge carrier trapped at the interfaces should have an adverse effect on the carrier mobilities. Therefore, to confirm charge trappings, mobility measurements were planned and performed on the single and multilayer devices. The estimated mobilities from transfer characteristics of single and five layers are presented in Table 3.8. It is clear that as number of layer increases from one to five, the hole mobilities was reduced from  $1.28 \times 10^{-4}$  to  $7.36 \times 10^{-5} \text{ cm}^2/\text{Vs}$  (Fig. 3.18). That can be related directly to increased capacitance values of multilayer devices which reflect that charge holding capacities and multiple scatterings at the interfaces. When a multiple layer device was given identical THF treatment, a significant enhancement was observed and it increased from  $7.36 \times 10^{-5}$  to  $1.19 \times 10^{-4} \text{ cm}^2/\text{Vs}$ . However, for single layer devices the mobility value was marginally reduced. Thus the THF treatment has enhanced the mobilities which confirms that extra capacitance is being observed due to charge holding at the interfaces.

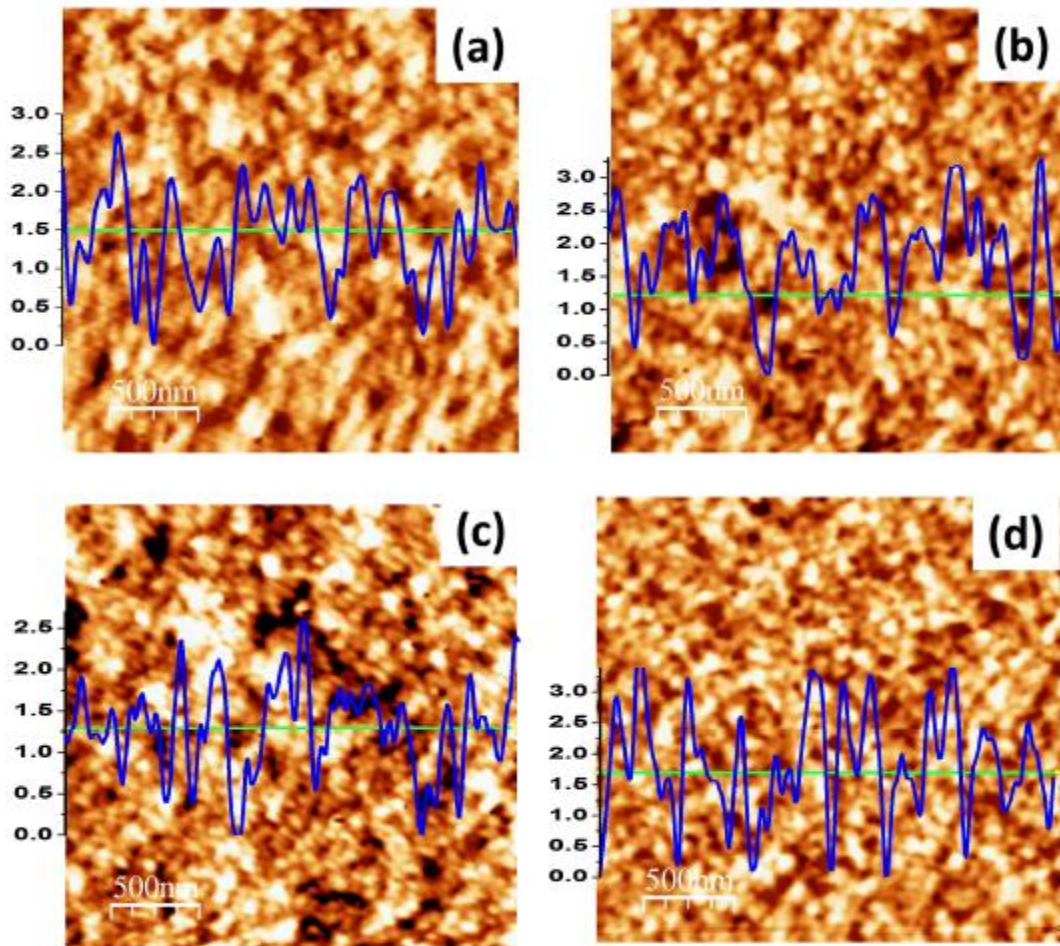


**Fig 3.19.** AFM images of the PCDTBT films before solvent annealing (a) single layer and (b) thick active layer and after solvent annealing (c) single layer and (d) thick active layer.

**Table 3.8.** Hole mobilities in single and five layer device.

	<b>Single Layer</b>	<b>Five Layer</b>
<b>Pristine</b>	$1.28 \times 10^{-4} \text{ cm}^2/\text{Vs}$	$7.36 \times 10^{-5} \text{ cm}^2/\text{Vs}$
<b>After THF</b>	$1.12 \times 10^{-4} \text{ cm}^2/\text{Vs}$	$1.19 \times 10^{-4} \text{ cm}^2/\text{Vs}$

### 3.5. Conclusions

The effect of charge trapping at interfaces in polymer solar cells was investigated in PCDTBT:PC<sub>71</sub>BM based polymer solar cells. The active layer thickness of devices was varied

and charge trapping centers were deliberately created following the approach of layer by layer growth. It has been observed that the open circuit voltage ( $V_{OC}$ ) gradually increases from 0.52 V for a single layer device to 0.80 V for a multilayer (5 layers) device. Absorption of solar energy is a crucial step for any photovoltaic device and as the thickness was increased more light was absorbed in the solar cell, However, the efficiency has not increased in this proportion but reduced. The main reason for this reduction is the short circuit current density ( $J_{SC}$ ) which found to decrease from 17.33 to 7.51 mA/cm<sup>2</sup>. Due to this reduction in current density the efficiency of multilayer devices is reduced down to 1.53% from 3.55%. This shows that enhancement due to absorption has been countered by increased losses in these devices. It has been inferred that  $J_{SC}$  is not limited due to external fields but a pronounced recombination process due to charge trapping is hindering a significant fraction of the separated charge to reach respective electrodes. This charge trapping at the interfaces was confirmed by impedance spectroscopy and mobility measurements. The solvent annealing of the thick active layers by THF vapors results elimination of charge trap and thereby leading to improvement in all photovoltaic parameters and therefore, results in overall efficiency improvement to 3.9% as compared to 1.53% (before solvent annealing). The efficiency improvement has been attributed to the suppression of the resistive losses occurring at various interfaces of the active layer as supported by impedance spectroscopy measurements.

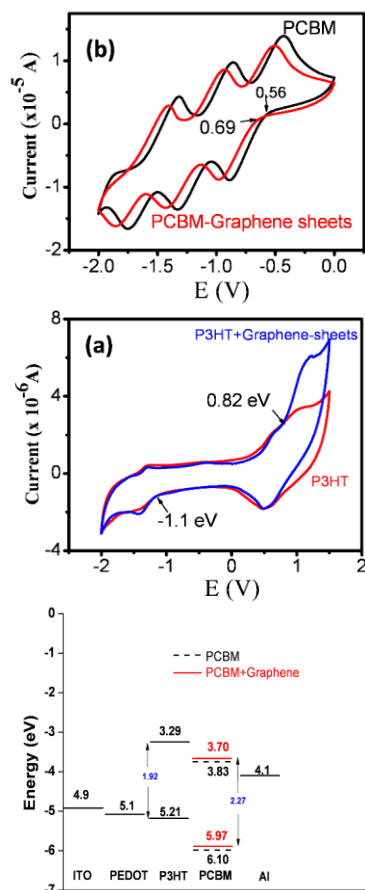
In summary, an overall improvement in the efficiency of PCDTBT:PCBM based bulk heterojunction (BHJ) solar cell is demonstrated by using a mixed approach of using thick active layer as well as solvent annealing. The use of thicker active layer of 290 nm as compared to thin active layer of thickness 75 nm allows enhanced light harvesting but also resulted in an increased recombination due to presence of charge traps. The impedance spectroscopy confirmed that

major problems associated with lower efficiency for higher thickness devices could be charge trapping at the interfaces, which is related to roughening of interior morphology. This has been successfully proved by a deliberate creation of imperfect interfaces between successive layers. The solvent annealing of the thick active layers by tetrahydrofuran vapors results in the elimination of charged trap and thereby leads to the improvement in all photovoltaic parameters and overall efficiency improvement of 3.9% as compared to 3.55% for device using thin layer. The efficiency improvement has been attributed to the suppression of the resistive losses occurring at various interfaces of the active layer as supported by impedance spectroscopy measurements.

## Chapter 4

### Efficiency enhancement in BHJ solar cells using graphene nanosheets

---



#### Highlights

1. Efficiency enhancement in P3HT:PCBM and PCDTBT:PCBM solar cells using graphene nanosheets in the active layer of solar cells.
2. The cyclic voltammetry technique has revealed the chemical  $\pi$ - $\pi$  interaction that PCBM undergoes when graphene is used with PCBM which shifts the energy levels of PCBM, with HOMO shifting from -6.10 eV to -5.97 eV.
3. The shifts in the energy levels improved the open circuit voltage of the P3HT:PCBM solar cells which improved the photovoltaic performance of the solar cells.
4. The addition of graphene sheets in the active layer have also shown improvement in the photovoltaic performance of P3HT:PCBM solar cells due to the improved packaging of the active layer.

---

*\*part of the work has been published in AIP Conf. Proc. 1665, 050122 (2015) and Appl. Phys.*

*Let. 104 (2014) 133901.*

---

## 4.1 Introduction

One of the reasons for the low efficiency in the polymer solar cells is attributed to the large band gap in the polymer solar cells. The low band gap polymers cover more spectrum of the incident light upto the longer wavelength because of the direct dependency of the energy of the photons on longer wavelength end of the spectrum on the band gap of the materials used as the active layer. The donor type polymer which has been widely used in the active layers of the solar cells is P3HT [99, 100] with which the efficiencies have been reported upto 2-6% [101, 102, 103]. For a long time fullerene based derivatives like PCBM have used as the acceptor materials in combination with P3HT shown in bulk heterojunction solar cells. But it has been argued that such fullerene based acceptor materials may have to be optimized with tuning its properties in order to give better photovoltaic performance. It has also been proposed that other materials like carbon allotropes, nanotubes or graphene can be used as acceptor material in the polymer solar cells [103,104,105]. We speculated that instead of complete replacement of PCBM with such materials based on carbon, the better approach would be to use a combination of both PCBM and a carbon based material as an acceptor material. Such combination must be first studied for its variation in the properties and then an appropriate optimized combination must be used which would give better photovoltaic performance as compared when both of these materials were used alone as acceptor material in P3HT:PCBM solar cells.

In our studies we aimed at finding the way to tune the properties of PCBM in order to enhance the performance of P3HT:PCBM solar cells. One such property is the LUMO of PCBM which plays important role in the open circuit voltage and the absorption of the spectrum of the light incident on it. For this we used graphene to be used along with PCBM as an acceptor material in the P3HT:PCBM solar cells. Graphene after its functionalization has been used and

reported [106,107,108,109, 110,111,112,113,114]to be used as an additive in the P3HT:PCBM solar cells. However, in all the previous attempts the improvements in the efficiency has been reported to be 1.22% in case of the fullerene grafted graphene in polymer solar cells [115,116]. Others have reported efficiencies of 0.44% and 1.05% using either graphene with fullerene or a mixture of graphene with carbon nano tubes [105]. The studies also aimed at using this approach for the P3HT:PCBM solar cells fabricated on the flexible substrates as the large scale production of the polymer solar cells is done using the flexible substrates and the efficiencies of these solar cells have been reported to be low [117,118,119,120,121,122,123].

This has led us to investigate graphene in the mixture of PCBM to be used as an acceptor type material for the P3HT:PCBM solar cells. However, in our approach we have developed the composites of the graphene and PCBM rather than just a mixture of the graphene and PCBM. This has been done in order to investigate the chemical  $\pi$ - $\pi$  interaction [124,125] that PCBM undergoes when graphene is used with PCBM. Also we fabricated the P3HT:PCBM solar cells on the flexible substrate PEN coated with ITO with efficiencies achieved upto 2.51%.

#### **4.1.1 Preparation of graphene for graphene-PCBM composite as acceptor type material**

We have prepared the graphene-PCBM composite by using thin sheets of graphene and thin flakes of graphene, each prepared in separate ways. Thus we have two types of composites – graphene sheet:PCBM composite and graphene flake:PCBM composite. In order to prepare these graphene-PCBM composites we kept the suspension of 0.1 mg of graphene flakes in 10 ml of DCB for a period of 20 days for ultrasonication (30kHz, 250 W). The graphene flakes which were used in the graphene flake:PCBM composite were used as such in the composite preparation. However the thin graphene sheets to be used in the graphene sheet:PCBM

composite were derived from the graphene flakes through the ultrasonication by breaking the graphene flakes into thin sheets of graphene. This is a simple exfoliation process gives the thin sheets of graphene. These thin sheets were then further filtered using 0.2  $\mu$  filter before adding into the PCBM to form the graphene:PCBM composite.

#### **4.1.2 Fabrication of the P3HT:PCBM solar cells**

All the procedure of fabrication of the P3HT:PCBM solar cells was carried out inside MBraun Glove Box, with inert atmosphere having oxygen and moisture < 0.1ppm. The fabrication of the P3HT:PCBM solar cells has been done in both glass substrates and flexible PEN substrates, for their better thermoelectric properties [126], using the graphene:PCBM composite in both types of the solar cells. The architecture of the solar cell consists of PEN/PEDOT:PSS/P3HT:PCBM/Al, each layer of material deposited upon other with optimized thicknesses. ITO coated on the substrates with thickness of 100nm are having the resistivity of 12 ohm/sq. These ITO coated substrates were cut into size of 25mm  $\times$  25mm for device fabrication. The optimized thicknesses for the various layers are – 120 nm of PEDOT:PSS, 100nm of P3HT:PCBM (including graphene sheet:PCBM and graphene flake:PCBM) and 70 nm of Al deposited through evaporation technique. The ITO on the substrates was etched into three strips per substrate through chemical etching process using a mixture of HNO<sub>3</sub>:H<sub>2</sub>O:HCl in 1:10:1 as an etchant for 30 minutes. The substrates were then thoroughly cleaned by ultrasonicing them in the soap solution, de-ionized water, high purity grade acetone and finally with methanol each for 15 minutes. The cleaned substrates were then dried with ultra pure nitrogen gas and given UV- Ozone treatment for 20 minutes. The substrates were then coated with a layer of PEDOT:PSS (HTL) of thickness nearly 120 nm using spin coating technique and thermally annealed for 120 minutes at the temperature of 120<sup>0</sup>C before transferring into Glove

Box. After thermal annealing, a layer of P3HT:PCBM active layer (100 nm) was coated on the substrates using the spin coating inside the Glove Box. The active layers consisting of P3HT and graphene sheet/PCBM composite and P3HT and graphene flake/PCBM composite were deposited with same thickness in the similar fashion on the substrates inside the Glove Box. The concentration of the P3HT and PCBM in DCB used was 18. mg/ml and 20 mg/ml with 200  $\mu$ l/ml of filtered DCB consisting of graphene sheets. The active layer coated substrates were the left for drying overnight in the Gove Box. After the active layer deposition, Al (thickness nearly 70 nm) was deposited on the substrates through thermal evaporation inside the Gove Box at ultra low pressure of  $6 \times 10^{-6}$  mBar. The fabricated devices consisted of 9 device pixels each with an area of  $6 \text{ mm}^2$  in each substrate.

### **4.1.3 Characterization of the P3HT:PCBM solar cells and graphene composites**

The morphological, IV, CV and impedance spectroscopy characterization of the P3HT:PCBM solar cells, P3HT:PCBM films, P3HT:PCBM-graphene composite films has been done to study the chemical interaction of graphene with PCBM and its effects on the photovoltaic performance, morphology and JV characteristics of the P3HT:PCBM solar cells.

#### **4.1.3.1 Cyclic Voltammetry**

In order to understand the chemical interaction of graphene on P3HT and PCBM, cyclic voltammetry was carried out. Since the band gap between the P3HT and PCBM depends on the difference of the HOMO of P3HT and LUMO of PCBM, cyclic voltammetry is an effective tool for the study of any changes in such levels [127, 128]. From CV measurements in Fig. 4.1., it can be seen that graphene is non-interacting with P3HT as both the onset of redox peaks for P3HT and P3HT-graphene sheets is same at 0.82 eV and -1.1 eV. However with PCBM and PCBM-

graphene sheets composite a shift in the onset of the first reduction peak has been found from 0.56 eV to 0.69 eV which shows that there is  $\pi$ - $\pi$  interaction between PCBM and PCBM-graphene composites.

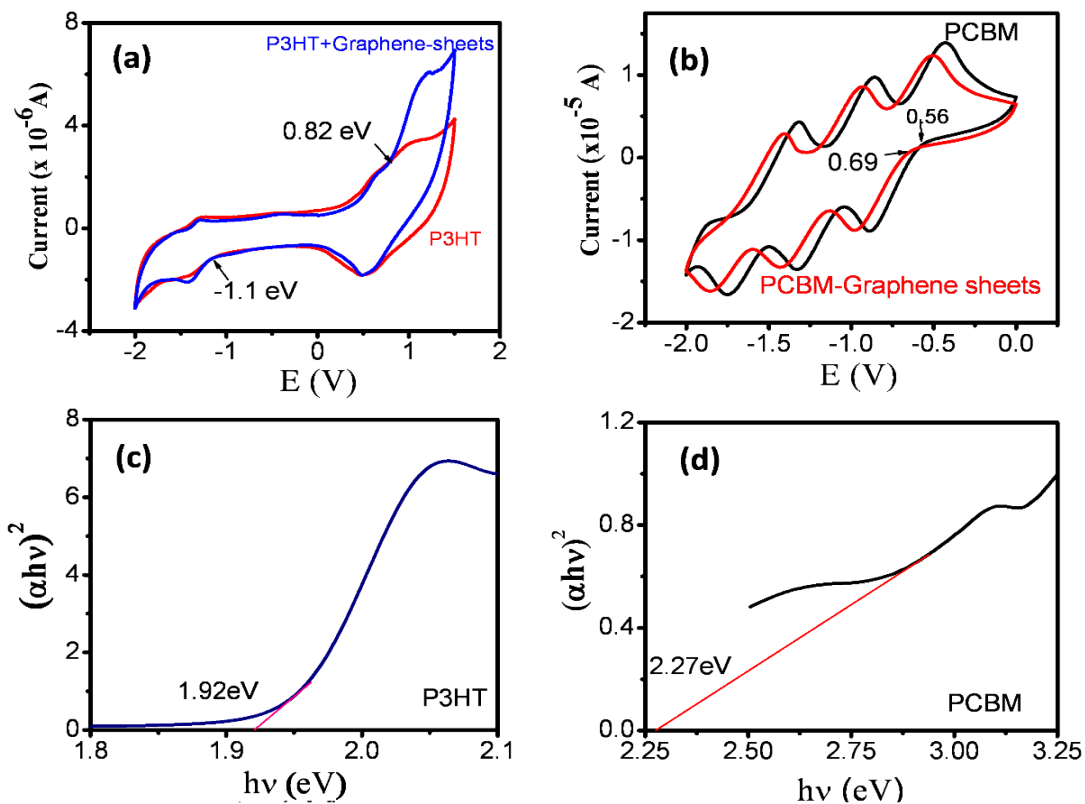


**Fig. 4.1.** Cyclic voltammograms recorded for the solution of (a) P3HT and P3HT + graphene-sheets and (b) PCBM and PCBM + graphene-sheets.  $(\alpha hv)^2$  vs  $h\nu$  plots obtained for (c) P3HT and (d) PCBM films.

Such shift in the onset of the reduction potential of PCBM is further directly related to the shift in the energy levels of the PCBM when graphene sheets are added to it. This can be understood by the relation between energy levels of PCBM with redox potential values given by:

$$E_{\text{LUMO}} = [(E_{\text{red}} - E_{1/2(\text{ferrocene})}) + 4.8] \text{ eV} \quad (4.1)$$

$$E_{\text{HOMO}} = [(E_{\text{ox}} - E_{1/2(\text{ferrocene})}) + 4.8] \text{ eV} \quad (4.2)$$

where  $E_{\text{ox}}$  and  $E_{\text{red}}$  are the onsets of oxidation and reduction potentials, respectively.

The value of  $E_{1/2(\text{ferrocene})}$  was chosen as 0.41, an average of redox ferrocene peaks recorded at 0.37 and 0.44 V. Ferrocene is used as an external standard while carrying the CV measurements.

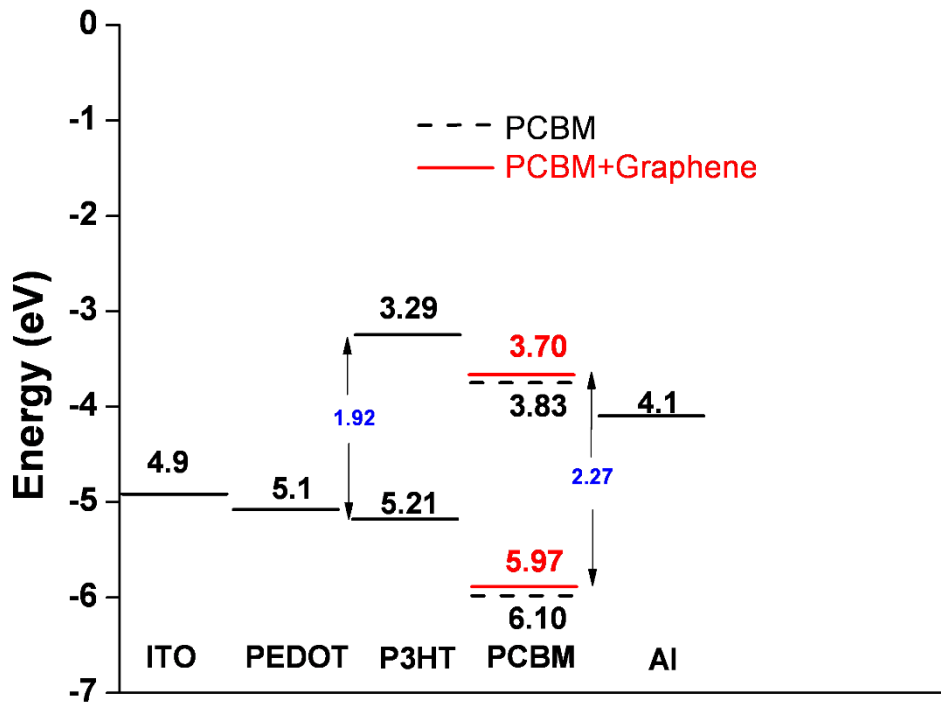


**Fig. 4.2.** Energy level diagrams for the solar cell structures:ITO/PEDOT/P3HT:PCBM/Al and ITO/PEDOT/P3HT:PCBM-graphenesheets/Al.

In order to confirm this, we also carried out UV-Visible spectroscopy to measure the energy gap. It has been found out that there is shift in the energy levels of PCBM, with HOMO shifting from -6.10 to -5.97 eV and LUMO shifting from -3.83 to -3.70 eV, as shown in Fig. 4.2. However

since there is no chemical interaction between the P3HT and graphene sheets, so no shift in the energy levels of P3HT has been found out. The change in the HOMO of the PCBM when added with graphene sheets has been established as there is no change in the band gap of the PCBM even after adding graphene sheets in it.

Such shift in the energy levels of PCBM after the addition of graphene sheets in it has an advantageous impact on the open circuit voltage of the P3HT:PCBM-graphene solar cells. As the open circuit voltage is directly depending on the difference of the HOMO of the P3HT and LUMO of the PCBM, which is given by

$$V_{OC} = 1/e (-|E_{HOMO}^D| + |E_{LUMO}^A|) - 0.3 \text{ V} \quad (4.3)$$

Where 0.3 V, empirical value represents losses due to charge transfer [129,130].

This establishes that the open circuit voltage of the devices based on P3HT:PCBM-graphene should be higher as compared to that of P3HT:PCBM devices.

#### **4.1.3.2 Morphological characterization**

We also carried out the AFM studies on the morphology of the active layer of P3HT:PCBM and P3HT:PCBM-graphene using Atomic Force Microscope (AFM) (Nanonicsmodel MV-4000). The AFM microscopy images as shown in Fig. 4.3.has revealed that in the films of P3HT:PCBM-graphene, the rms roughness is 3.2 nm, while in case of the P3HT:PCBM, it is higher upto 4.2 nm. Thus, there is better packing of the active layer offered by the addition of graphene sheets in the active layers. Such an improved morphology can be attributed for the smooth charge transfer in the P3HT:PCBM-graphene solar cells as compared to that P3HT:PCBM solar cells thus could give higher short circuit current density.

### 4.1.3.3 Raman characterization

The presence of the filtered graphene sheets in the DCB is confirmed by carrying out Raman spectroscopy as shown in the Fig. 4.3. It can be seen from the Fig. 4.3. that there is presence of peaks at  $1380$  and  $1450\text{ cm}^{-1}$  corresponding to the presence of P3HT and  $1430$ ,  $1465$ ,  $1573\text{ cm}^{-1}$  corresponding to PCBM. With these peaks, shifted peaks of G-band position ( $\text{sp}^2$  carbon) from  $1587\text{ cm}^{-1}$  to  $1571\text{ cm}^{-1}$  and D-band position ( $\text{sp}^3$  carbon) has been found [131, 132]. This shows the presence of graphene in the active layer as well as the shift shows that there is strong chemical interaction between the graphene and PCBM in the active layer.

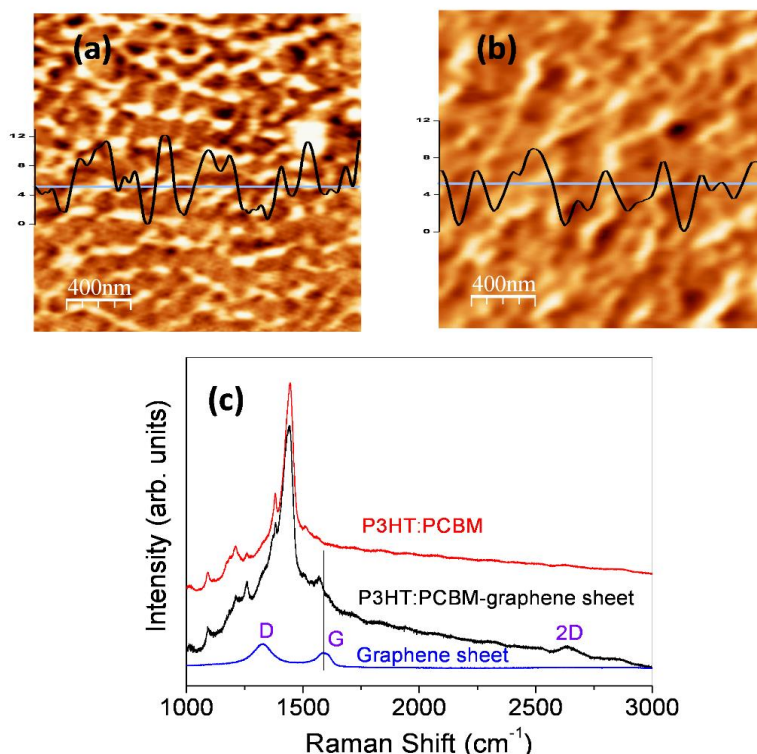


**Fig. 4.3.** AFM images of active layer blend films of (a) P3HT:PCBM and (b) P3HT:PCBM-graphene-sheets. The shown line profile is scaled in nm. (c) Raman spectra recorded for the films of pure graphene-sheets, P3HT:PCBM and P3HT:PCBM-graphene c

#### 4.1.3.4 JV Characterization

The JV results of P3HT:PCBM and P3HT:PCBM-graphene are shown in Fig. 4.4. Addition of graphene sheets in the active layer decreases the series resistance of the across the film from 63 to 27  $\Omega$  (Table 4.1). On the other hand, the shunt resistance value is improved from 1.17 to 4.26 k $\Omega$ . Also, open circuit voltage has higher value of 0.76 V in case of the solar cells based on P3HT:PCBM-graphene sheet as compared to that of 0.67 V of P3HT:PCBM solar cells. This enhancement of the open circuit voltage is already predicted by the change in the energy levels of the PCBM after the addition of graphene sheets into it.

**Table. 4.1.** Summary of various photovoltaic parameters obtained for flexible bulk-heterojunction solar cells using different active layer.

Active Layer	V <sub>OC</sub> (V)	J <sub>SC</sub> (mA/cm <sup>2</sup> )	Fill Factor (%)	Efficiency (%)	R <sub>S</sub> ( $\Omega$ )	R <sub>P</sub> (k $\Omega$ )
P3HT:PCBM	0.67	5.6	33	1.23	63	1.17
P3HT:PCBM-graphene sheets	0.76	7.2	46	2.51	27	4.26
P3HT:PCBM-graphene flakes	0.52	1.03	32	0.91	178	2.15

In addition to the open circuit voltage, the FF has also improved in case of the P3HT:PCBM-graphene sheets from 33 to 46%. As predicted from the improved morphology of the P3HT:PCBM active layer due to the addition of graphene sheets in it, we also observed an improvement in the short circuit current density from a value of 5.6 to 7.2 mA/cm<sup>2</sup>. However

there are two mechanisms that determine the efficient charge transfer across the active layer to the electrodes which finally determines the short circuit current density of the device. The first mechanism being the dissociation of the charge at the donor-acceptor interface which depends upon the energy difference of LUMO levels of donor and acceptor. A threshold value of 0.8 eV is proposed for the same, however, in case of the P3HT:PCBM-graphene due to the shifting of the LUMO in case of the PCBM, this difference has increased to 0.13 eV. This increase in the difference of LUMO levels of the P3HT and PCBM decreases the probability of the dissociation of the exciton across the P3HT and PCBM interface. This mechanism causes a reduction in the charge transfer across the interface and thus the short circuit current density. However, the improved packaging of P3HT:PCBM due to addition of graphene sheets in the active layer improves the charge transfer across the interface resulting in the higher short circuit current density. Since there is an overall improvement in the short circuit current density, this shows that the improved morphology of the active due to addition of graphene sheets into the active layer has compensated for the decreased probability of the exciton dissociation across the interface due to higher difference in the LUMO levels of the P3HT and PCBM [133].

An improvement in the shunt resistance  $R_p$  which shows reduction in the losses [134, 135] and decrement in the series resistance  $R_s$  has also been found. These effects can again be attributed to the better packaging of the films due to graphene sheets which provides a direct path for charge transfer rather than hopping mechanism of charge transfer usually found in the P3HT:PCBM solar cells [136].

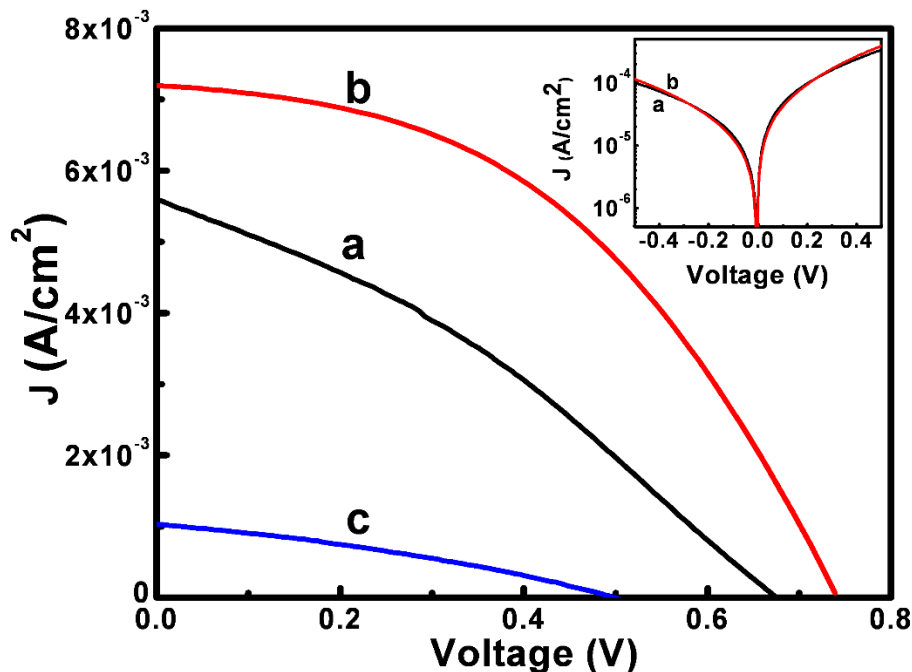


**Fig. 4.4.** JV characteristics for the bulk heterojunction solar cells fabricated using different active layers: (a) P3HT:PCBM, (b) P3HT:PCBM-graphene-sheets, and (c) P3HT:PCBM-graphene-flakes. The inset shows the dark current for (a) P3HT:PCBM and (b) P3HT:PCBM-graphene-sheets based devices.

#### 4.1.4 Efficiency enhancement in PCDTBT:PCBM using graphene nanosheets

Experiments were also carried out to improve the efficiency of PCDTBT:PCBM solar cells using thinner graphene sheets as an additive in the hole transport layer (HTL) and active layers of these solar cells. The required graphene nanosheets were exfoliated by mechanical process using rigorous ultrasonication of graphene flakes. It has been found that devices with graphene nanosheets mixed in the HTL have shown improvement in the efficiency, however

other devices shown a degradation. The improvement in the efficiency in the devices has been attributed to the improved charge transport for photo-generated carriers across the interfaces.

The photovoltaic performance of these solar cells can be improved by modifying the properties of the active layer or HTL and their interfaces in these solar cells. Graphene nanosheets have been demonstrated to alter energy levels of active layer components and improve the efficiency of P3HT:PCBM solar cells. This encourage us to fabricate and study PCDTBT:PCBM devices having graphene nanosheets in active layer, hole transport layer and both.

#### **4.1.4.1 Experimental details**

For the preparation of the graphene nanosheets, graphene flakes were mixed in the solvents of 1,2-dichlorobenzene and dimethyl sulfoxide and were ultrasonicated for 45 days, which exfoliated the graphene flakes into thin nanosheets of graphene. For the fabrication of the PCDTBT:PCBM solar cells, ITO coated glass sheets of resistivity nearly  $20\Omega/\text{sq}$  were first cleaned using deionized water, acetone and methanol and the HTL layer of PEDOT:PSS was deposited on it through spin coating with thickness of 50 nm. The active layer of PCDTBT:PCBM with concentration of 10mg/ml in the ratio of 1:4 was then deposited on it with active layer thickness of 70 nm. After the active layer deposition, aluminum electrodes were deposited on it through thermal evaporation with thickness of  $\sim 100$  nm. The solar cells were fabricated in a GloveBox (MBraun) where oxygen and moisture levels were controlled within 0.1ppm. For studying the effects of addition of graphene in the PCDTBT:PCBM on the photovoltaic performance of solar cells, four different sets of substrates were fabricated with eachset consisting of 9 devices. These set was fabricated with (i) no graphene nanosheets, (ii) graphene nanosheets in the HTL alone, (iii) graphene sheets inactive layer alone, and (iv) graphene sheets both in HTL and active layer. For adding the graphene in the HTL, 200  $\mu\text{l}$  of

dimethyl sulfoxide solvent consisting of graphene nanosheets was added into PEDOT:PSS, while for adding the graphene nanosheets in the active layer, 200  $\mu\text{l}$  of 1,2-dichlorobenzene solvent consisting of graphene nanosheets was added into freshly prepared active layer blend having total volume of 1ml.

#### **4.1.4.2 Results and Discussion**

The PCDTBT:PCBM solar cells were then characterized for JV measurements under incident light intensity of  $30 \text{ mW/cm}^2$  inside the GloveBox (as shown in Fig. 4.5). The JV results show that addition of graphene in the HTL improve the short circuit current density from  $11.3$  to  $15.5 \text{ mA/cm}^2$  and fill factor from  $29$  to  $31\%$ , which results in an overall improvement in efficiency from  $4.9$  to  $6.4 \%$ . However the open circuit voltage decreases from  $0.45$  to  $0.4 \text{ V}$ . In case of the solar cells with graphene nanosheets in active layer, addition of graphene reduces the short circuit current density to  $6.65 \text{ mA/cm}^2$  and improves both the open circuit voltage and fill factor to  $0.47 \text{ V}$  and  $34\%$ . This result is in conformation with the previous obtained results in which it has been found that graphene chemically interacts through  $\pi$ - $\pi$  interaction and modifies the energy levels of PCBM which results in the improved open circuit voltage. The improvement in the fill factor can be attributed to the improved morphology due to the graphene nanosheets present in the active layer of PCDTBT:PCBM solar cells which provide a better arrangement of the grains across the bulk. This improved morphology leads to the decrement in the roughness of the surface of the active layer (which was confirmed by AFM) and thus improves charge transfer across the interfaces between the active layer and aluminum electrodes and between active layer and HTL. The reduction in the short circuit current density, which can be attributed to dominant charge recombination phenomenon in such solar cells, the overall efficiency reduces to  $3.6 \%$ . In case of solar cells with addition of graphene in both HTL and active layer the decrement in the

short circuit current density due to graphene in the active layer is compensated by the improvements due to graphene in the HTL. The measured photovoltaic parameters are summarized in Table 4.2.

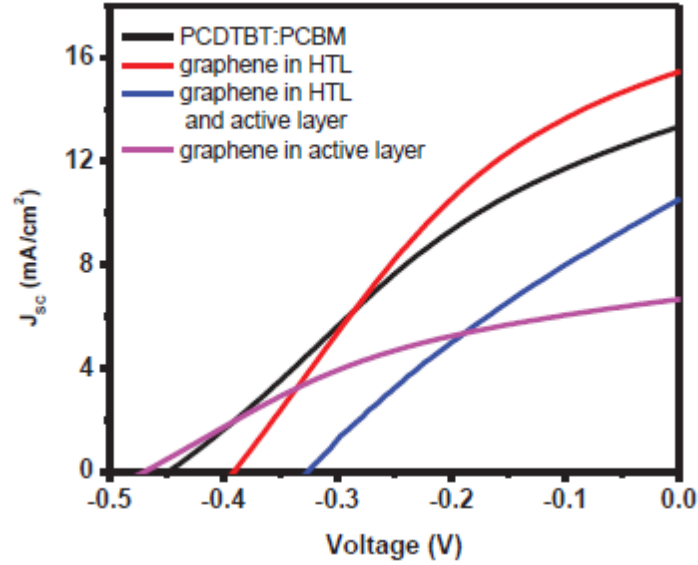


**Fig. 4.5.** JV characteristics with different set of devices under 30 mW/cm<sup>2</sup>.

**Table. 4.2.** Photovoltaic parameters with different set of devices under 30 mW/cm<sup>2</sup>

Parameters	V <sub>oc</sub> (V)	J <sub>sc</sub> (mA/cm <sup>2</sup> )	FF (%)	Efficiency (%)
PCDTBT_PCBM_no graphene	0.45	13.31	29	4.9
HTL_graphene	0.40	15.49	31	6.4
Active_graphene	0.47	6.65	34	3.6
Active_HTL_graphene	0.33	10.48	27	3.1

## 4.2 Conclusions

We also carried out the fabrication of P3HT:PCBM-graphene flakes solar cells where the graphene flakes rather than the thin sheets of graphene were added into the active layer. In such solar cells, the devices have shown degraded performance as compared to the P3HT:PCBM solar cells. This shows that mixing the graphene flakes in the active layer degrade the photovoltaic performance of the solar cells due to their poor miscibility in the active layer. This occurs because of the aggregation of the graphene flakes in the active layer which prevent the effective transfer of the charge across the films. Due to their larger size they have poor interfacial contacts with PCBM which does not result in the strong interactions between the graphene flakes and PCBM. Thus, as compared to the graphene sheets, the graphene flakes are not better to be used in the active layer for the improvement in the photovoltaic performance of the solar cells.

The experimental studies also showed that graphene can be used in combination with the HTL of the PCDTBT:PCBM solar cells for the improvement in the overall efficiency. Such improved efficiency is attributed to improved charge transfer across the bulk and the interfaces which is shown in the improved short circuit current density and fill factor. However, addition of graphene in the active layer alone and both active layer and HTL does not result in any improvement in the overall efficiency due to decrement in the short circuit current density which cannot be compensated by the improvements in the open circuit voltage and fill factor resulting in lower overall efficiency.

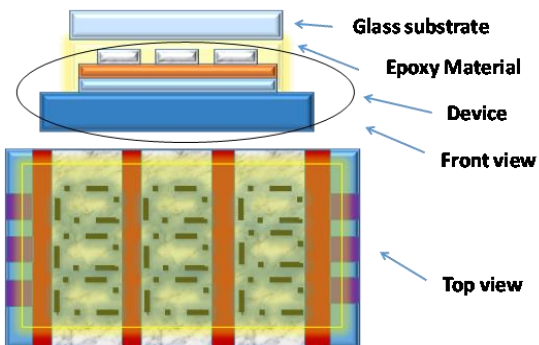
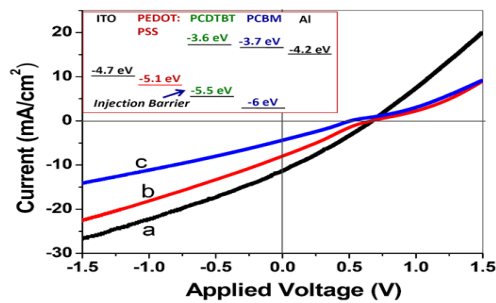
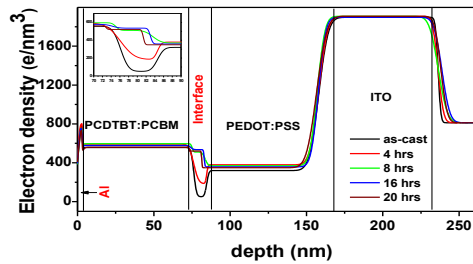
Thus, a simple exfoliation process has been used to produce the thin graphene sheets to be used in the active layer. Such addition of graphene sheets in the active layer have shown improvement in the photovoltaic performance of P3HT:PCBM solar cells due to the improved packaging of the active layer and change in the energy levels of the PCBM in the active layer.

# Chapter 5

## Summary and Conclusions

### Highlights

1. The main studies that were carried out during the thesis work are discussed.
2. The main results obtained during the thesis work are presented in light of the state of the art.
3. The key challenges that need to be addressed further with the developed understanding and employed techniques are presented.



With the high global energy demands, different renewable sources of energy have been explored for the production of the energy. The solar energy is the most promising of such renewable sectors of the energy. The solar energy can be harnessed using different types of solar cells belonging to the different generations depending upon the types of the materials and processes used in their fabrication. The focus of the thesis is to understand the factors responsible for understanding the effects of the factors like thickness of the layers in the solar cells, nature of the interfaces and morphology on the low efficiency in BHJs, adoption of the novel techniques for the improvement of the efficiency and understanding their stability issues.

Even with the development of different materials for the fabrication of the polymer solar cells, architectures and techniques for the improvement of the efficiency of the polymer solar cells, these solar cells show a large variation in the reported efficiencies and lack reproducibility in the these efficiencies under the similar fabrication conditions. In addition to it, the chemical and morphological stability over the period of the operation of these solar cells also forms one of the key challenges among the various issues of the polymer solar cells. The various factors controlling the morphology of the interfaces between the various layers and bulk of the layers are responsible for the ineffective charge transfer across the interface and bulk of the devices. This inefficient charge transfer is responsible for the lower efficiency in the polymer solar cells. Even with the techniques of encapsulation of the devices, the diffusion of the ambient oxygen and moisture into the device layers cannot be effectively prevented through the encapsulation of the device. With all the above mentioned issues in view, this thesis thus aims at the development of the BHJ polymer solar cells based on PCDTBT and P3HT donor polymers and addressing the key challenges by the application of the novel techniques for the enhancement of the efficiency of the solar cells.

Following are the main studies that were carried out during the thesis work:

- [1] The polymer solar cells based on PCDTBT and P3HT were fabricated with optimized conditions and parameters in order to obtain the maximum average efficiency.
- [2] In order to improve the efficiency of the solar cells based on PCDTBT, the approach of the thermal annealing of the devices was carried out. The thermal annealing approach has previously shown a significant improvement in the photovoltaic performance of the solar cells based on P3HT. However, with the solar cells based on PCDTBT, a significant degradation in the photovoltaic performance was observed after thermal annealing of the devices. This degradation leads to the generation of the S-kinks in the IV characteristics of the solar cells.
- [3] In order to determine the factors responsible for such degradation of the photovoltaic performance of these solar cells, the XRR technique was employed in order to determine the electron density profiles at the interfaces between the various layers of the solar cells. This was carried out in addition to other techniques like XPS, Kelvin probe microscopy, Raman spectroscopy and UV-Vis spectroscopy for determining the changes in the parameters like binding energies, work function or the bonding in the structure of the materials used in the fabrication of the solar cells.
- [4] For the solar cells based on both P3HT and PCDTBT, novel approach of application of graphene nanosheets in the active layer of the solar cells was employed. In case of the solar cells based PCDTBT, the application of the graphene in both the HTL and the active layer was carried out in different combinations to obtain the optimized combination for the maximum average efficiency in the solar cells.

[5] For the solar cells based on PCDTBT, another approach of the solvent annealing of the active layer in addition to increase in the thickness of the active layer was also carried out. This was achieved by depositing various layers of the active material over the top of the previous layer. The maximum thickness of the active layer was then optimized and solvent annealing of the devices with the various layers was carried out.

[6] The encapsulation of the devices was carried out after the aluminum electrodes are deposited on the top of the device. The devices fabricated are characterized under one sun and are to be used for operation in the ambient environmental conditions. The materials used for the fabrication of the solar cells are prone to the degradation by the oxygen and moisture present in the environment, thus it is necessary to prevent the exposure of the device to the ambient oxygen and moisture through the encapsulation procedure. The encapsulation was done by using an epoxy material which is dropped on the top surface of the device and is then covered and pressed with a thin glass plate to cover the surface of the device. The deposited epoxy material is then treated under UV light for 30 minutes which hardens the epoxy material and prevents the exposure of the device to the ambient environmental conditions.

With the above mentioned studies carried out, various results regarding the performance of the polymer solar cells were obtained which developed the further understanding of the factors and processes responsible for affecting the performance of the solar cells. Also significant improvements in the efficiencies of the solar cells were achieved with the adoption of the novel approaches for such improvements. Following are the main results that were obtained during the thesis work:

[1] In order to improve the photovoltaic performance of the solar cells based on PCDTBT, the approach of thermal annealing of the devices was adopted. However, it has been found that the thermal annealing of these solar cells degrades the performance of the solar cells. In order to determine the possible reasons for the degradation of the thermally annealed devices, UV-Vis and Raman spectroscopy measurements were carried out on PCDTBT, PCBM and PCDTBT:PCBM blend. A modification in the intensity of the UV-Vis absorption spectra peaks of PCDTBT: PCBM with respect to the PCDTBT and PCBM was found. This modification is responsible for the interaction between the polymer and the PCBM molecules. There are two band transitions at 450 and 578 nm for PCDTBT corresponding to  $\pi$ - $\pi^*$  transition and two peaks at 345 and 520 nm corresponding to  $\pi$ - $\pi^*$  transition and asymmetry of the  $C_{60}$  molecules. In addition, the absorption intensity in the spectra does not change with the thermal annealing suggesting no crystallization or disordering in the PCDTBT:PCBM and there is slight increase in the intensity of the C-C intra stretch ( $1374\text{cm}^{-1}$ ) relative to in-plane skeleton mode ( $1445\text{cm}^{-1}$  and  $1538\text{cm}^{-1}$ ) after the thermal annealing. This change has been attributed to the increase in the degree of the molecular ordering of the PCDTBT:PCBM after thermal annealing which can improve the device performance. Thus, it has been concluded that the thermal annealing does not degrades the bulk of the device but the interfaces between the various layers of the solar cells can be degraded by the thermal annealing which further degrades the performance of the solar cells.

[2] In order to understand the S-kinks, the XRR technique was employed to determine the electron density profiles at the various interfaces layers of the solar cells. It has been found that a direct correlation exist between the electron density profile at the interface

and observed S-kink in the J-V characteristics of the PCDTBT:PCBM based BHJ solar cells. The Kelvin Probe and XPS analyses suggested that the chemisorbed oxygen ( $O_2^-$ ) in PEDOT:PSS layer is responsible for the enhanced electron density at the interface and give rise to S-shape in JV characteristics upon light illumination. In addition, annealing of the devices causes increase in the surface roughness and electron density of the interfaces owing to re-organization of materials at the interface and may lead to S-kink in the devices.

[3] For the solar cells based on both P3HT and PCDTBT, incorporation of graphene nanosheets in the active layer of the solar cells was investigated. The experiments were carried out on BHJ solar cells based on P3HT:PCBM using the composites of the graphene mixed in PCBM in the active layer of the BHJ solar cell. The solution of thin graphene-sheets obtained from a simple ultrasonic exfoliation process was found to chemically interact with PCBM molecules. The thinner graphene-sheets significantly altered the positions of highest occupied molecular orbital and lowest unoccupied molecular orbital of PCBM, which was found to be beneficial for the enhancement of the open circuit voltage of the solar cells. Flexible BHJ solar cells fabricated P3HT:PCBM-graphene exhibited a power conversion efficiency of 2.51%, which is a 2-fold increase as compared to those fabricated using P3HT:PCBM. The experimental studies also showed that graphene can be used in combination with the HTL of the PCDTBT:PCBM solar cells for the improvement in the overall efficiency. Such improved efficiency is attributed to the improved charge transfer across the bulk and the interfaces that improves the short circuit current density and fill factor.

[4] Additionally, for efficiency improvement in the BHJ polymer solar cells based on PCDTBT:PCBM, an approach of enhancing the active layer thickness was adopted. The efficiency of PCDTBT:PCBM based BHJ solar cell is limited by the thickness of the active layer. In order to improve the efficiency of the BHJ solar cell by a mixed approach of use of thicker active layer as well as solvent annealing was adopted. It has been observed that a higher thickness of 290 nm of PCDTBT:PCBM active layer via multilayer deposition aids in more light absorption as compared to the thickness of 75 nm active layer. The BHJ solar cells fabricated using thick active layer show enhanced open circuit voltage, and reduced short circuit current density and fill factor as compared with devices fabricated using thin active layer. The solvent annealing of the thick active layer by tetrahydrofuran vapors results in improvement of all photovoltaic parameters and therefore overall efficiency improvement of 3.9% as compared to 3.55% for device using thin layer. The efficiency improvement has been attributed to the suppression of the resistive losses occurring at various interfaces of the active layer as has been supported by impedance spectroscopy measurements.

[5] The encapsulation of the devices has shown that the non-encapsulated devices undergo a degradation in their photovoltaic performance after 120 minutes of their fabrication while the encapsulated devices show nearly the same photovoltaic performance for a testing period upto 45 days. The present studies on the encapsulation of the polymer solar cells confirmed that the encapsulation of the devices is crucial for their stable operation for longer period of times.

### **Further scope of the present work**

This thesis aims at the development of the BHJ polymer solar cells based on PCDTBT and P3HT donor polymers and addressing the key challenges in the performance these solar cells. This was achieved by the application of the novel techniques for the enhancement of the efficiency of the solar cells. Various results regarding the performance of the polymer solar cells were obtained which developed the further understanding of the factors and processes responsible for affecting the performance of the solar cells. In addition, significant improvements in the efficiencies of the solar cells were achieved with the adoption of the novel approaches for such improvements. However, there are various other challenges that can be addressed further with the understanding developed with the work and the techniques employed in this thesis. The following are the key challenges that can be addressed further with the developed understanding and employed techniques:

- [1] The application of XRR technique can also be applied to the solar cells with different architectures and types of the materials and such accumulation of the electrons and the reorganization of the materials at the interfaces can also be observed in the case of such solar cells. Further, in case of devices with higher thickness there is a significant decrease in the short circuit current density and the fill factor of the devices. Both the parameters depend significantly on the successful charge generation, charge separation and charge transfer across the bulk and the interfaces to the electrodes of the devices. Such decrease in both the parameters can also be attributed to the charge accumulation at the interfaces between the various active layers deposited on the top of the previous layers. Thus, the technique of the XRR can also be employed for determining the electron density profiles

at these interfaces which can be related to the degraded performance of the devices with higher thickness.

[2] In addition, the XRR technique can also be employed for determining the change in the electron density profiles at the interfaces of the devices after solvent annealing which can thus be attributed to the improved charge transfer across the interfaces of the devices.

[3] The application of the graphene nanosheets in the active layer of the solar cells can also be further applied to the solar cells with different architectures and types of the materials for improvement in the performance of these solar cells. A better understanding of the improved performance of the bulk of the devices with graphene nanosheets can be developed by determining the electron density profiles in these devices. Such electron density profiles at the interfaces of these devices can show an improved charge transfer across the bulk of these devices.

In summary, some of the major achievements in the efficiencies of the polymer solar cells are summarized in Table 5.1. It can be seen that the work on polymer photovoltaics has evolved from the simple molecules to more complex polymers with addition of new properties in the materials. This has made it possible for efficiencies to scale up from less than 1% to more than 10% over this duration of the evolution of the polymer solar cells. With further research in the polymer photovoltaics, new polymers with tuned properties offering the advantage of the higher efficiencies, much better stability and thus longer durations of operating times will be developed.

**Table 5.1** Major achievements and evolution of the polymer solar cells

<b>Donor Polymer</b>	<b>Acceptor material</b>	<b>Year</b>	<b>Efficiency (%)</b>
Tetracene		1974	$10^{-3}$ - $10^{-4}$ [137]
Merocyanine dyes		1978	1 [138]
p type metalfree phthalocyanine (H <sub>2</sub> Pc)	n type perylene-tetracarboxylic derivative (MePTC)	1991	0.7 [139]
MEH-PPV	C <sub>60</sub>	1993	1 [140]
MEH-PPV	cyano PPV	1995	0.9 [141]
MDMO-PPV	C <sub>60</sub>	2001	3 [142]
P3HT	methanofullerene	2005	5 [143]
PTB7	PC <sub>71</sub> BM	2010	7.4 [144]
PTB7	PC <sub>71</sub> BM	2011	9.2 [145]
PDTP-DFBT	PC <sub>71</sub> BM	2013	10.2 [146]

## References

---

- [1] "2014 Key World Energy Statistics" <http://www.iea.org/publications/freepublications/.IEA>, (2014), pp. 6, 24, 28.
- [2] D. M. Chapin, C. S. Fuller, G. L. Pearson, A New Silicon p-n Junction Photocell for Converting Solar Radiation into Electrical Power, *J. Appl. Phys.*, 25 (1954) 676–677.
- [3] M. L. Tsai, W. C. Tu, L. Tang, T. C. Wei, W. R. Wei, S. P. Lau, L. J. Chen, J. H. He, Efficiency Enhancement of Silicon Heterojunction Solar Cells via Photon Management Using Graphene Quantum Dot as Downconverters, *NanoLett.*, 16 (2016) 309–313.
- [4] H. Shirakawa, E. J. Louis, A. G. MacDiarmid, C. K. Chiang, A. J. Heeger, Synthesis of electrically conducting organic polymers: Halogen derivatives of polyacetylene (CH)<sub>x</sub>, *Chem. Comm.*, 16 (1977) 578.
- [5] J. Yan, B. R. Saunders, Third-generation solar cells: a review and comparison of polymer:fullerene, hybrid polymer and perovskite solar cells, *RSC Adv.*, 4 (2014) 43286–43314.
- [6] C. Winder, N. S. Sariciftci, Low bandgap polymers for photon harvesting in bulk heterojunction solar cells, *J. Mater. Chem.*, 14 (2004) 1077–1086.
- [7] Z. He, C. Zhong, S. Su, M. Xu, H. Wu, Y. Cao, Enhanced power-conversion efficiency in polymer solar cells using an inverted device structure, *Nature Photonics*, 6(2012)591–595.
- [8] Z. He, B. Xiao, F. Liu, H. Wu, Y. Yang, S. Xiao, C. Wang, T. P. Russell, Y. Cao, Single-junction polymer solar cells with high efficiency and photovoltage, *Nature Photonics* 9,(2015)174–179.

- 
- [9] J. You, L. Dou, K. Yoshimura, T. Kato, K. Ohya, T. Moriarty, K. Emery, C. C. Chen, J. Gao, G. Li, Y. Yang, A polymer tandem solar cell with 10.6% power conversion efficiency, *Nature Comm.*, 4 (2013) 1446.
- [10] H. Zhou, Y. Zhang, C. K. Mai, S. D. Collins, G. C. Bazan, T. Q. Nguyen, A. J. Heeger, Polymer Homo-Tandem Solar Cells with Best Efficiency of 11.3%, *Adv. Mater.*, 27 (2015) 1767–1773.
- [11] S. Liu, P. You, J. Li, J. Li, C. S. Lee, B. S. Ong, C. Sury, F. Yan, Enhanced efficiency of polymer solar cells by adding a high-mobility conjugated polymer, *Energy Environ. Sci.*, 8 (2015) 1463-1470.
- [12] J. Liu, Q. Liang, H. Wang, M. Li, Y. Han, Z. Xie, L. Wang, Improving the Morphology of PCDTBT:PC70BM Bulk Heterojunction by Mixed-Solvent Vapor-Assisted Imprinting: Inhibiting Intercalation, Optimizing Vertical Phase Separation, and Enhancing Photon Absorption, *J. Phys. Chem. C*, 9, 118 (2014) 4585-4595.
- [13] T. Y. Chu, S. Alem, S. W. Tsang, S. C. Tse, S. Wakim, J. Lu, G. Dennler, D. Waller, R. Gaudiana, Y. Tao, Morphology control in polycarbazole based bulk heterojunction solar cells and its impact on device performance, *Appl. Phys. Lett.*, 25 (2011) 98.
- [14] D. Chi, S. Qu, Z. Wang, J. Wang, High efficiency P3HT:PCBM solar cells with an inserted PCBM layer, *J. Mater. Chem. C*, 2 (2014) 4383-4387.
- [15] L. Lu, Z. Luo, T. Xu, L. Yu, Cooperative Plasmonic Effect of Ag and Au Nanoparticles on Enhancing Performance of Polymer Solar Cells, *NanoLett.* 13 (1) (2013) 59-64.
- [16] M. Zhang, Y. Gu, X. Guo, F. Liu, S. Zhang, L. Huo, T. P. Russell, J. Hou, Efficient Polymer Solar Cells Based on Benzothiadiazole and Alkylphenyl Substituted Benzodithiophene with a Power Conversion Efficiency over 8%, *Adv. Mater.*, 25 (2013) 4944–4949.

- 
- [17] H. Zhou, Y. Zhang, J. Seifert, S. D. Collins, C. Luo, G. C. Bazan, T. Q. Nguyen, A. J. Heeger, High-Efficiency Polymer Solar Cells Enhanced by Solvent Treatment, *Adv. Mater.*, 25 (2013) 1646–1652.
- [18] J. H. Tsai, Y. C. Lai, T. Higashihara, C. J. Lin, M. Ueda, W. C. Chen, Enhancement of P3HT/PCBM Photovoltaic Efficiency Using the Surfactant of Triblock Copolymer Containing Poly(3-hexylthiophene) and Poly(4-vinyltriphenylamine) Segments, *Macromolecules*, 43 (14) (2010) 6085-6091.
- [19] D. Mühlbacher, M. Scharber, M. Morana, Z. Zhu, D. Waller, R. Gaudiana, C. Brabec, High Photovoltaic Performance of a Low-Bandgap Polymer, *Adv. Mater.*, 18 (2006) 2884–2889.
- [20] P. Vanlaeke, G. Vanhoyland, T. Aernouts, D. Cheyens, C. Deibel, J. Manc, P. Heremans, J. Poortmans, Polythiophene based bulk heterojunction solar cells: Morphology and its implications, *Thin Solid Films*, 511–512 (2006) 358–361.
- [21] S. Albrecht, S. Janietz, W. Schindler, J. Frisch, J. Kurpiers, J. Kniepert, S. Inal, P. Pingel, K. Fostiropoulos, N. Koch, D. Neher, Fluorinated Copolymer PCPDTBT with Enhanced Open-Circuit Voltage and Reduced Recombination for Highly Efficient Polymer Solar Cells, *J. Am. Chem. Soc.*, 134 (36) (2012) 14932-14944.
- [22] J. Hou, H. Y. Chen, S. Zhang, G. Li, Y. Yang, Synthesis, Characterization, and Photovoltaic Properties of a Low Band Gap Polymer Based on Silole-Containing Polythiophenes and 2,1,3-Benzothiadiazole, *J. Am. Chem. Soc.*, 130 (48) (2008) 16144-16145.
- [23] X.H. Li, Wei E.I. Sha, Wallace C.H. Choy, Dixon D. S. Fung, F. X. Xie, Efficient Inverted Polymer Solar Cells with Directly Patterned Active Layer and Silver Back Grating, *J. Phys. Chem. C*, 116 (12) (2012) 7200-7206.

- 
- [24] S. H. Park, A. Roy, S. Beaupré, S. Cho, N. Coates, J. S. Moon, D. Moses, M. Leclerc, K. Lee, A. J. Heeger, Bulk heterojunction solar cells with internal quantum efficiency approaching 100%, *Nature Photon.*, 3 (2009) 297 - 302.
- [25] M. Jørgensen, K. Norrman, F. C. Krebs, Stability/degradation of polymer solar cells, *Sol. Energy Mater. Sol. Cells*, 92 (2008) 686–714.
- [26] K. Norrman, M. V. Madsen, S. A. Gevorgyan, F. C. Krebs, Degradation Patterns in Water and Oxygen of an Inverted Polymer Solar Cell, *J. Am. Chem. Soc.*, 132 (2010) 16883-16892.
- [27] N. Dam, R. D. Scurlock, B. Wang, L. Ma, M. Sundahl, P. R. Ogilby, Singlet Oxygen as a Reactive Intermediate in the Photodegradation of Phenylenevinylene Oligomers, *Chem. Mater.*, 11 (1999) 1302-1305.
- [28] M.G. Matturro, R.P. Reynolds, R.V. Kastrup, C.F. Pictroski, Thioozonide decomposition. Sulfur and oxygen atom transfer. Evidence for the formation of a carbonyl O-sulfide intermediate, *J. Am. Chem. Soc.*, 108, (1986), 2775.
- [29] K. Norrman, N.B. Larsen, F.C. Krebs, Lifetimes of organic photovoltaics: Combining chemical and physical characterisation techniques to study degradation mechanisms, *Sol. Energy Mater. Sol. Cells*, 90 (2006), 2793.
- [30] M. Lögdlund, J.L. Brédas, Theoretical studies of the interaction between aluminum and poly(p-phenylenevinylene) and derivatives, *J. Chem. Phys.*, 101 (1994), 4357.
- [31] M.P. de Jong, L.J. van Ijzendoorn, M.J.A. de Voigt, Stability of the interface between indium-tin-oxide and poly(3,4-ethylenedioxythiophene)/poly(styrenesulfonate) in polymer light-emitting diodes, *Appl. Phys. Lett.*, 77 (2000), 2255.

- 
- [32] Wei-Ru Wu, U-SerJeng, Chun-Jen Su, Kung-Hwa Wei, Ming-Shin Su, Mao-Yuan Chiu, Chun-Yu Chen, Wen-Bin Su, Chiu-Hun Su, and An-Chung Su, Competition between Fullerene Aggregation and Poly(3-hexylthiophene) Crystallization upon Annealing of Bulk Heterojunction Solar Cells, *ACS Nano*, 5 (8)(2011), 6233-6243.
- [33] D. H.Wang, K. H.Park, J. H.Seo, J. Seiffter, J. H.Jeon, J. K. Kim, J. H. Park, O. O. Park, A. J.Heeger, Enhanced Power Conversion Efficiency in PCDTBT/PC<sub>70</sub>BM Bulk Heterojunction Photovoltaic Devices with Embedded Silver Nanoparticle Clusters, *Adv. Energy Mater.*, 1 (2011) 766–770.
- [34] J. Liu, Q. Liang, H. Wang, M. Li, Y. Han, Z. Xie, L. Wang, Improving the Morphology of PCDTBT:PC<sub>70</sub>BM Bulk Heterojunction by Mixed-Solvent Vapor-Assisted Imprinting: Inhibiting Intercalation, Optimizing Vertical Phase Separation, and Enhancing Photon Absorption, *J. Phys. Chem. C*, 118 (9) (2014) 4585-4595.
- [35] C. Shim, M. Kim, S. G. Ihn, Y. S. Choi, Y. Kim, K. Cho, Controlled nanomorphology of PCDTBT–fullerene blends via polymer end-group functionalization for high efficiency organic solar cells, *Chem. Comm.*, 48 (2012) 7206-7208.
- [36] D. Chi, S. Qu, Z. Wang, J. Wang, High efficiency P3HT:PCBM solar cells with an inserted PCBM layer, *J. Mater. Chem. C*, 2 (2014) 4383-4387.
- [37] D. Chen, A. Nakahara, D. Wei, D. Nordlund, T. P. Russell, P3HT/PCBM Bulk Heterojunction Organic Photovoltaics: Correlating Efficiency and Morphology, *NanoLett.*, 11 (2) (2011) 561-567.
- [38] D. M.González, V.Körstgens, Y.Yao, L.Song, G.Santoro, S. V.Roth, P.Müller-Buschbaum, Improved Power Conversion Efficiency of P3HT:PCBM Organic Solar Cells by Strong

- 
- Spin–Orbit Coupling-Induced Delayed Fluorescence, *Adv. Energy Mater.*, 5 (2015) 1401770.
- [39] E. Bundgaard, F. C. Krebs, Low band gap polymers for organic photovoltaics, *Sol. Energy Mater. Sol. Cells*, 91, 11 (2007) 954–985.
- [40] F. Machui, S. Langner, X. Zhu, S. Abbott, C. J. Brabeca, Determination of the P3HT:PCBM solubility parameters via a binary solvent gradient method: Impact of solubility on the photovoltaic performance, *Sol. Energy Mater. Sol. Cells*, 100 (2012) 138–146.
- [41] C. H. Peters, I. T. Sachs-Quintana, J. P. Kastrop, S. Beaupré, M. Leclerc, M. D. McGehee, High Efficiency Polymer Solar Cells with Long Operating Lifetimes, *Adv. Energy Mater.*, 1 (2011) 491–494.
- [42] B. Kim, H. R. Yeom, M. H. Yun, J. Y. Kim, C. Yang, A Selenophene Analogue of PCDTBT: Selective Fine-Tuning of LUMO to Lower of the Bandgap for Efficient Polymer Solar Cells, *Macromolecules*, 45 (21)(2012) 8658–8664.
- [43] J. S. Moon, J. Jo, A. J. Heeger, Nanomorphology of PCDTBT:PC70BM Bulk Heterojunction Solar Cells, *Adv. Energy Mater.*, 2 (2012) 304–308.
- [44] M. O. Reese, M. S. White, G. Rumbles, D. S. Ginley, S. E. Shaheen, Optimal negative electrodes for poly(3-hexylthiophene): [6,6]-phenyl C61-butyric acid methyl ester bulk heterojunction photovoltaic devices, *Appl. Phys. Lett.*, 92 (2008) 053307.
- [45] W. Tress, K. Leo, M. Riede, Influence of Hole-Transport Layers and Donor Materials on Open-Circuit Voltage and Shape of I–V Curves of Organic Solar Cells, *Adv. Funct. Mater.*, 21 (2011) 2140–2149.

- 
- [46] A. Wagenpfahl, D. Rauh, M. Binder, C. Deibel, V. Dyakonov, S-shaped Current-Voltage Characteristics of Organic Solar Devices, *Phys. Rev. B*, 82 (2010) 115306.
- [47] J. Wagner, M. Gruber, A. Wilke, Y. Tanaka, K. Topczak, A. Steindamm, U. Hörmann, A. Opitz, Y. Nakayama, H. Ishii, J. Pflaum, N. Koch, W. Brütting, Identification of different origins for s-shaped current voltage characteristics in planar heterojunction organic solar cells, *J. Appl. Phys.*, 111 (2012) 054509.
- [48] C. Falkenberg, S. Olthof, R. Rieger, M. Baumgarten, K. Muellen, K. Leo, M. Riede, The role of energy level matching in organic solar cells — Hexaazatriphenylenehexacarbonitrile as transparent electron transport material, *Sol. Energy Mater. Sol. Cells*, 95 (2011) 0927-0932.
- [49] J.C. Wang, X.C. Ren, S.Q. Shi, C.W. Leung, P. K. L. Chan, Charge accumulation induced S-shape J – V curves in bilayer heterojunction organic solar cells, *Org. Electron.*, 12 (2011) 880-885.
- [50] A. Kumar, S. Sista, Y. Yang, Dipole induced anomalous S-shape I-V curves in polymer solar cells, *J. Appl. Phys.*, 105 (2009) 094512.
- [51] F. A.de Castro, J. Heier, F. Nüesch, R. Hany, Origin of the Kink in Current-Density Versus Voltage Curves and Efficiency Enhancement of Polymer-C60Heterojunction Solar Cells, *IEEE J. Sel. Top. Quantum Electron.*, 16 (2010) 1690–1699.
- [52] W. Tress, A. Petrich, M. Hummert, M. Hein, K. Leo, M. Riede, Imbalanced mobilities causing S-shaped I–V curves in planar heterojunction organic solar cells, *Appl. Phys. Lett.*, 98 (2011) 063301.

- 
- [53] Y. H. Sona, G. W. Kima, W. S. Jeona, R. Podeb, J. H. Kwona, Thermal Annealing Effect of Subphthalocyanine (SubPc) Donor Material in Organic Solar Cells, *Mol. Cryst. Liquid Cryst.*, 1 565 (2012) 8-13.
- [54] G. K. Mor, T. P. Le, K. Vakhshouri, D. R. Kozub, E. D. Gomez ,*ACS Appl. Mater. Interfaces*, 6 (22) (2014) 19638–19643.
- [55] Q. Yang, J. Wang, X. Zhang, J. Zhang, Y. Fu, Z. Xie, Constructing vertical phase separation of polymer blends via mixed solvents to enhance their photovoltaic performance, *Science China Chemistry*, 58 (2015) 309-316.
- [56] W. Tress, S. Corvers, K. Leo, M. Riede, Investigation of Driving Forces for Charge Extraction in Organic Solar Cells: Transient Photocurrent Measurements on Solar Cells Showing S-Shaped Current–Voltage Characteristics, *Adv. Energy Mater.*, 3(2013) 873–880.
- [57] W. Tress, O. Inganäs, Simple experimental test to distinguish extraction and injection barriers at the electrodes of (organic) solar cells with S-shaped current–voltage characteristics, *Sol. Energy Mater. Sol. Cells*, 117 (2013) 599–603.
- [58] Abhay Gusain, V. Saxena, P. Veerender, P. Jha, S. P. Koiry, A. K. Chauhan, D. K. Aswal, S. K. Gupta, Investigation on the Effects of Thermal Annealing on PCDTBT:PCBM Bulk-heterojunction Polymer Solar Cells, *AIP Conf. Proc.*, 776 (2013) 1512.
- [59] Z. Li, H. C. Wong, Z. Huang, H. Zhong, C. H. Tan, W. C. Tsoi, J. S. Kim, J. R. Durrant, J. T. Cabral, Performance Enhancement of Fullerene-based Solar Cells by Light Processing, *Nature Comm.*, 4 (2013) 2227.
- [60] M. R. Fitzsimmons, C. Majkrzak, Modern Techniques for Characterizing Magnetic Materials, *Springer, New York*, Chap. 3 (2005) pp. 107–155.

- 
- [61] G. Luo, W. Bu, M. Mihaylov, I. Kuzmenko, Mark L. Schlossman, L. Soderholm, X-ray reflectivity reveals a nonmonotonic ion-density profile perpendicular to the surface of ErCl<sub>3</sub> aqueous solutions, *J. Phys. Chem. C*, 117 (2013) 19082-19090.
- [62] S. Wakim, S. Beaupr, N. Blouin, B. R. Aich, S. Rodman, R. Gaudiana, Ye Tao, M. Leclerc, Highly efficient organic solar cells based on a poly(2,7-carbazole) derivative, *J. Mater. Chem.*, 19 (2009) 5351–5358.
- [63] J. W. Kingsley, P. P. Marchisio, H. Yi, A. Iraqi, C. J. Kinane, S. Langridge, R. L. Thompson, A. J. Cadby, A. J. Pearson, D. G. Lidzey, R. A. L. Jones, A. J. Parnell, Molecular weight dependent vertical composition profiles of PCDTBT:PC<sub>71</sub>BM blends for organic photovoltaics, *Sci. Rep.*, 4 (2014) 5286.
- [64] S. H. Park, A. Roy, S. Beaupre, S. Cho, N. Coates, J. S. Moon, D. Moses, M. Leclerc, K. Lee, A. J. Heeger, Bulk heterojunction solar cells with internal quantum efficiency approaching 100%, *Nature Photon.*, 3 (2009) 297–303.
- [65] E. A. Parlak, T. A. Tumay, N. Tore, S. Sarıođlan, P. Kavak, F. Turksoy, Efficiency improvement of PCDTBT solar cells with silver nanoparticles, *Sol. Energy Mater. Sol. Cells*, 110 (2013) 58–62.
- [66] F. Etzold, I. A. Howard, R. Mauer, M. Meister, T. D. Kim, K. W. Lee, N. S. Back, F. Laquai, Ultrafast exciton dissociation followed by nongeminate charge recombination in PCDTBT:PCBM photovoltaic blends, *J. Am. Chem. Soc.*, 133 (2011) 9469–9479.
- [67] N. Koch, A. Elschner, J. Schwartz, A. Kahn, Organic molecular films on gold versus conducting polymer: Influence of injection barrier height and morphology on current–voltage characteristics, *Appl. Phys. Lett.*, 82 (2003) 2281.

- 
- [68] N. Koch, A. Elschner, J. P. Rabe, R. L. Johnson, Energy level alignment at interfaces with pentacene: metals versus conducting polymers, *Adv. Mater.*, 17 (2005) 330.
- [69] F. Petraki, S. Kennou, S. Nespurek, The electronic properties of the interface between nickel phthalocyanine and a PEDOT:PSS, *J. Appl. Phys.*, 103 (2008) 033710.
- [70] G. Greczynski, T. Kugler, W.R. Salaneck, Characterization of the PEDOT-PSS system by means of X-ray and ultraviolet photoelectron spectroscopy, *Thin Solid Films*, 354 (1999) 129-135.
- [71] K. Fehse, R. Meerheim, K. Walzer, K. Leo, W. Lövenich, A. Elschner, Lifetime of organic light emitting diodes on polymer anodes, *Appl. Phys. Lett.*, 93 (2008) 083303.
- [72] K. Norrman, Morten V. Madsen, S. A. Gevorgyan, F. C. Krebs, Degradation Patterns in Water and Oxygen of an Inverted Polymer Solar Cell, *J. Am. Chem. Soc.*, 132 (2010) 16883–16892.
- [73] T. Nagata, S. Oh, T. Chikyow, Y. Wakayama, Effect of UV–ozone treatment on electrical properties of PEDOT:PSS film, *Org. Electron.*, 12 (2011) 279-284.
- [74] J. W. Kiel, B. J. Kirby, C. F. Majkrzak, B. B. Maranville, M. E. Mackay, Nanoparticle concentration profile in polymer-based solar cells, *Soft Matter*, 6 (2010) 641-646.
- [75] Y. Xie, Y. Bao, J. Du, C. Jiang, Q. Qiao, Understanding of morphology evolution in local aggregates and neighboring regions for organic photovoltaics, *Phys. Chem. Chem. Phys.*, 29 (2012) 10168-77.
- [76] S. Singh, M. R. Fitzsimmons, T. Lookman, J. D. Thompson, H. Jeen, A. Biswas, M. A. Roldan, M. Varela, Magnetic non uniformity and thermal hysteresis of magnetism in a manganite thin film, *Phys. Rev. Lett.*, 108 (2012) 077207.

- 
- [77] L. G. Parratt, Surface studies of solids by total reflection of X-rays, *Phys. Rev.*, 95 (1954) 359-369.
- [78] Y. G. Ko, W. D. Kwon, M. Kim, K. Kim, Y. S. Gal, M. Ree, Electrically permanent memory characteristics of an ionic conjugated polymer, *Polym. Chem.*, 3 (2012) 2028.
- [79] F. C. Krebs, K. Norrman, Analysis of the failure mechanism for a stable organic photovoltaic during 10,000 h of testing, *Progress in Photovoltaics: Research and Applications*, 15 (2007) 697–712.
- [80] G. Namkoong, J. Kong, M. Samson, I. -W. Hwang, K. Lee, Active layer thickness effect on the recombination process of PCDTBT:PC71BM organic solar cells, *Org. Elect.*, 14 (2013) 74.
- [81] Y. Sun, C. J. Takacs, S. R. Cowan, J. H. Seo, X. Gong, A. Roy and A. J. Heeger, Efficient, Air-Stable Bulk Heterojunction Polymer Solar Cells Using MoO<sub>x</sub> as the Anode Interfacial Layer, *Adv. Mater.*, 23 (2011) 2226.
- [82] F. Nickel, C. Sprau, M.F.G. Klein, P. Kapetana, N. Christ, X. Liu, S. Klinkhammer, U. Lemmer, A. Colsmann, Spatial mapping of photocurrents in organic solar cells comprising wedge-shaped absorber layers for an efficient material screening, *Sol. Energy Mater. Sol. Cells*, 104 (2012) 18.
- [83] S. Beaupr e and M. Leclerc, PCDTBT: en route for low cost plastic solar cells, *J. Mater.Chem.A*, 1 (2013) 11097.
- [84] N. Blouin, A. Michaud, D. Gendron, S. Wakim, E. Blair, R. N. -Plesu, M. Bellete, G. Durocher, Y. Tao, M. Leclerc, Toward a Rational Design of Poly(2,7-Carbazole) Derivatives for Solar Cells, *J. Am. Chem. Soc.*, 130 (2008)732.

- 
- [85] M. C. Scharber , D. Mühlbacher , M. Koppe , P. Denk , C. Waldauf , A. J. Heeger , C. J. Brabec, Design rules for donors in bulk-heterojunction solar cells - Towards 10 % energy-conversion efficiency, *Adv. Mater.*, 18 (2006) 789.
- [86] T. M. Clarke, J. Peet, A. Nattestad, N. Drolet, G. Dennler, C. Lungenschmied, M. Leclerc, A. J. Mozer, Charge carrier mobility, bimolecular recombination and trapping in polycarbazolecopolymer:fullerene (PCDTBT:PCBM) bulk heterojunction solar cells, *Org. Elect.*, 13 (2012) 2639–2646.
- [87] P. A. Staniec, A. J. Parnell, A. D. F. Dunbar, H. Yi, A. J. Pearson, T. Wang, P. E. Hopkinson, C. Kinane, R. M. Dalgliesh, A. M. Donald, A. J. Ryan, A. Iraqi, R. A. L. Jones and D. G. Lidzey, The Nanoscale Morphology of a PCDTBT:PCBM Photovoltaic Blend, *Adv. Energy Mater.*, 1 (2011) 499.
- [88] N. C. Cates, R. Gysel, J. E. P. Dahl, A. Sellinger, M. D. McGehee, *Chem. Mater.*, 2010, 22, 3543.
- [89] H. Yi, S. Al-Faifi, A. Iraqi, D. C. Watters, J. Kingsley and D. G. Lidzey, Carbazole and thienylbenzo[1,2,5]thiadiazole based polymers with improved open circuit voltages and processability for application in solar cells, *J. Mater. Chem.*, 21 (2011) 13649.
- [90] G. Fang, J. Liu, Y. Fu, B. Meng, B. Zhang, Z. Xie, L. Wang, Improving the nanoscale morphology and processability for PCDTBT-based polymer solar cells via solvent mixtures, *Org. Elect.*, 13 (2012) 2733.
- [91] J. Liu, L. Chen, B. Gao, X. Cao, Y. Han, Z. Xie, L. Wang, Constructing the Nanointerpenetrating Structure of PCDTBT:PC70BM Bulk Heterojunction Solar Cells Induced by Aggregation of PC70BM via Mixed-Solvent Vapor Annealing, *J. Mater. Chem. A*, 1 (2013) 6216.

- 
- [92] H. Klauk, *Chem. Soc. Rev.*, 39 (2010) 2643–2666.
- [93] C. Scharsich, F. S. U. Fischer, K. Wilma, R. Hildner, S. Ludwigs, A. Kohler, Revealing Structure Formation in PCPDTBT by Optical Spectroscopy, *J. Polym. Sci. B: Polym. Phys.*, 53 (2015) 1416.
- [94] D. Di Nuzzo, A. Aguirre, M. Shahid, V. S. Gevaerts, S. C. J. Meskers, and R. A. J. Janssen, Improved Film Morphology Reduces Charge Carrier Recombination into the Triplet Excited State in a Small Bandgap Polymer-Fullerene Photovoltaic Cell, *Adv. Mater.*, 22 (2010) 4321.
- [95] J. Bisquert, Theory of the Impedance of Electron Diffusion and Recombination in a Thin Layer, *J. Phys. Chem.*, 106 (2001) 325.
- [96] J. Bisquert, Chemical capacitance of nanostructured semiconductors: Its origin and significance for nanocomposite solar cells, *Phys. Chem. Chem. Phys.*, 5 (2003) 5360.
- [97] G. Garcia-Belmonte, P. P. Boix, J. Bisquert, M. Sessolo, H. J. Bolink, Sol. Energy Mater. Sol. Cells, Simultaneous determination of carrier lifetime and electron density-of-states in P3HT:PCBM organic solar cells under illumination by impedance spectroscopy, *Sol. Energy Mater. Sol. Cells*, 94 (2), (2010) 366-375.
- [98] A. Guerrero, S. Loser, G. Garcia-Belmonte, C. J. Bruns, J. Smith, H. Miyauchi, S. I. Stupp, J. Bisquert and T. J. Marks, Solution-processed small molecule:fullerenebulkheterojunction solar cells: impedance spectroscopy deduced bulk and interfacial limits to fill-factors, *Phys. Chem. Chem. Phys.*, 15, (2013) 16456.
- [99] G. Dennler, M. C. Scharber, C. J. Brabec, *Adv. Mater.*, 21(13), (2009) 1323.
- [100] X. Yang, A. Uddin, *Renewable Sustainable Energy Rev.*, 30, (2014) 324.

- 
- [101] J. Kniepert, I. Lange, N. J. van der Kaap, L. J. A. Koster, D. Neher, A conclusive view on charge generation, recombination, and extraction in as-prepared and annealed P3HT:PCBM blends: Combined experimental and simulation work, *Adv. Energy Mater.*, 4 (2014), 1301401.
- [102] O. Oklobia, T. S. Shafai, *Solid-State Electron.*, 87, (2013) 64.
- [103] T. Wang, A. J. Pearson, D. G. Lidzey, R. A. L. Jones, *Adv. Funct. Mater.*, 21(8), (2011)1383.
- [104] Z. Yin, J. Zhu, Q. He, X. Cao, C. Tan, H. Chen, Q. Yan, H. Zhang, *Adv. Energy Mater.*, 4(1), (2014) 1300574.
- [105] D. Chen, H. Zhang, Y. Liu, J. Li, *Energy Environ. Sci.*, 6(5), (2013) 1362.
- [106] A. Iwan, A. Chuchmała, *Prog. Polym. Sci.*, 37 (12), (2012) 1805.
- [107] K. S. Novoselov, A. K. Geim, S. V. Morozov, D. Jiang, Y. Zhang, S. V. Dubonos, I. V. Grigorieva, A. A. Firsov, *Science*, 306 (5696), (2004) 666.
- [108] C. N. R. Rao, A. K. Sood, K. S. Subrahmanyam, A. Govindaraj, *Angew. Chem. Int. Ed.*, 48 (42), (2009) 7752.
- [109] F. Bonaccorso, Z. Sun, T. Hasan, A. C. Ferrari, *Nature Photon*, 4 (9), (2010) 611.
- [110] D. Jinhong, C. H. Ming, *Macromol. Chem. Phys.*, 213 (10–11), (2012) 1060.
- [111] S. Xuemei, S. Hao, L. Houpu, P. Huisheng, *Adv. Mater.*, 25 (37), (2013) 5153.
- [112] S. Sasha, A. D. Dmitriy, H. B. D. Geoffrey, M. K. Kevin, J. Z. Eric, A. S. Eric, D. P. Richard, T. N. SonBinh, S. R. Rodney, *Nature*, 442 (7100), (2006) 282.
- [113] Q. Liu, Z. Liu, X. Zhang, N. Zhang, L. Yang, S. Yin, Y. Chen, *Appl. Phys. Lett.*, 92(22), (2008) 223303.
- [114] D. Yu, Y. Yang, M. Durstock, J.-B. Baek, L. Dai, *ACS Nano*, 4(10), (2010) 5633.

- 
- [115] D. Chen, H. Zhang, Y. Liu, J. Li, *Energy Environ. Sci.*, 6(5), (2013) 1362.
- [116] D. Yu, K. Park, M. Durstock, L. Dai, *J. Phys. Chem. Lett.*, 2(10), (2011) 1113.
- [117] R. Søndergaard, M. Hösel, D. Angmo, T. T. Larsen-Olsen, F. C. Krebs, *Mater. Today*, 15 (1–2), (2012) 36.
- [118] J. E. Carle, M. Helgesen, M. V. Madsen, E. Bundgaard, F. C. Krebs, *J. Mater. Chem. C*, 2(7), (2014) 1290.
- [119] S. Lee, J. S. Yeo, Y. Ji, C. Cho, D. Y. Kim, S. I. Na, B. H. Lee, T. Lee, *Nanotechnology* 23(34), (2012) 344013.
- [120] S. I. Na, S. S. Kim, J. Jo, D. Y. Kim, *Adv. Mater.*, 20(21), (2008) 4061.
- [121] M. Ohzeki, S. Fujii, Y. Arai, T. Yanagidate, Y. Yanagi, T. Okukawa, A. Yoshida, H. Kataura, Y. Nishioka, *Jpn. J. Appl. Phys., Part 1* 53(2S), 02BE04 (2014).
- [122] Z. Yin, J. Zhu, Q. He, X. Cao, C. Tan, H. Chen, Q. Yan, H. Zhang, *Adv. Energy Mater.*, 4(1), (2014)1300574.
- [123] A. K. Manna, S. K. Pati, *Chem. Phys. Chem*, 14(9), (2013) 1844.
- [124] W. Chen, H. Huang, A. Thye, S. Wee, *Chem. Comm.*, 36, (2008) 4276.
- [125] V. Zardetto, T. M. Brown, A. Reale, A. D. Carlo, *J. Polym. Sci., Part B: Polym. Phys.*, 49(9), (2011) 638.
- [126] B. W. D'Andrade, S. Datta, S. R. Forrest, P. Djurovich, E. Polikarpov, M. E. Thompson, *Org. Electron.*, 6(1), (2005) 11.
- [127] B. W. Larson, J. B. Whitaker, X. B. Wang, A. A. Popov, G. Rumbles, N. Kopidakis, S. H. Strauss, O. V. Boltalina, *J. Phys. Chem. C*, 17(29), (2013) 14958.
- [128] R. A. J. Janssen, J. Nelson, *Adv. Mater.*, 25(13), (2013) 1847.

- 
- [129] F. B. Kooistra, J. Knol, F. Kastenberg, L. M. Popescu, W. J. H. Verhees, J. M. Kroon, J. C. Hummelen, *Org. Lett.*, 9(4), (2007) 551.
- [130] E. Klimov, W. Li, X. Yang, G. G. Hoffmann, J. Loos, *Macromolecules*, 39(13), (2006) 4493.
- [131] Y. C. Huang, Y. C. Liao, S. S. Li, M. C. Wu, C. W. Chen, W.-F. Su, *Sol. Energy Mater. Sol. Cells*, 93(6–7), (2009) 888.
- [132] A. C. Ferrari, D. M. Basko, *Nature Nano.*, 8(4), (2013) 235.
- [133] B. Qi, J. Wang, *Phys. Chem. Chem. Phys.*, 15(23), (2013) 8972.
- [134] C. R. McNeill, *Energy Environ. Sci.*, 5(2), (2012) 5653.
- [135] M. Campoy-Quiles, T. Ferenczi, T. Agostinelli, P. G. Etchegoin, Y. Kim, T. D. Anthopoulos, P. N. Stavrinou, D. D. C. Bradley, J. Nelson, *Nature Mater.*, 7(2), (2008)158.
- [136] A. Guerrero, T. R. Sanchis, P. P. Boix, G. Garcia-Belmonte, *Org. Electron.*, 13(11), (2012)2326.
- [137] P. H. Fang, Analysis of conversion efficiency of organic semiconductor solar cells, *J. Appl. Phys.*, 45, (1974) 4672.
- [138] D. L. Morel, A. K. Ghosh, T. Feng, E. L. Stogryn, P. E. Purwin, R. F. Shaw and C. Fishman, High efficiency organic solar cells, *Appl. Phys. Lett.*, 32,(1978) 495.
- [139] M. Hiramoto, H. Fujiwara, M. Yokoyama, Three layered organic solar cell with a photoactive interlayer of codeposited pigments, *Appl. Phys. Lett.*, 58, (1991)1062.
- [140] N. S. Sariciftci, L. Smilowitz, A. J. Heeger, F. Wudl, Photoinduced Electron Transfer from a Conducting Polymer to Buckminsterfullerene, *Science*, 258, 5087, (1993) 1474-1476.

- 
- [141] G. Yu and A. J. Heeger, Charge separation and photovoltaic conversion in polymer composites with internal donor/acceptor heterojunctions, *J. Appl. Phys.*, 78, (1995) 4510.
- [142] C. J. Brabec, N. S. Sariciftci, and J. C. Hummelen, Plastic Solar Cells., *Adv. Funct. Mater.*, 11, (2001)15–26.
- [143] G. Li, V. Shrotriya, J. Huang, Y. Yao, T. Moriarty, K. Emery, Y. Yang, High-efficiency solution processable polymer photovoltaic cells by self-organization of polymer blends, *Nature Materials*, 4, (2005) 864 - 868.
- [144] Y. Liang, Z. Xu, J. Xia, S. T. Tsai, Y. Wu, G. Li, C. Ray, L. Yu, For the Bright Future—Bulk Heterojunction Polymer Solar Cells with Power Conversion Efficiency of 7.4%, *Adv. Mater.*, 22 (2010) 135–138.
- [145] Z. He, C. Zhong, S. Su, M. Xu, H. Wu, Y. Cao, Enhanced power-conversion efficiency in polymer solar cells using an inverted device structure, *Nature Photonics*, 6, (2012) 591–595.
- [146] J. You, C. C. Chen, Z. Hong, K. Yoshimura, K. Ohya, R. Xu, S. Ye, J. Gao, G. Li, Y. Yang, 10.2% Power Conversion Efficiency Polymer Tandem Solar Cells Consisting of Two Identical Sub-Cells, *Adv. Mater.*, 25, (2013) 3973–3978.